

# UC Santa Cruz

## UC Santa Cruz Electronic Theses and Dissertations

### Title

Renormalization Group Constraints on the Two-Higgs Doublet Model

### Permalink

<https://escholarship.org/uc/item/7zn2j5k0>

### Author

Santos, Edward Regalado

### Publication Date

2015

Peer reviewed|Thesis/dissertation

UNIVERSITY OF CALIFORNIA  
SANTA CRUZ

**RENORMALIZATION GROUP CONSTRAINTS ON THE  
TWO-HIGGS DOUBLET MODEL**

A dissertation submitted in partial satisfaction of the  
requirements for the degree of

DOCTOR OF PHILOSOPHY

in

PHYSICS

by

**Edward R. Santos III**

June 2015

The Dissertation of Edward R. Santos III  
is approved:

---

Professor Howard Haber, Chair

---

Professor Michael Dine

---

Professor Stefano Profumo

---

Dean Tyrus Miller  
Vice Provost and Dean of Graduate Studies

Copyright © by  
Edward R. Santos III  
2015

# Table of Contents

List of Figures	v
List of Tables	viii
Abstract	ix
Dedication	xi
Acknowledgments	xii
<b>1 Introduction</b>	<b>1</b>
1.1 Standard Model . . . . .	6
1.1.1 Higgs mechanism . . . . .	6
1.1.2 Yukawa Lagrangian . . . . .	9
1.1.3 Scalar potential constraints . . . . .	12
1.2 Beyond the Standard Model . . . . .	22
1.2.1 Constraints on non-minimal Higgs sectors . . . . .	23
<b>2 Two-Higgs Doublet Model</b>	<b>28</b>
2.1 Basis-Independent Formalism . . . . .	30
2.1.1 Higgs mass eigenstates . . . . .	32
2.1.2 Decoupling limit . . . . .	33
2.2 Bounded from below conditions for a general 2HDM potential . . . . .	35
2.3 Yukawa sector and flavor-alignment . . . . .	40
<b>3 Renormalization Group Stability and Perturbativity Analysis</b>	<b>45</b>
3.1 Numerical Analysis . . . . .	52
3.1.1 Results from one-loop RG running . . . . .	52
3.1.2 The effects of two-loops RG running . . . . .	59

<b>4</b>	<b>Flavor Violation via Planck Scale Flavor-Alignment</b>	<b>64</b>
4.1	Planck scale flavor-alignment . . . . .	66
4.1.1	Leading logarithm approximation . . . . .	69
4.2	Experimental Bounds . . . . .	72
4.2.1	Flavor-changing top decays . . . . .	73
4.2.2	Leptonic $B$ decays . . . . .	75
<b>5</b>	<b>Conclusions</b>	<b>81</b>
<b>A</b>	<b>One-Loop Renormalization Group Equations for 2HDM</b>	<b>86</b>
A.1	Yukawa Couplings . . . . .	87
A.2	Scalar Parameters . . . . .	95
	<b>Bibliography</b>	<b>99</b>

# List of Figures

1.1	Left panel: The probability that electroweak vacuum decay happened in our past light-cone, taking into account the expansion of the universe. Right panel: The life-time of the electroweak vacuum, with two difference assumptions for future cosmology: universes dominated by the cosmological constant ( $\Lambda$ CDM) or by dark matter (CDM). Figures taken from Ref. [1]. . . . .	18
1.2	The instability scale $\Lambda_I$ at which the SM potential becomes negative as a function of the Higgs mass (left) and of the top mass (right). The theoretical error is not shown and corresponds to a $\pm 1$ GeV uncertainty in $m_h$ . Figures taken from Ref. [2]. . . . .	20
1.3	Left panel: Regions of absolute stability, meta-stability and instability of the SM vacuum in the $m_t - m_h$ plane. Right panel: Zoom in the region of the preferred experimental range of $m_h$ and $m_t$ (the gray areas denote the allowed region at 1, 2, and $3\sigma$ ). The three boundary lines correspond to $\alpha_s(m_Z) = 0.1184 \pm 0.0007$ , and the grading of the colors indicates the size of the theoretical error. The dotted contour-lines show the instability scale $\Lambda$ in GeV assuming $\alpha_s(m_Z) = 0.1184$ . Figures taken from Ref. [2]. . . . .	21
3.1	Distribution of absolute values of the flavor-alignment parameters, for regions of 2HDM parameter space which remain valid up to the Planck scale, assuming $\Lambda_H = 500$ GeV. . . . .	51
3.2	RG running of 2HDM quartic scalar couplings, with $\Lambda_H = 1$ TeV. Red points correspond to parameter choices for which an instability occurs in the scalar potential; blue points indicate the presence of a Landau pole. The upper solid black line indicates the occurrence of a Landau pole in the SM. The lower solid black line indicates the limit for which the SM potential becomes unstable. . . . .	53

3.3	Histograms of squared-mass differences of the heavy scalar states for $\Lambda_H = 500$ GeV. The left panel shows values of squared-mass difference between the two heavier neutral states. The middle and right panels shows the values of the squared-mass difference between the lighter and heavier of the two heavy neutral states and the charged Higgs boson, respectively. The histograms correspond to 2HDM parameters for which there are no Landau poles and vacuum stability is satisfied at all energies below the Planck scale. . .	56
3.4	Histograms of squared-mass differences of the heavy scalar states for $\Lambda_H = 1$ TeV. The left panel shows values of squared-mass difference between the two heavier neutral states. The middle and right panels shows the values of the squared-mass difference between the lighter and heavier of the two heavy neutral states and the charged Higgs boson, respectively. The histograms correspond to 2HDM parameters for which there are no Landau poles and vacuum stability is satisfied at all energies below the Planck scale. . . . .	57
3.5	Left panel: Scale shift for converting the one-loop scalar potential instability boundary to the two-loop scalar potential instability boundary for a SM-like Higgs boson. Right panel: Higgs boson mass bounds in the flavor-aligned 2HDM, incorporating the scale shift shown in the left panel, assuming that $\Lambda_H = 1$ TeV. Red points indicate an instability in the running; blue points indicate the presence of a Landau pole. . . . .	61
3.6	Histograms of squared-mass differences of the heavy scalar states for $\Lambda_H = 1$ TeV, using the two-loop extended procedure. The left panel shows values of squared-mass difference between the two heavier neutral states. The middle and right panels shows the values of the squared-mass difference between the lighter and heavier of the two heavy neutral states and the charged Higgs boson, respectively. The histograms correspond to 2HDM parameters for which there are no Landau poles and vacuum stability is satisfied at all energies below the Planck scale. . . . .	63
4.1	Regions of the A2HDM parameter space where $ \rho_{ij}^U  \gg  \rho_{ji}^U $ (green points) and $ \rho_{ij}^U  \ll  \rho_{ji}^U $ (blue points), for $i > j$ . The left panel is for $i, j = 2, 1$ , the middle panel is for $i, j = 3, 1$ , and the right panel is for $i, j = 3, 2$ . . . . .	71

4.2	Regions of the A2HDM parameter space where $ \rho_{ij}^D  \gg  \rho_{ji}^D $ (green points) and $ \rho_{ij}^D  \ll  \rho_{ji}^D $ (blue points), for $i > j$ . The left panel is for $i, j = 2, 1$ , the middle panel is for $i, j = 3, 1$ , and the right panel is for $i, j = 3, 2$ . . . . .	72
4.3	Histogram of branching ratios for $t \rightarrow uh$ and $t \rightarrow ch$ , in the left and right panels, respectively. Although enhancements with respect to the SM rate are possible, the resulting decay rate is many orders of magnitudes below the current experimental bound of $\text{BR}(t \rightarrow qh) \lesssim 10^{-3}$ , for both $q = u, c$ . . . . .	75
4.4	Tree level neutral Higgs boson mediated $B_s \rightarrow \mu^+\mu^-$ in the 2HDM.	77
4.5	A2HDM branching ratio for $B_s \rightarrow \mu^+\mu^-$ relative the the SM, as a function of $ \alpha^D $ . Left panel: results for $ \rho_{32}^D  \ll  \rho_{23}^D $ , corresponding to the small alignment parameter limit. Right panel: results for $ \rho_{32}^D  \gg  \rho_{23}^D $ , corresponding to the large alignment parameter limit, implying large branching ratios relative to the SM are generated only when $ \rho_{32}^D  \gg  \rho_{23}^D $ . . . . .	79
4.6	Constraints on the A2HDM parameter space from $B_s \rightarrow \mu^+\mu^-$ . The blue points correspond to regions of parameter space that deviate from $\text{BR}(B_s \rightarrow \mu^+\mu^-)_{SM}$ by less than 10%. The red points correspond to regions of parameter space that deviate from $\text{BR}(B_s \rightarrow \mu^+\mu^-)_{SM}$ between 10% - 20%. The green points indicate the region of parameter space that deviate from $\text{BR}(B_s \rightarrow \mu^+\mu^-)_{SM}$ by more than 20%. . . . .	80

# List of Tables

2.1	$q_{ki}$ as a function of the neutral Higgs mixing angles in the Higgs basis. . . . .	33
3.1	Squared mass splittings of the heavier Higgs bosons of the 2HDM with $\Lambda_H = 500$ GeV, for $124 \lesssim m_h \lesssim 126$ GeV, for points that survive up to the Planck scale, using one-loop calculations. . . . .	58
3.2	Squared mass splittings of the heavier Higgs bosons of the 2HDM with $\Lambda_H = 1$ TeV, for $124 \lesssim m_h \lesssim 126$ GeV, for points that survive up to the Planck scale, using one-loop calculations. . . . .	59
3.3	Squared-mass splittings of the heavy Higgs bosons of the 2HDM with $\Lambda_H = 1$ TeV, for $m_h \simeq 125$ GeV, for points that survive to the Planck scale, using the two-loop extended procedure. . . . .	62

## Abstract

Renormalization Group Constraints on the Two-Higgs Doublet Model

by

Edward R. Santos III

We examine the constraints on the two Higgs doublet model (2HDM) due to the stability of the scalar potential and absence of Landau poles at energy scales below the Planck scale. We employ the most general 2HDM that incorporates an approximately Standard Model (SM) Higgs boson with a flavor-aligned Yukawa sector to eliminate potential tree-level Higgs-mediated flavor-changing neutral currents. Using basis independent techniques, we exhibit regimes of the 2HDM parameter space with a 125 GeV SM-like Higgs boson that is stable and perturbative up to the Planck scale. Implications for the heavy scalar spectrum are exhibited.

The most general 2HDM contains an extended Yukawa sector that includes new sources of flavor changing neutral currents (FCNCs), which must be suppressed due to experimental bounds. The flavor-alignment ansatz asserts a proportionality between the Yukawa matrices that couple the up-type (down-type) fermions to the two respective Higgs doublet fields of the 2HDM, thereby eliminating FCNCs at tree-level. If flavor-alignment is imposed at a high energy scale, such as the Planck scale, tree-level FCNCs can be generated at the electroweak scale via renormalization group running. We determine the size of FCNCs that

can be generated at the electroweak scale via Planck scale flavor-alignment, and use experimental bounds on flavor-changing observables to place constraints on the flavor-aligned 2HDM parameter space.

To my Grandfather,

Papa Juan.

## Acknowledgments

This dissertation completes a long journey that began when I was a high school junior. At the time, I was an unmotivated student struggling to find reason to continue my education. One of my teachers Tom Kaplan, was aware of the potential I possessed and was among the first educators that challenged me to perform up to it, thus starting a long academic journey culminating in this dissertation. Thanks Mr. Kaplan, you helped me find the inner power to do extraordinary things that we all possess. I've always done my best to pass this along to those who have looked up to me.

I would like to acknowledge some of the my favorite teachers I had throughout my academic career: the aforementioned Tom Kaplan, Carol Cho, Shari Stockwell, Tom Weiss, Oshri Karmon, Michael Connor, Ron Rusay, David Griffiths, Steve Shenker, Stefano Profumo, Howard Haber, and Michael Dine. Thank you all for providing unforgettable learning experiences. I would also like to thank Patricia Burchat, my undergraduate research advisor at Stanford, who inspired me in many ways.

It really is impossible to adequately thank all of the people I have known and befriended here in Santa Cruz, and so I'll stick those those who might one day read this. Firstly, my physics classmates: Andy Kuhl, Carena Church, Greg Bowers, Jonathan Cornell, Matt Wittmann, Milton Bose, Nicole Moody, Omar Moreno,

TJ Torres, Zach Nadler – you guys were great, and I hope our friendships endure. Laura Fava, my academic sister, who has always been so helpful and thoroughly enjoyable to talk to. Eric Carlson, for being such a great friend, and my future political officemate. Patrick Draper, for useful conversations, but maybe more so for all the useless ones. Tim Stefaniak, for providing much help in the later stages of this dissertation process.

To Stefano Profumo, thanks so much for being a great friend and for always looking out for me. As one of the most competitive people I have ever met, I've always appreciated the fact that you were going to give me your best, whether in the classroom or on the bike, which in turn always helped me better myself. But along with your best, you've given me many laughs and great memories while killing each other (and ourselves) in the mountains of Santa Cruz, and I'm very grateful for our friendship.

I'm very fortunate to have had a great relationship with my advisor, Howie Haber. On a professional level, any amount of Howie's attention to detail that has rubbed off on me has undoubtedly made me a better analytical thinker, and I'm very thankful for having had the opportunity to work with him. On a personal level, I'll cherish the stories shared while traveling to and from SLAC, being there together for Matt Cain's perfect game, and five great years on the Re-Entry softball team, filled with championship runs.

To my siblings, it's still weird to me to see you guys all grown up and have your own families, but I'm proud of you guys. It's not always been easy, but I'm glad we have each other. To my Mother, Mercy, who has always had my back and had never ending belief in me during this journey, thank you. I appreciate all of the lessons and qualities that you have passed on to me, and I couldn't ask for a better Mom.

To Melissa, one of the funniest and silliest people I have ever met. Your presence in my life has provided me a large source of happiness and has helped me realize what the important things in life are. Thank you so much for your support and patience over the last few years. I'm looking forward to our future together, which hopefully includes a vacation sooner than later.

*The text of this thesis includes reprints of the following previously published material in Refs. [3] and [4]. The co-author listed in this publication directed and supervised the research which forms the basis for the thesis.*

# Chapter 1

## Introduction

The discovery of the Higgs boson at the Large Hadron Collider (LHC) in 2012 (Refs. [5, 6]) has proven to be a major success for particle physics, providing a confirmation of the long sought-after mechanism for electroweak symmetry breaking (EWSB). With the existence of the Higgs boson now confirmed, the attention has now turned to deciphering the Higgs properties, in order to determine and whether it is the SM Higgs boson or the lightest Higgs boson of a larger set. Whereas the standard model (SM) has been very successful in explaining much of particle physics to a high degree of accuracy, there exists many motivations for physics Beyond the Standard Model (BSM), including dark matter, dark energy, sufficient CP-violation required for baryogenesis, the question of naturalness, among others. Most recently, SM Renormalization Group (RG) calculations (Refs.

[2, 7]) have shown that the SM is most likely not consistent at all energy scales up to the Planck scale, due to the existence of a deeper minimum of the scalar potential at large field values. To avoid the corresponding instability of the electroweak vacuum would require new physics entering at an intermediate energy scale.

Although the prospect of existence of new BSM physics is exciting, there is no guarantee that the scale of the new physics is close to the electroweak scale. Nevertheless, arguments motivated by naturalness of the electroweak symmetry breaking (EWSB) mechanism suggest that BSM physics should be present at or near the TeV scale (see e.g., Refs. [8, 9] for a review and a guide to the literature). Many models of new physics have been proposed to address the origin of EWSB, and many of these approaches possess extended Higgs sectors. However, in such models one must specify the BSM physics in order to study the behavior of running couplings between the electroweak scale and some very high energy scale  $\Lambda$ . At present, there is no direct experimental evidence that the origin of the EWSB scale is a consequence of naturalness. Adding additional Higgs multiplets at or near the TeV scale by themselves does not address the origin of EWSB. Indeed, one could argue that it makes matters worse by adding additional fine-tuning constraints. Nevertheless, in this paper we shall accept the fine-tunings required to sustain an extended Higgs sector near the TeV scale. After all, we know that multiple generations exist in the fermionic sector of the Standard Model. Thus,

we should be prepared for the possibility that the scalar sector of the theory is also non-minimal.

Here, we shall focus on the two-Higgs doublet model (2HDM), which was initially proposed by Lee in 1973 [10] (for a review, see e.g. Ref. [11]). It provides a richer Higgs particle spectrum, namely three neutral scalars and a charged pair. The 2HDM admits the possibility of CP-violation in the scalar potential, both explicit or spontaneous. In the limit of CP-conservation, two of the neutral scalars are CP-even, typically denoted by  $h$  and  $H$ , (where  $m_h < m_H$ ) while the other neutral scalar is CP-odd, denoted by  $A$ . We shall consider a very general version of the 2HDM that is not inconsistent with present data. Such a model must possess a SM-like Higgs boson (within the accuracy of the present Higgs data). In addition, Higgs-mediated tree-level flavor changing neutral currents (FCNCs) must be either absent or highly suppressed. These conditions are achieved if the non-minimal Higgs states of the model have masses above about 350 GeV and if the Yukawa couplings are aligned in such a way that the neutral Higgs couplings are diagonal in the mass-basis for the neutral Higgs bosons. The most general 2HDM parameter space allowed by the present data is somewhat larger than the one specified here. Nevertheless, the restricted parameter space outlined above is still quite general and incorporates the more constrained 2HDMs considered in the literature.

Chapter 1 of this thesis begins with a review of the SM Higgs mechanism, recapping the scalar potential and mechanism in which masses are generated for gauge bosons and fermions. We then review constraints on the SM scalar potential by imposing perturbativity, meta-stability, and stability. After a brief mention of several BSM models, we recap constraints from precision electroweak data and FCNCs, the latter in the context of the minimal flavor violation (MFV) framework.

Chapter 2 reviews the most general 2HDM, one of the simplest extensions to the SM Higgs sector, positing the existence of a second heavier Higgs doublet, in addition to that of the SM. The most general 2HDM provides a richer spectrum of Higgs bosons and introduces additional sources of CP-violation, however, in its most general form it allows FCNCs that are severely constrained experimentally. We recap the most general 2HDM with the flavor-alignment ansatz, in which the two sets of Yukawa matrices are proportional and thus simultaneously bi-diagonalizable. We present the 2HDM in the basis-independent formalism (as first presented in Ref. [12]), making no CP assumptions that would result in constraints on the scalar potential and Higgs-fermion interactions. Conditions for tree-level stability of the CP-violating 2HDM are also presented in the basis-independent formalism.

Chapter 3 is based on work presented in Ref. [3], where we show that if the recently discovered 125 GeV Higgs boson is lightest scalar, then the 2HDM

could potentially survive up to the Planck scale under renormalization group (RG) evolution. For regions of the parameter space that survive stability and perturbativity requirements up to Planck scale, we provide bounds on the squared mass differences between two of the heavier Higgs bosons. In particular, we find that the heavy Higgs bosons are roughly degenerate with small deviations resulting from the presence of constrained quartic couplings of the 2HDM scalar potential. We also present a rough estimate of the leading two-loop effects by taking into account the two-loop contributions to the SM RG evolution.

Chapter 4 is based on work presented in Ref. [4], where we study the effects of imposing Planck scale flavor-alignment between the two sets of Yukawa matrices in the most general 2HDM Yukawa sector. The implications for FCNC processes from both Higgs mediated tree-level and one-loop radiative effects are examined. We use current experimental results to constrain the parameter space of the alignment parameters.

In Chapter 5, we conclude by summarizing the implications of Chapters 3 and 4 for the 2HDM. Appendix A contains the derivations of the one-loop renormalization group equations RGEs for the 2HDM scalar potential parameters and the Yukawa couplings.

## 1.1 Standard Model

The ATLAS and CMS experiments have recently reported (Refs. [5, 6]) the discovery a SM-like Higgs boson at a mass of about 125 GeV. The LHC by itself cannot claim discovery of the SM Higgs boson, only discovery of a SM-like Higgs boson. The SM has proven to be very robust, with the Higgs boson being that of the SM or very close to it. Precision Higgs data from future colliders are needed to determine the exact nature of the observed Higgs boson. In this section we review the SM Higgs mechanism as a means of EWSB and review the implications the observed Higgs mass has on the scalar potential during RG evolution, Finally, we briefly review the experimental constraints on non-minimal Higgs sectors.

### 1.1.1 Higgs mechanism

The Standard Model of particle physics, which obeys an  $SU(3)_c \times SU(2)_L \times U(1)_Y$  gauge symmetry, does not allow explicit mass terms for gauge bosons or fermions. For gauge bosons, mass terms violate local gauge invariance, thereby requiring a mechanism to break the  $SU(2)_L \times U(1)_Y$  electroweak symmetry. The left and right handed fermions transform as doublets and singlets, respectively, under  $SU(2)_L$ , and thus it is not possible to construct an  $SU(2)_L$  invariant mass term for fermions. The Higgs mechanism provides a means for EWSB by introducing a hypercharge-one ( $Y = 1$ ), complex scalar  $SU(2)_L$  doublet with four real fields,

$$\phi = \begin{pmatrix} \phi_0^+ + i\phi_1^+ \\ \phi_2 + i\phi_3 \end{pmatrix}, \quad (1.1)$$

with a tree-level scalar potential of the form,

$$V_H = -m^2\phi^\dagger\phi + \frac{\lambda}{2}(\phi^\dagger\phi)^2. \quad (1.2)$$

We require the minimum of the potential, defined to be the vacuum expectation value (vev)  $v$ , be non-zero to induce spontaneous symmetry breaking, thereby requiring  $m^2 > 0$ . For the potential to be bounded from below at tree-level, we must also have  $\lambda > 0$ . By minimizing the scalar potential (eq. 1.2) with respect to  $\phi$ , we find the the vev is  $v = \sqrt{m^2/\lambda} = (\sqrt{2}G_F)^{-1/2} = 246$  GeV. By expanding  $\phi$  around the vev,

$$\phi = \begin{pmatrix} G^+ \\ \frac{1}{\sqrt{2}}(v + h + iG^0) \end{pmatrix}, \quad (1.3)$$

and inserting this expansion into the scalar potential (eq. 1.2), we generate a mass term  $-\lambda v^2 h^2$  for the scalar field  $h$ , now identified as the field of the physical Higgs boson. The fields  $G^0$  and  $G^\pm$  are identified as the massless Goldstone bosons. Thus, the shape of the scalar potential is controlled by two parameters: the mass of the Higgs boson (or equivalently, the Higgs self-coupling), and the vacuum expectation value, both of which have now been determined experimentally.

The  $W^\pm$  and  $Z$  bosons, being massless before EWSB, each have two degrees of freedom for a total of six. The scalar doublet (eq. 1.1) has four degrees of freedom, one of which becomes the physical Higgs boson, the rest of which are identified as massless Goldstone bosons. Through the Higgs mechanism, the Goldstone bosons become the longitudinal modes of the  $W^\pm$  and  $Z$  gauge boson, which now each have three degrees of freedom and therefore effectively acquire masses. This occurs via the scalar kinetic terms in the Lagrangian, where the covariant derivative terms of the scalar field are given by  $D_\mu\phi = (\partial_\mu + igW_\mu^a\tau^a + i\frac{1}{2}Yg'B_\mu)\phi$ . Expanding  $\phi$  around the vev (eq. 1.3) and inserting into the scalar kinetic term yields

$$\mathcal{L}_{KE} = |D_\mu\phi|^2 = \frac{v^2}{8} [g^2((W_\mu^1)^2 + (W_\mu^2)^2) + (g'B_\mu - gW_\mu^3)^2]. \quad (1.4)$$

Identifying the vector boson mass eigenstates of definite electric charge,

$$W_\mu^\pm = \frac{1}{\sqrt{2}}(W_\mu^1 \mp iW_\mu^2), \quad (1.5)$$

$$Z_\mu = \frac{1}{\sqrt{g^2 + g'^2}}(gW_\mu^3 - g'B_\mu), \quad (1.6)$$

$$A_\mu = \frac{1}{\sqrt{g^2 + g'^2}}(gW_\mu^3 + g'B_\mu). \quad (1.7)$$

Inserting these fields into eq. 1.4, we obtain the mass terms for the physical gauge bosons,

$$\mathcal{L}_{KE} = \left(\frac{gv}{2}\right)^2 W_\mu^+ W^{\mu-} + \frac{1}{2} \left(\frac{1}{2} \sqrt{g^2 + g'^2} v\right) Z_\mu Z^\mu + \frac{1}{2} (0) A_\mu A^\mu. \quad (1.8)$$

In summary, the Higgs mechanism, via the inclusion of a complex hypercharge one scalar SU(2) doublet  $\phi$  with a non-zero vev, along with a scalar potential of the form eq. 1.2, generates a new massive particle, the Higgs boson, and gives mass to the  $W^\pm$  and  $Z$  bosons, while recovering the massless photon:

$$m_h = \sqrt{\lambda} v, \quad (1.9)$$

$$m_W = \frac{1}{2} g v, \quad (1.10)$$

$$m_Z = \frac{1}{2} \sqrt{g^2 + g'^2} v = m_W / \cos \theta_W, \quad (1.11)$$

$$m_A = 0, \quad (1.12)$$

where  $\tan \theta_W = g'/g$ , is the weak mixing angle.

### 1.1.2 Yukawa Lagrangian

The Higgs mechanism also provides a means to generate mass terms for chiral fermions. Naively, we would write a chiral fermion mass term as  $m_f \bar{f} f = m_f (\bar{f}_L f_R + \bar{f}_R f_L)$ , but since left and right-handed fermions are SU(2) doublets and singlets, respectively, such a mass term is not SU(2) invariant. We can,

however, couple the left-handed fermions to the scalar field to generate a SU(2) invariant term,

$$-\mathcal{L}_Y = y_f \bar{F}_L \cdot \phi f_R + h.c., \quad (1.13)$$

where  $y_f$  is an arbitrary coupling constant, and  $F_L$  is a left-handed SU(2) fermion doublet, which generates a mass term after the scalar field acquires a vev,

$$-\mathcal{L}_Y = \frac{v}{\sqrt{2}} y_f \bar{f}_L f_R + h.c.. \quad (1.14)$$

Thus, fermions couple to the Higgs boson with a magnitude proportional to their masses,  $m_f = y_f v / \sqrt{2}$ . The strength of these couplings are determined once the fermion mass has been measured.

In generalizing to three generations, we shall focus only on the quark sector (the extension to leptons is fairly straightforward). With three generations, the Yukawa couplings,  $y_f$ , now become two  $3 \times 3$  matrices in flavor space,  $Y_Q^0$ , where  $Q = U, D$ . The Yukawa Lagrangian is now written as

$$-\mathcal{L}_Y = \bar{Q}_L^0 \cdot \tilde{\phi} Y_U^0 U_R^0 + \bar{Q}_L^0 \cdot \phi Y_D^{0\dagger} D_R^0 + h.c., \quad (1.15)$$

where  $\tilde{\phi} = i\tau_2 \phi^*$  and  $Q$  is the left-handed SU(2) quark doublet,

$$Q_L^i = \begin{pmatrix} U^i \\ D^i \end{pmatrix}_L. \quad (1.16)$$

To find the quark-mass eigenstates, we apply the following unitary transformations to diagonalize the Yukawa matrices

$$P_L U = V_L^U P_L U^0, \quad (1.17)$$

$$P_L D = V_L^D P_L D^0, \quad (1.18)$$

$$P_R U = V_R^U P_R U^0, \quad (1.19)$$

$$P_R D = V_R^D P_R D^0, \quad (1.20)$$

where  $P_{R,L} \equiv \frac{1}{2}(1 \pm \gamma_5)$ , and the Cabibbo-Kobayashi-Maskawa (CKM) matrix is defined to be  $K \equiv V_L^U V_L^{D\dagger}$ . Redefining  $\mathcal{U} \equiv K^\dagger U$ , and  $\mathcal{Q} = \begin{pmatrix} \mathcal{U} \\ D \end{pmatrix}_L$ , we can rewrite eq. 1.15 as

$$-\mathcal{L}_Y = \bar{\mathcal{Q}}_L \cdot \tilde{\phi} Y_U \mathcal{U}_R + \bar{\mathcal{Q}}_L \cdot \phi Y_D^\dagger D_R + h.c., \quad (1.21)$$

where  $Y_U$  and  $Y_D$  are the Yukawa matrices in the quark-mass eigenstate, which are diagonalized by the rotation

$$Y_U = V_L^U Y_U^0 V_R^{U\dagger}, \quad (1.22)$$

$$Y_D = V_R^D Y_D^0 V_L^{D\dagger}. \quad (1.23)$$

The quarks mass matrices are then identified in terms of the diagonalized Yukawa matrices and vev as

$$M_U = \frac{v}{\sqrt{2}} Y_U = \text{diag}(m_u, m_c, m_t), \quad (1.24)$$

$$M_D = \frac{v}{\sqrt{2}} Y_D^\dagger = \text{diag}(m_d, m_s, m_b). \quad (1.25)$$

### 1.1.3 Scalar potential constraints

In this thesis, we analyze the scalar potential of the 2HDM with a SM-like Higgs of mass 125 GeV to test validity of the theory up to the Planck scale given the appropriate stability and perturbativity requirements. In the 2HDM, these constraints can be much more complicated given the increased parameter space. Thus, we review the concepts of stability, meta-stability, and perturbativity for the scalar potential in the SM, to build intuition for how these phenomena are exhibited in the 2HDM. Recent two-loop calculations (Refs. [1, 2]) suggest that a 125 GeV Higgs boson leads to a scenario in which the scalar potential is in the metastable regime.

Stability of the scalar potential requires that the potential is bounded from below at all energy scales during RG evolution. Here we follow the effective potential approach reviewed in Ref. [13], taking into account quantum loop corrections to the tree-level potential. For the SM Higgs, the effective potential is given by

$$V_{eff}(\phi) = V^{(0)}(\phi) + \hbar V^{(1)}(\phi), \quad (1.26)$$

where  $V^{(0)}$  is the tree-level scalar potential (eq. 1.2) and  $V^{(1)}$  accounts for the one-loop quantum corrections

$$V^{(1)} = -m_0^2\phi^2 + \frac{1}{2}\lambda_0\phi^4 + \frac{1}{16\pi^2} \left[ \frac{1}{4}H^2 \left( \ln \frac{H}{\Lambda_0^2} - \frac{3}{2} \right) + \frac{3}{4}G^2 \left( \ln \frac{G}{\Lambda_0^2} - \frac{3}{2} \right) \right. \\ \left. + \frac{3}{2}W^2 \left( \ln \frac{W}{\Lambda_0^2} - \frac{5}{6} \right) + \frac{3}{4}Z^2 \left( \ln \frac{Z}{\Lambda_0^2} - \frac{5}{6} \right) - 3T^2 \left( \ln \frac{T}{\Lambda_0^2} - \frac{3}{2} \right) \right], \quad (1.27)$$

with

$$H = -m_0^2 + \lambda_0\phi^2/2, \quad (1.28)$$

$$G = -m_0^2 + \lambda_0\phi^2/6, \quad (1.29)$$

$$W = g_0'^2\phi^2/4, \quad (1.30)$$

$$Z = (g_0^2 + g_0'^2)\phi^2/4, \quad (1.31)$$

$$T = g_0^2\phi^2/2. \quad (1.32)$$

For large  $\phi$ , the one-loop potential can be written as

$$V^{(1)}(\phi) = \phi^4 \left[ \lambda_0 + [\beta_\lambda(\lambda_0, g_0, g_0') - 4\lambda_0\gamma(\lambda_0, g_0, g_0')] \ln \left( \frac{\phi}{\mu_0} \right) \right. \\ \left. + \mathcal{O}(\lambda_0^2, g_0^2, g_0'^2) \right], \quad (1.33)$$

which is just the expansion of the quartic term in the RG improved potential,

$$V_{RG}^{(1)} = \lambda(t)[\xi(t)\phi]^4 + \mathcal{O}(\lambda(t)^2, g(t)^2, g'(t)^2), \quad (1.34)$$

where

$$\xi(t) = e^{-\int_0^t \gamma(\lambda(t'), g(t'), g'(t')) dt'}, \quad (1.35)$$

$\gamma$  is the anomalous dimension,  $t = \ln(\mu/\mu_0)$ , and  $\mu_0$  is the renormalization scale.

Within the approximation of eq. 1.34 we see that the stability of  $V(\phi)$  is equivalent to requiring  $\lambda(\Lambda) > 0$  for all  $\Lambda$ . If at some scale before  $\Lambda = M_{PL}$ ,  $\lambda(\Lambda) < 0$ , then the scalar potential is either completely unstable, or there exists a deeper potential minimum at  $\phi > \Lambda$ . The latter case would correspond to a metastable vacuum, which is described in more detail later in this section. In the former case, to avoid the scalar potential becoming unstable, new physics is required before the scale of the instability. To illustrate this phenomena, we analyze the one-loop RGE for the Higgs self coupling  $\lambda$ ,

$$16\pi^2 \frac{d\lambda}{dt} = 12\lambda^2 + 12y_t^2\lambda - 12y_t^4 - 3(g'^2 + 3g^2)\lambda + \frac{3}{4}(g^4 + 2g'^2g^2 + 3g^4). \quad (1.36)$$

The RHS of eq. 1.36 is dominated by three terms:  $12\lambda^2$ ,  $12y_t^2\lambda$ , and  $-12y_t^4$ . The effect of the first two is to increase the value of  $\lambda$  during RG evolution, driving the coupling constant to the non-perturbative regime, and the last to decrease

$\lambda$ , driving the potential to become unstable. To reach the Planck scale, these three terms must balance each other out appropriately, leading to a range of Higgs masses that satisfy this condition, which at one-loop is  $140 \text{ GeV} \lesssim m_h \lesssim 175 \text{ GeV}$ , where the lower and upper bounds are from requiring stability and perturbativity, respectively.

The perturbativity requirement is sometimes confused as being an upper bound on Higgs masses. Instead, it indicates the energy scale at which the theory becomes non-perturbative, at which point the one-loop RGEs cease to be reliable, and the inclusion of higher-order or non-perturbative corrections to the one-loop RGEs is necessary. In the SM, this occurs when the Higgs self coupling (mass) is large, so that the one-loop beta function for  $\lambda$  (eq. 1.36) is dominated by the  $\lambda^2$  term, so to crude approximation, we get

$$16\pi^2 \frac{d\lambda}{dt} \approx 12\lambda^2, \tag{1.37}$$

This allows for an analytic solution for  $\lambda(\Lambda)$ ,

$$\lambda(\Lambda) \approx \frac{1}{\frac{2v^2}{m_h^2} - \frac{3}{4\pi^2} \ln(\Lambda/v)}. \tag{1.38}$$

Taking the limit  $\lambda(\Lambda) \rightarrow \infty$  (known as a Landau Pole), implies that the denominator of eq. 1.38 goes to zero. Solving for  $\Lambda$ , we get

$$\Lambda \lesssim e^{\frac{8\pi^2 v^2}{3m_h^2}} v \approx 10^{46} \text{ GeV}. \quad (1.39)$$

Eq. 1.39 provides the largest scale at which the theory becomes non-perturbative, such that higher-order loop corrections or non-perturbative methods must be used, and/or new physics introduced, given a Higgs mass. The inclusion of higher order and non-perturbative calculations provides a very similar result. Of course, perturbativity would have long ceased before Higgs self coupling reached a Landau pole, and so conversely, the perturbativity requirement provides an upper bound for Higgs masses that can reach the Planck scale. Including all of the terms in the eq. 1.36, and taking a softer perturbativity requirement  $\lambda(M_{PL}) \lesssim 1$ , yields an upper bound of  $m_h \lesssim 175 \text{ GeV}$ .

Eq. 1.39 informs us that the SM is well within the perturbative regime. Extended Higgs sectors (with the lightest scalar corresponding to a SM-like Higgs), however, contain additional quartic couplings in the scalar potential that can lead to perturbativity issues at an energy scale well below the Planck scale. It is beneficial to use the SM as an illustration of phenomena, as the concept can be extended to understand perturbativity constraints in BSM models with extended Higgs sectors.

In the metastable scenario, i.e. requiring that the lifetime of the metastable electroweak vacuum is less than the age of the universe, one finds a lower bound

on  $m_h$  that is not as strict as that from stability, as reviewed in Ref. [14]. Current values of the Higgs mass and the top quark mass indicate that the SM Higgs vacuum is not the true vacuum, and here we recap the meta-stability requirements as reviewed in Ref. [1], who provide the vacuum-decay probability for the electroweak vacuum to have decayed during the past history of the universe as

$$\wp_0 = 0.15 \frac{\Lambda_B^4}{H_0^4} e^{-S(\Lambda_B)}, \quad (1.40)$$

where  $H_0$  is the present Hubble constant, and  $S(\Lambda_B)$  is the action of the bounce of size  $R = \Lambda_B^{-1}$ ,

$$S(\Lambda_B) = \frac{8\pi^2}{3|\lambda(\Lambda_B)|}. \quad (1.41)$$

Fig. 1.1a (taken from Ref. [1]) shows  $\wp_0$  as a function of the top quark mass, where we see that the probability for our current vacuum to decay to the true vacuum is incredibly small. In the regime that the universe is matter dominated in the future, the lifetime of the electroweak vacuum,  $\tau_{EW}$  is given by

$$\tau_{EW} = \left(\frac{55}{3\pi}\right)^{1/4} \frac{e^{S(\Lambda_B)/4}}{\Lambda_B} \approx \frac{T_U}{\wp_0^{1/4}}, \quad (1.42)$$

where  $T_U \approx 0.96H_0$ , having defined the ‘radius’ of the present day universe to be  $cT_U$ . If the future of the universe is dominated by the cosmological constant, i.e. dark energy, the lifetime of the electroweak vacuum is

$$\tau_{EW} = \frac{3H^3 e^{S(\Lambda_B)}}{4\pi\Lambda_B^4} \approx \frac{0.02T_U}{\wp_0}, \quad (1.43)$$

where  $H = H_0\sqrt{\Omega_\Lambda}$ . The lifetime of the electroweak vacuum for both the matter and cosmological constant dominated cases are both particularly large, and are shown in Fig. 1.1b (taken from Ref. [1]) as a function of the top quark mass. Such large values for  $\tau_{EW}$  indicate that the current SM electroweak vacuum lifetime is much greater than the current lifetime of our universe, and thus is metastable.

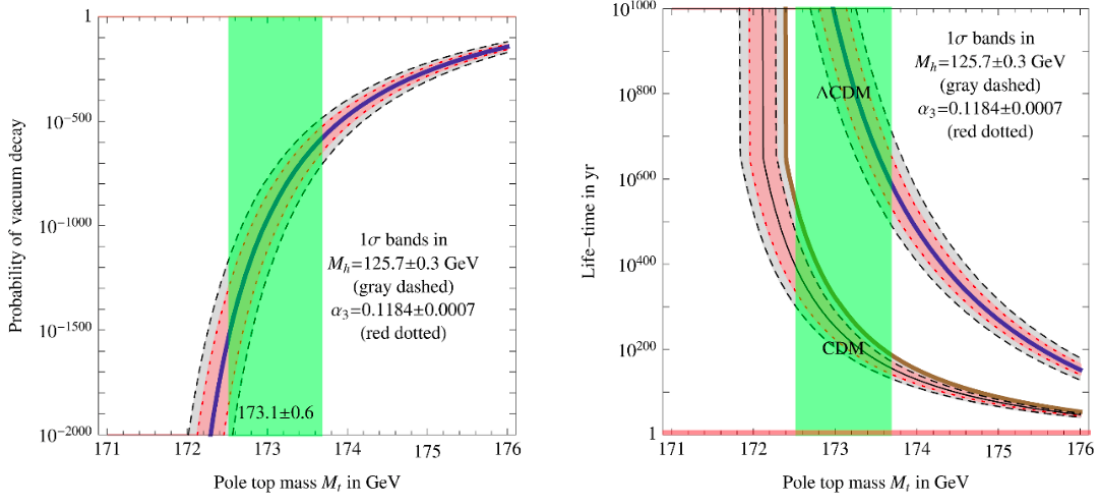


Figure 1.1: Left panel: The probability that electroweak vacuum decay happened in our past light-cone, taking into account the expansion of the universe. Right panel: The life-time of the electroweak vacuum, with two difference assumptions for future cosmology: universes dominated by the cosmological constant ( $\Lambda$ CDM) or by dark matter (CDM). Figures taken from Ref. [1].

Ref. [1] also shows that the SM scalar potential is stable up to the Planck

scale for a Higgs mass satisfying

$$m_h > 129.6 \text{ GeV} + 2.0(m_t - 173.34 \text{ GeV}) - 0.5 \text{ GeV} \left( \frac{\alpha_s(m_z) - 0.1184}{0.0007} \right) \pm 0.3 \text{ GeV}, \quad (1.44)$$

where  $m_t$  is the top quark pole mass and  $\alpha_s(m_z)$  is the strong coupling constant at the electroweak scale. Taking into account the theoretical uncertainty with the uncertainty in the top quark mass and the strong coupling constant, the requirement for the scalar potential to be stable is

$$m_h > (129.6 \pm 1.5) \text{ GeV}, \quad (1.45)$$

and  $m_h < 126 \text{ GeV}$  being valid up to the Planck scale is excluded at  $2.8\sigma$  (99.8% C.L. one sided). Similarly, the instability scale  $\Lambda_V$  is found to be

$$\log_{10} \frac{\Lambda_V}{\text{GeV}} = 9.5 + 0.7 \left( \frac{m_h}{\text{GeV}} - 125.15 \right) - 1.0 \left( \frac{m_t}{\text{GeV}} - 173.34 \right) + 0.3 \left( \frac{\alpha_s(m_z) - 0.1184}{0.0007} \right). \quad (1.46)$$

Thus, the most current results suggest that if the SM is the only source of physics up to the Planck scale, the Higgs self coupling will become negative at  $\Lambda_V = 10^{9.5} \text{ GeV}$ , up to the uncertainties in the Higgs and top quark masses, as well as the strong coupling constant, as seen in Fig. 1.2 (taken from Ref. [2]). In this scenario, it appears that our current vacuum is metastable, though the

probability of tunneling to the true vacuum state is incredibly small, as shown in Fig. 1.1a (taken from Ref. [1]). The current situation is recapped in Fig. 1.3 (taken from Ref. [2]), and will need further precision measurements for the top quark and Higgs masses to clarify the picture.

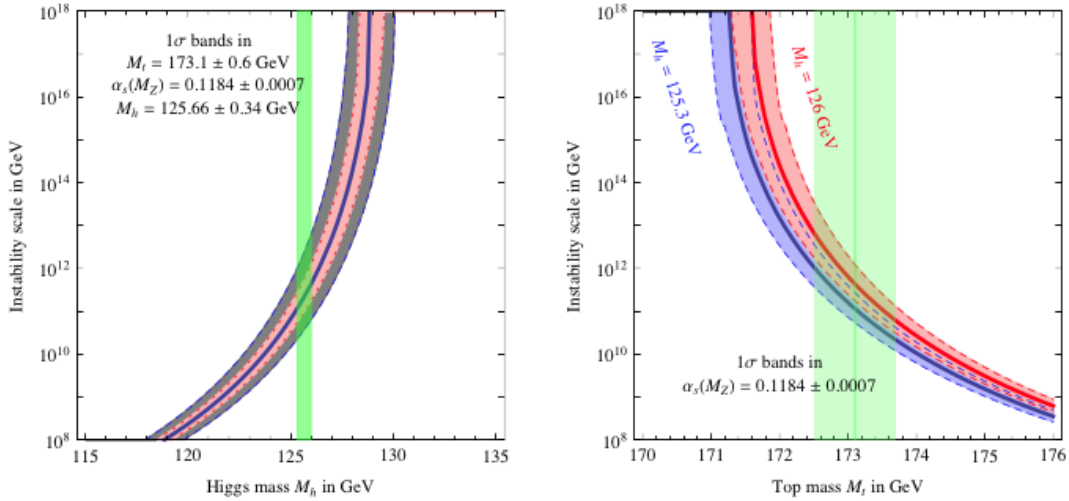


Figure 1.2: The instability scale  $\Lambda_I$  at which the SM potential becomes negative as a function of the Higgs mass (left) and of the top mass (right). The theoretical error is not shown and corresponds to a  $\pm 1$  GeV uncertainty in  $m_h$ . Figures taken from Ref. [2].

The existence of additional scalar degrees of freedom in an extended Higgs sector provides an opportunity to cure the vacuum metastability problem of the SM Higgs boson. However, by demanding no Landau poles and requiring a stable scalar potential at all energy scales up to the Planck scale, one imposes strong constraints on the parameter space of the extended Higgs sector. Investigations

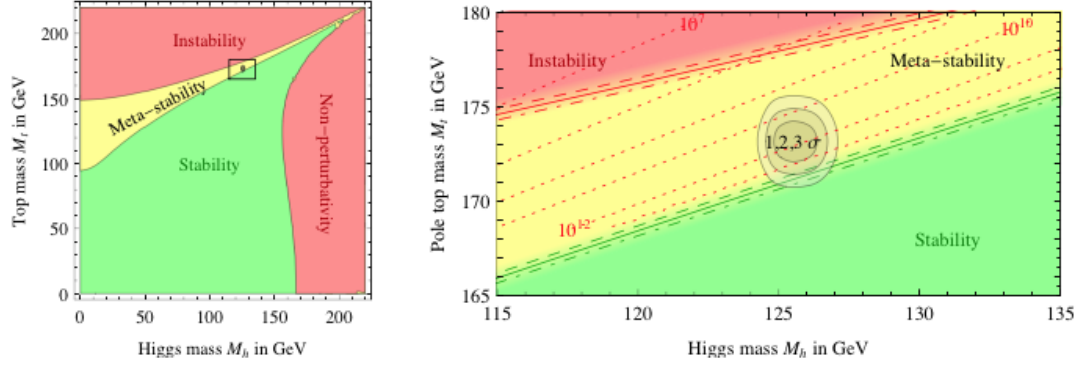


Figure 1.3: Left panel: Regions of absolute stability, meta-stability and instability of the SM vacuum in the  $m_t - m_h$  plane. Right panel: Zoom in the region of the preferred experimental range of  $m_h$  and  $m_t$  (the gray areas denote the allowed region at 1, 2, and  $3\sigma$ ). The three boundary lines correspond to  $\alpha_s(m_Z) = 0.1184 \pm 0.0007$ , and the grading of the colors indicates the size of the theoretical error. The dotted contour-lines show the instability scale  $\Lambda$  in GeV assuming  $\alpha_s(m_Z) = 0.1184$ . Figures taken from Ref. [2].

of this type have been performed in extended Higgs sectors that add additional singlet scalar fields [15, 16, 17, 18, 19] and in various constrained 2HDMs. Examples of the latter [20, 21, 22, 23, 24] invoke a  $\mathbb{Z}_2$  discrete symmetry to simplify the 2HDM scalar potential. In Ref. [25] this latter assumption was relaxed (while imposing CP conservation) and the Higgs-fermion Yukawa couplings, apart from the Higgs couplings to the top quark, were neglected.

## 1.2 Beyond the Standard Model

Despite the successes of the Standard Model, there exist many motivations for BSM physics. For one, the SM cannot account for dark matter or dark energy. There is also insufficient sources of CP-violation in the SM to adequately explain the electro baryogenesis. The hierarchy problem asks why weak scale is so much smaller than the Planck scale? The bare mass parameter of the Higgs boson is subject to radiative corrections that are quadratically sensitive to the scale of new physics, which naively should correspond to  $M_{PL}$ . The Planck scale, however would correspond to fine-tuning at 1 part in  $10^{34}$ , suggesting that SM by itself suffers when considering the notion of *naturalness*. Theories such as supersymmetry and those postulating extra dimensions have been invented to solve the hierarchy problem, though no evidence of such theories has yet been observed. It could be possible that our universe is part of a multiverse, and the

parameters of our universe are randomly determined.

Borrowing motivation from the fact that fermions come in three generations for no obvious reason, we have to be prepared for the possibility that the scalar sector exhibits similar multiplicity. While an extended Higgs sector need not necessarily solve any of the aforementioned issues of the SM, it is possible that an extended Higgs sector (such as the 2HDM) is a low-energy effective theory for a more complete theory at higher energies.

### 1.2.1 Constraints on non-minimal Higgs sectors

In BSM models with non-minimal Higgs sectors, there exist two key constraints that must be satisfied. The first is due to the experimental fact that  $\rho = m_W^2/m_Z^2 \cos^2 \theta_W$  is approximately one. The *custodial* symmetry  $SU(2)_V$  responsible for the tree-level relationship between the  $W$  and  $Z$  masses, is the diagonal vector subgroup of  $SU(2)_L \times SU(2)_R$ , which in the SM is an accidental symmetry of the scalar potential (eq. 1.2). The  $\rho$  parameter would be exactly unity if this symmetry were exact, but the  $U(1)_Y$  hypercharge gauge interactions and the Higgs-fermion Yukawa couplings break the custodial symmetry, leading to finite one-loop radiative corrections to the  $\rho$  parameter. It should be noted that the SM with any number of singlets and doublets would also exhibit a custodial symmetry, hence providing  $\rho \approx 1$  at tree-level. In general,

$$\rho = \frac{\sum_{T,Y} [4T(T+1) - Y^2] |V_{T,Y}|^2 c_{T,Y}}{\sum_{T,Y} 2Y^2 |V_{T,Y}|^2}, \quad (1.47)$$

where  $V_{T,Y} = \langle \phi(T, Y) \rangle$  is the vevs of the neutral fields,  $T$  and  $Y$  describe the  $SU(2)_L$  isospin and hypercharge of the Higgs representation, respectively, and  $c_{T,Y} = 1, c_{T,0} = 1/2$  for  $T, Y$  in the complex and real representations, respectively (Ref. [26]).

In the modified minimal subtraction  $\overline{\text{MS}}$  scheme (denoted by the caret), we can define the  $\hat{\rho}$  parameter, assuming the validity of the SM, as

$$\hat{\rho} \equiv \frac{m_W^2}{m_Z^2 \hat{c}_Z^2}, \quad (1.48)$$

where  $\hat{c}_Z \equiv \cos \hat{\theta}_W(m_Z)$ , and is less sensitive than  $\cos \theta_W$  to  $m_t$  and most types of new physics. We can define the  $\rho_0$  parameter to describe new sources of  $SU(2)$  breaking that cannot be accounted for by the top quark or the SM Higgs,

$$\rho_0 = \frac{m_W^2}{m_Z^2 \hat{c}_Z^2 \hat{\rho}} = 1.00040 \pm 0.00024, \quad (1.49)$$

which is  $1.7\sigma$  above the SM expected value of  $\rho_0 = 1$ , after simultaneously fitting  $\rho_0, m_h, m_t$ , and  $\alpha_s$  to the data.

The dominant radiative corrections due to new physics appears through vacuum-polarization amplitudes. These correction are described by the oblique ‘‘Peskin-Takeuchi’’ parameters  $S, T$ , and  $U$ , introduced in Refs. [27, 28], though here we

follow the more recent description of the oblique parameters described in Ref. [29], in which they receive contributions only from new physics and not loop contributions from  $m_t$  or  $m_h$ :

$$S \equiv \frac{4\widehat{s}_Z^2 \widehat{c}_Z^2}{\widehat{\alpha}(m_Z)} \left[ \frac{\Pi_{ZZ}^{\text{new}}(m_Z^2) - \Pi_{ZZ}^{\text{new}}(0)}{m_Z^2} - \frac{\widehat{c}_Z^2 - \widehat{s}_Z^2}{\widehat{c}_Z \widehat{s}_Z} \frac{\Pi_{Z\gamma}^{\text{new}}(m_Z^2)}{m_Z^2} - \frac{\Pi_{\gamma\gamma}^{\text{new}}(m_Z^2)}{m_Z^2} \right], \quad (1.50)$$

$$T \equiv \frac{1}{\widehat{\alpha}(m_Z)} \left[ \frac{\Pi_{WW}^{\text{new}}(0)}{m_W^2} - \frac{\Pi_{ZZ}^{\text{new}}(0)}{m_Z^2} \right], \quad (1.51)$$

$$S + U \equiv \frac{4\widehat{s}_Z^2}{\widehat{\alpha}(m_Z)} \left[ \frac{\Pi_{WW}^{\text{new}}(m_W^2) - \Pi_{WW}^{\text{new}}(0)}{m_W^2} - \frac{\widehat{c}_Z}{\widehat{s}_Z} \frac{\Pi_{Z\gamma}^{\text{new}}(m_Z^2)}{m_Z^2} - \frac{\Pi_{\gamma\gamma}^{\text{new}}(m_Z^2)}{m_Z^2} \right], \quad (1.52)$$

$$(1.53)$$

and have been experimentally determined:

$$S = -0.03 \pm 0.10, \quad (1.54)$$

$$T = 0.01 \pm 0.12, \quad (1.55)$$

$$U = 0.05 \pm 0.10, \quad (1.56)$$

Fixing  $U = 0$  (as is the case in many BSM models),

$$S = 0.00 \pm 0.08, \tag{1.57}$$

$$T = 0.05 \pm 0.07, \tag{1.58}$$

$$\tag{1.59}$$

both cases of which are in good agreement with the SM.

The second key constraint stems from the possibility of FCNCs introduced by additional sources of Higgs-fermion couplings. FCNCs are absent in the SM at tree-level, but are generated through quantum loop corrections. These corrections, however, are highly suppressed by the Glashow-Iliopoulos-Maiani (GIM) mechanism (Ref. [30]). Experimentally, FCNC processes are highly constrained, and any BSM model must have a mechanism in place to control FCNC processes.

In the most general 2HDM, for example, the Yukawa Lagrangian includes two sets of Yukawa matrices that cannot be simultaneously diagonalized. One set of diagonalized Yukawa matrices can be associated with the quark mass matrices, but the other set of Yukawa matrices are arbitrary, complex  $3 \times 3$  matrices that provide source of FCNCs at tree-level, requiring a mechanism to constrain the FCNCs to be a phenomenologically viable model. Perhaps the most popular approach in the literature, *natural flavor conservation* (NFC), was introduced by Glashow, Weinberg, and Paschos (Refs. [31, 32]), in which discrete symmetries between the two scalar doublets could be implemented so that FCNCs are eliminated at tree-

level by requiring at most, one scalar multiplet is responsible for providing masses for quarks or leptons. The cost of implementing NFC, however, is that the scalar potential becomes explicitly CP-conserving. In this thesis, we invoke the more general flavor-alignment ansatz proposed in Ref. [33], which we review in section 2.3.

Another popular approach to constrain FCNCs in extended Higgs sectors is to invoke *minimal flavor violation* (MFV), introduced in Ref. [34] as a framework for BSM models to extend the SM with small flavor-changing perturbations that obey experimental constraints. MFV essentially requires that all flavor and CP-violating interactions are linked to the known structure of Yukawa couplings. The MFV hypothesis can be consistently defined independently of the structure of the new-physics model. In the context of MFV, it is possible to relate various FCNC processes, as MFV implies that all flavor-changing effective operators are proportional to the same non-diagonal structure.

# Chapter 2

## Two-Higgs Doublet Model

The Two-Higgs Doublet Model (2HDM) is amongst the simplest of extensions to the SM Higgs sector, and postulates the existence of a second heavier scalar doublet. This results in a richer Higgs spectrum consisting of three neutral Higgs bosons, one of which resembles the SM Higgs, and two charged Higgs bosons. Many BSM models, including supersymmetric models, incorporate a 2HDM for their Higgs sector, though a 2HDM makes sense by itself. In fact, a general 2HDM has many benefits such as the possibility of CP-violation in the scalar and Yukawa sectors, that are not present in models such as supersymmetry.

One of the distinguishing features of the most general 2HDM is the fact that the two scalar doublet, hypercharge-one fields are indistinguishable. One is always free to define new linear combinations of the scalar doublets that preserves the

form of the kinetic energy terms of the Lagrangian. A specific choice for the scalar fields is called a *basis*, and any physical prediction of the theory must be *basis independent*. In this thesis, we employ a basis-independent formalism introduced in Ref. [12]. We consider the most general 2HDM scalar potential (which is potentially CP-violating) and the most general Yukawa sector, which introduces three additional independent  $3 \times 3$  matrix Yukawa couplings. Without additional assumptions, the latter yields Higgs-mediated tree-level FCNCs, in conflict with observed data. In order to circumvent this, we impose an “alignment ansatz”, introduced in Ref. [33], which postulates that the independent Yukawa coupling matrices are proportional to the corresponding quark and charged lepton mass matrices. In this case one finds that, in the mass basis for the quarks and leptons, the matrix Yukawa couplings are flavor diagonal, and the Higgs-mediated tree-level FCNCs are absent. One way to achieve flavor-alignment in the Yukawa sector is to introduce a set of discrete symmetries which constrain the Higgs scalar potential and Yukawa couplings. The so-called Type-I and II 2HDMs [35], and the related Type X and Type Y 2HDMs [36, 37] provide examples of this type. Indeed, Ref. [38] showed that the flavor-alignment is preserved under RGE running if and only if such discrete symmetries are present. The flavor-alignment ansatz is more general, but requires fine-tuning in the absence of an underlying symmetry.

## 2.1 Basis-Independent Formalism

In a generic basis, the most general renormalizable  $SU(3)_C \times SU(2)_L \times U(1)_Y$  gauge-invariant 2HDM scalar potential is given by

$$\begin{aligned} \mathcal{V} = & m_{11}^2 (\Phi_1^\dagger \Phi_1) + m_{22}^2 (\Phi_2^\dagger \Phi_2) - [m_{12}^2 \Phi_1^\dagger \Phi_2 + \text{h.c.}] \\ & + \frac{1}{2} \lambda_1 (\Phi_1^\dagger \Phi_1)^2 + \frac{1}{2} \lambda_2 (\Phi_2^\dagger \Phi_2)^2 + \lambda_3 (\Phi_1^\dagger \Phi_1) (\Phi_2^\dagger \Phi_2) + \lambda_4 (\Phi_1^\dagger \Phi_2) (\Phi_2^\dagger \Phi_1) \\ & + \left\{ \frac{1}{2} \lambda_5 (\Phi_1^\dagger \Phi_2)^2 + [\lambda_6 (\Phi_1^\dagger \Phi_1) + \lambda_7 (\Phi_2^\dagger \Phi_2)] (\Phi_1^\dagger \Phi_2) + \text{h.c.} \right\}, \end{aligned} \quad (2.1)$$

where  $\Phi_1, \Phi_2$  are two hypercharge-one complex scalar doublets. The two doublets separately acquire vacuum expectation values (vevs)  $\langle \Phi_1^0 \rangle = v_1/\sqrt{2}$  and  $\langle \Phi_2^0 \rangle = v_2/\sqrt{2}$  with the constraint  $v^2 = |v_1|^2 + |v_2|^2 \simeq (246 \text{ GeV})^2$ . The parameters  $\lambda_{1,2,3,4}$  and  $m_{11}^2, m_{22}^2$  are real whereas  $\lambda_{5,6,7}$  and  $m_{12}^2$  are potentially complex. The 2HDM is CP-conserving if there exists a basis in which all of the parameters and the vacuum expectation values are simultaneously real.

We shall adopt a basis-independent formalism as developed in Ref. [12], which provides basis-independent 2HDM potential parameters that are invariant under a global  $U(2)$  transformation of the two scalar doublet fields,  $\Phi_a \rightarrow U_{a\bar{b}} \Phi_b$  ( $a, \bar{b} = 1, 2$ ).

It is convenient to define the so-called *Higgs basis* of scalar doublet fields,

$$H_1 = \begin{pmatrix} H_1^+ \\ H_1^0 \end{pmatrix} \equiv \frac{v_1^* \Phi_1 + v_2^* \Phi_2}{v}, \quad H_2 = \begin{pmatrix} H_2^+ \\ H_2^0 \end{pmatrix} \equiv \frac{-v_2 \Phi_1 + v_1 \Phi_2}{v}, \quad (2.2)$$

so that  $\langle H_1^0 \rangle = v/\sqrt{2}$  and  $\langle H_2^0 \rangle = 0$ . The Higgs basis is uniquely defined up to a rephasing of the  $H_2$  field,  $H_2 \rightarrow e^{i\chi} H_2$ . In the Higgs basis, the scalar potential takes the familiar form,<sup>1</sup>

$$\begin{aligned} \mathcal{V} = & Y_1(H_1^\dagger H_1) + Y_2(H_2^\dagger H_2) + [Y_3 H_1^\dagger H_2 + \text{h.c.}] + \frac{1}{2} Z_1 (H_1^\dagger H_1)^2 + \frac{1}{2} Z_2 (H_2^\dagger H_2)^2 \\ & + Z_3 (H_1^\dagger H_1) (H_2^\dagger H_2) + Z_4 (H_1^\dagger H_2) (H_2^\dagger H_1) + \left\{ \frac{1}{2} Z_5 (H_1^\dagger H_2)^2 + [Z_6 (H_1^\dagger H_1) \right. \\ & \left. + Z_7 (H_2^\dagger H_2)] (H_1^\dagger H_2) + \text{h.c.} \right\}, \end{aligned} \quad (2.3)$$

where  $Y_1, Y_2$ , and  $Z_{1,2,3,4}$  are real parameters and uniquely defined, whereas  $Y_3$  and  $Z_{5,6,7}$  transform under a rephasing of  $H_2$ , viz.,  $[Y_3, Z_6, Z_7] \rightarrow e^{-i\chi} [Y_3, Z_6, Z_7]$  and  $Z_5 \rightarrow e^{-2i\chi} Z_5$ . Minimizing the scalar potential then yields

$$Y_1 = -\frac{1}{2} Z_1 v^2, \quad Y_3 = -\frac{1}{2} Z_6 v^2. \quad (2.4)$$

The scalar potential is CP-violating if no choice of  $\chi$  can be found in which all Higgs basis scalar potential parameters are simultaneously real.

---

<sup>1</sup>As discussed in Appendix A, the squared-mass and coupling coefficients,  $Y_1, Y_2$ , and  $Z_{1,2,3,4}$  can be expressed as U(2)-invariant combinations of the scalar potential coefficients and the vevs, whereas  $Y_3$  and  $Z_{5,6,7}$  are U(2)-pseudoinvariant combinations of the scalar potential coefficients and the vevs that are rephased under a U(2) transformation [12].

### 2.1.1 Higgs mass eigenstates

The tree-level mass eigenstates of the neutral scalars can be obtained by diagonalizing the neutral scalar squared-mass matrix in the Higgs basis [39, 40],

$$\mathcal{M} = v^2 \begin{pmatrix} Z_1 & \text{Re}(Z_6) & -\text{Im}(Z_6) \\ \text{Re}(Z_6) & \frac{1}{2}[Z_3 + Z_4 + \text{Re}(Z_5)] + Y_2/v^2 & -\frac{1}{2}\text{Im}(Z_5) \\ -\text{Im}(Z_6) & -\frac{1}{2}\text{Im}(Z_5) & \frac{1}{2}[Z_3 + Z_4 - \text{Re}(Z_5)] + Y_2/v^2 \end{pmatrix}. \quad (2.5)$$

The diagonalizing matrix is a real orthogonal  $3 \times 3$  matrix that is parameterized by three mixing angles  $\theta_{12}$ ,  $\theta_{13}$ , and  $\theta_{23}$  (details can be found in Ref. [40]). In terms of U(2)-invariant combinations of the mixing angles and scalar potential parameters, the squared-masses of the three neutral Higgs bosons, denoted by  $h_1$ ,  $h_2$  and  $h_3$  respectively, are given by [40],

$$m_k^2 = |q_{k2}|^2 Y_2 + v^2 \left\{ q_{k1}^2 Z_1 + \frac{1}{2}|q_{k2}|^2 [Z_3 + Z_4 - \text{Re}(Z_5 e^{-2i\theta_{23}})] \right. \\ \left. + \text{Re}(q_{k2})\text{Re}(q_{k2} Z_5 e^{-2i\theta_{23}}) + 2q_{k1}\text{Re}(q_{k2} Z_6 e^{-i\theta_{23}}) \right\}, \quad \text{for } k = 1, 2, 3, \quad (2.6)$$

where the  $q_{ki}$  are invariant combinations of the mixing angles shown in Table 2.1. It is convenient to choose a convention where  $m_1 < m_2 < m_3$  (which can always be arranged by an appropriate choice of neutral Higgs mixing angles). The squared-mass of the charged scalars is given by

$$m_{H^\pm}^2 = Y_2 + \frac{1}{2}Z_3 v^2. \quad (2.7)$$

Table 2.1:  $q_{ki}$  as a function of the neutral Higgs mixing angles in the Higgs basis.

$k$	$q_{k1}$	$q_{k2}$
1	$\cos \theta_{12} \cos \theta_{13}$	$-\sin \theta_{12} - i \cos \theta_{12} \sin \theta_{13}$
2	$\sin \theta_{12} \cos \theta_{13}$	$\cos \theta_{12} - i \sin \theta_{12} \sin \theta_{13}$
3	$\sin \theta_{13}$	$i \cos \theta_{13}$

### 2.1.2 Decoupling limit

The decoupling limit corresponds to taking the squared-mass parameter of the Higgs basis field  $H_2$  large while holding the Higgs quartic coupling parameters fixed. The advantage of invoking the decoupling limit is to create an effective one-doublet model (i.e. a SM-like Higgs boson) and a set of heavier Higgs bosons roughly degenerate in mass. In the perturbative regime, we take  $|Z_i| \lesssim \mathcal{O}(1)$  and  $Y_2 \gg v^2$ . In this case [40, 41],

$$\sin \theta_{12} \sim \sin \theta_{13} \sim \mathcal{O}\left(\frac{v^2}{Y_2}\right). \quad (2.8)$$

In addition, the decoupling limit requires that

$$\text{Im}(Z_5 e^{-2i\theta_{23}}) \sim \mathcal{O}\left(\frac{v^2}{Y_2}\right), \quad (2.9)$$

which implies that

$$\text{Re}(Z_5 e^{-2i\theta_{23}}) = -|Z_5|. \quad (2.10)$$

The overall sign in eq. (2.10) [which is not determined by eq. (2.9)] is fixed in the convention where  $m_2 < m_3$ . Using the above results in eq. (2.6) yields

$$m_1^2 = Z_1 v^2 \left[ 1 + \mathcal{O}\left(\frac{v^2}{Y_2}\right) \right], \quad (2.11)$$

$$m_2^2 = Y_2 + \frac{1}{2} v^2 \left[ Z_3 + Z_4 - |Z_5| + \mathcal{O}\left(\frac{v^2}{Y_2}\right) \right], \quad (2.12)$$

$$m_3^2 = Y_2 + \frac{1}{2} v^2 \left[ Z_3 + Z_4 + |Z_5| + \mathcal{O}\left(\frac{v^2}{Y_2}\right) \right]. \quad (2.13)$$

At energy scales below  $Y_2$ , the effective low-energy theory corresponds to the Standard Model with one Higgs doublet. Consequently, in the decoupling limit the properties of  $h_1$  approach those of the SM Higgs boson. The non-minimal Higgs states are roughly degenerate in mass,  $m_2^2 \sim m_3^2 \sim m_{H^\pm}^2 \sim Y_2$ , with squared-mass splittings of  $\mathcal{O}(v^2)$ ,

$$m_3^2 - m_2^2 \simeq |Z_5| v^2, \quad (2.14)$$

$$m_3^2 - m_{H^\pm}^2 \simeq \frac{1}{2} (Z_4 + |Z_5|) v^2. \quad (2.15)$$

In the decoupling limit of a general 2HDM, the tree-level CP-violating and flavor-changing neutral Higgs couplings of the SM-like Higgs state  $h_1$  are suppressed by factors of  $\mathcal{O}(v^2/Y_2^2)$ . The corresponding interactions of the heavy neutral Higgs bosons ( $h_2$  and  $h_3$ ) and the charged Higgs bosons ( $H^\pm$ ) can exhibit both CP-violating and flavor non-diagonal couplings. If  $Y_2$  is sufficiently large, then FCNCs mediated by the lightest neutral scalar can be small enough to be consistent with experimental data. However, for values of  $Y_2$  of order 1 TeV and

below, tree-level Higgs-mediated FCNCs are problematical in the case of a generic Yukawa sector.

## 2.2 Bounded from below conditions for a general 2HDM potential

To ensure the existence of a stable electroweak vacuum, the 2HDM scalar potential must be bounded from below, *i.e.* it must assume positive values for any direction for which the fields are tending to infinity. If it ceases to be bound from below, then new sources of physics must arise at an intermediate energy scale to save the theory. This requirement places some restrictions on the allowed values of the quartic Higgs couplings. For the case of the scalar potential given in eq. (2.1) with  $\lambda_6 = \lambda_7 = 0$ , those necessary and sufficient conditions are given in eqs. (3.1)–(3.4).

We now review the analogous conditions for the most general renormalizable 2HDM potential, found in Refs. [42, 43]. It is particularly convenient to introduce a new notation for the scalar potential, based on gauge invariant field bilinears. Indeed in many 2HDM studies, such as the comparison of the value of the potential in different vacua, the classification of scalar symmetries and stability conditions, the bilinear formalism provides a significant simplification in the calculations. This

formalism also reveals a hidden Minkowski structure in the potential, which was established in Refs. [42, 43]. A similar Minkowskian notation has been employed in Refs. [44, 45, 46, 47, 48].

There are four independent gauge-invariant field bilinears, which are defined by

$$\begin{aligned}
r_0 &= \Phi_1^\dagger \Phi_1 + \Phi_2^\dagger \Phi_2, \\
r_1 &= -\left(\Phi_1^\dagger \Phi_2 + \Phi_2^\dagger \Phi_1\right) = -2 \operatorname{Re}\left(\Phi_1^\dagger \Phi_2\right), \\
r_2 &= i\left(\Phi_1^\dagger \Phi_2 - \Phi_2^\dagger \Phi_1\right) = -2 \operatorname{Im}\left(\Phi_1^\dagger \Phi_2\right), \\
r_3 &= -\left(\Phi_1^\dagger \Phi_1 - \Phi_2^\dagger \Phi_2\right).
\end{aligned} \tag{2.16}$$

These four quantities form the components of a covariant four-vector,  $r_\mu = (r_0, \vec{r})$  with respect to  $\text{SO}(3,1)$  transformations. We also define  $r^\mu = g^{\mu\nu} r_\nu = (r_0, -\vec{r})$  where  $g^{\mu\nu}$  is the usual Minkowski metric. It is straightforward to verify that  $r_0 \geq 0$  and  $r^\mu r_\mu \geq 0$ , the latter being a consequence of the Schwarz inequality. That is, the four-vector  $r_\mu$  lives on or inside the forward lightcone  $LC^+$ . The vacuum that preserves  $\text{SU}(2) \times \text{U}(1)$  electroweak symmetry [i.e.,  $\langle \Phi_1 \rangle = \langle \Phi_2 \rangle = 0$ ] corresponds to the apex of  $LC^+$ ; all neutral vacua correspond to the surface of  $LC^+$ , and any charge breaking vacua would lie on the interior of  $LC^+$ . Transformations of the scalar fields that preserve the scalar field kinetic energy terms leave  $r_0$  invariant and correspond to  $\text{SO}(3)$  rotations of the three-vectors,  $\vec{r}$ .

In terms of the bilinears defined in eq. (2.16), the scalar potential can be

written as

$$\mathcal{V} = -M_\mu r^\mu + \frac{1}{2} r^\mu \Lambda_\mu{}^\nu r_\nu, \quad (2.17)$$

with the 4-vector  $M_\mu$  and the mixed tensor  $\Lambda_\mu{}^\nu$  given by

$$M_\mu = \left( -\frac{1}{2}(Y_1 + Y_2), \quad \text{Re } Y_3, \quad -\text{Im } Y_3, \quad -\frac{1}{2}(Y_1 - Y_2) \right) \quad (2.18)$$

and

$$\Lambda_\mu{}^\nu = \frac{1}{2} \begin{pmatrix} \frac{1}{2}(Z_1 + Z_2) + Z_3 & -\text{Re}(Z_6 + Z_7) & \text{Im}(Z_6 + Z_7) & -\frac{1}{2}(Z_1 - Z_2) \\ \text{Re}(Z_6 + Z_7) & -Z_4 - \text{Re } Z_5 & \text{Im } Z_5 & -\text{Re}(Z_6 - Z_7) \\ -\text{Im}(Z_6 + Z_7) & \text{Im } Z_5 & -Z_4 + \text{Re } Z_5 & \text{Im}(Z_6 - Z_7) \\ \frac{1}{2}(Z_1 - Z_2) & -\text{Re}(Z_6 - Z_7) & \text{Im}(Z_6 - Z_7) & -\frac{1}{2}(Z_1 + Z_2) + Z_3 \end{pmatrix}. \quad (2.19)$$

To ensure that the scalar potential is bounded from below one needs to evaluate the eigenvalues and eigenvectors of the matrix  $\Lambda_\mu{}^\nu$ . Then one can determine conditions on the eigenvalues and eigenvectors such that  $r^\mu \Lambda_\mu{}^\nu r_\nu \geq 0$ . The eigenvalues  $\Lambda_a$  ( $a = 0, 1, 2, 3$ ) of the matrix  $\Lambda$  will be determined by the usual characteristic equation,

$$\det(\Lambda_\mu{}^\nu - \Lambda_a g_\mu{}^\nu) = 0. \quad (2.20)$$

since  $g_\mu{}^\nu = \delta_\mu^\nu$  is just the  $4 \times 4$  identity matrix. The corresponding eigenvectors corresponding to eigenvalue  $\Lambda_a$  will be denoted by  $V^{(a)}$ . For the most general 2HDM potential, the eigenvalues are the solutions of a quartic equation, which can in

principle be determined analytically (although the corresponding expressions are not particularly transparent). However, it is straightforward to numerically evaluate the eigenvalues and corresponding eigenvectors. Note that in general, some of the eigenvalues may be complex (since the real matrix  $\Lambda_\mu{}^\nu$  is not symmetric unless  $Z_6 = Z_7 = 0$  and  $Z_1 = Z_2$ ).

Having evaluated the eigenvalues and eigenvectors of  $\Lambda_\mu{}^\nu$ , we make use of *Proposition 10* of Ref. [42] to conclude that the 2HDM potential is bounded from below *if and only if* the following conditions are met:

1. All the eigenvalues  $\Lambda_a$  are real.
2.  $\Lambda_0 > 0$ .
3.  $\Lambda_0 > \{\Lambda_1, \Lambda_2, \Lambda_3\}$ . There may or may not be degeneracies among the three eigenvalues  $\Lambda_i$  ( $i = 1, 2, 3$ ).
4. There exist four linearly independent eigenvectors  $V^{(a)}$  corresponding to the four eigenvalues  $\Lambda_a$ , for  $a = 0, 1, 2, 3$ .
5. The eigenvector  $V^{(0)} = (v_{00}, v_{10}, v_{20}, v_{30})$ , corresponding to the eigenvalue  $\Lambda_0$ , is real and time-like. That is, it can be normalized so that

$$|V^{(0)}|^2 = v_{00}^2 - v_{10}^2 - v_{20}^2 - v_{30}^2 = 1.$$

6. The remaining three eigenvectors  $V^{(i)} = (v_{0i}, v_{1i}, v_{2i}, v_{3i})$  are real and space-

like, *i.e.* normalized so that

$$|V^{(i)}|^2 = v_{0i}^2 - v_{1i}^2 - v_{2i}^2 - v_{3i}^2 = -1.$$

To illustrate this technique, we shall reproduce the bounded from below conditions for a potential with a  $\mathbb{Z}_2$  symmetry in the Higgs basis so that  $Z_6 = Z_7 = 0$ . Without loss of generality, we can choose  $Z_5$  real by rephasing the Higgs basis field  $H_2$ . The matrix  $\Lambda = \Lambda_\mu{}^\nu$  is then given by

$$\Lambda = \frac{1}{2} \begin{pmatrix} \frac{1}{2}(Z_1 + Z_2) + Z_3 & 0 & 0 & -\frac{1}{2}(Z_1 - Z_2) \\ 0 & -Z_4 - Z_5 & 0 & 0 \\ 0 & 0 & -Z_4 + Z_5 & 0 \\ \frac{1}{2}(Z_1 - Z_2) & 0 & 0 & -\frac{1}{2}(Z_1 + Z_2) + Z_3 \end{pmatrix}, \quad (2.21)$$

so that two of its eigenvalues can be immediately read off as  $\Lambda_1 = -Z_4 - Z_5$  and  $\Lambda_2 = -Z_4 + Z_5$ . The remaining two eigenvalues are

$$\Lambda_\pm = Z_3 \pm \sqrt{Z_1 Z_2}. \quad (2.22)$$

Since the eigenvalues must be real, it follows that

$$Z_1 Z_2 > 0. \quad (2.23)$$

$\Lambda_+$  is the largest eigenvalue and thus must correspond to the time-like eigenvector.

Hence, we identify  $\Lambda_0 = Z_3 + \sqrt{Z_1 Z_2}$  and  $\Lambda_3 = Z_3 - \sqrt{Z_1 Z_2}$ . Imposing the

requirement that the scalar potential is bounded from below, it follows that the eigenvalues obtained above must all be real and obey the following inequalities:

$$\Lambda_0 > 0 \Rightarrow Z_3 > -\sqrt{Z_1 Z_2} \quad (2.24)$$

$$\Lambda_0 > \{\Lambda_1, \Lambda_2, \Lambda_3\} \Rightarrow Z_3 + Z_4 - |Z_5| > -\sqrt{Z_1 Z_2}, \quad (2.25)$$

which are the Higgs basis equivalents of eqs. (3.3) and (3.4). The time-like eigenvector is  $V^{(0)} = (x, 0, 0, y)$ , where the components  $x$  and  $y$  are related via the eigenvector equation by

$$y = \frac{Z_1 + Z_2 - \sqrt{Z_1 Z_2}}{Z_1 - Z_2} x. \quad (2.26)$$

Since the time-like normalization condition implies that  $x^2 - y^2 = 1$ , we obtain

$$x^2 = \frac{(Z_1 - Z_2)^2}{4\sqrt{Z_1 Z_2}(Z_1 + Z_2)}. \quad (2.27)$$

Thus we see that we must have  $Z_1 + Z_2 > 0$ , which when combined with eq. (2.23) yields

$$Z_1 > 0 \quad , \quad Z_2 > 0. \quad (2.28)$$

Thus we recover the Higgs basis equivalents of eqs. (3.1) and (3.2).

## 2.3 Yukawa sector and flavor-alignment

The most general 2HDM Yukawa sector, describing Higgs-fermion interactions, includes six Yukawa matrices (as compared to three in the SM). In a generic basis,

the Yukawa Lagrangian for the Higgs–quark interactions is given by eq. (A.1). Following the discussion of Appendix A, we can re-express the Yukawa Lagrangian in terms of the quark mass-eigenstate fields [49],

$$\begin{aligned}
-\mathcal{L}_Y &= \bar{U}_L(\eta_1^U \Phi_1^{0*} + \eta_2^U \Phi_2^{0*}) - \bar{D}_L K^\dagger(\eta_1^U \Phi_1^- + \eta_2^U \Phi_2^-)U^R \\
&+ \bar{U}_L K(\eta_1^{D\dagger} \Phi_1^+ + \eta_2^{D\dagger} \Phi_2^+)D^R + \bar{D}_L(\eta_1^{D\dagger} \Phi_1^0 + \eta_2^{D\dagger} \Phi_2^0)D^R + \text{h.c.}, \quad (2.29)
\end{aligned}$$

where  $\eta_{1,2}^{U,D}$  are  $3 \times 3$  Yukawa coupling matrices and  $K$  is the CKM matrix.

Using eq. (2.2), one can rewrite eq. (2.29) in terms of the Higgs basis scalar doublet fields,

$$\begin{aligned}
-\mathcal{L}_Y &= \bar{U}_L(\kappa^U H_1^{0\dagger} + \rho^U H_2^{0\dagger})U^R - \bar{D}_L K^\dagger(\kappa^U H_1^- + \rho^U H_2^-)U^R \\
&+ \bar{U}_L K(\kappa^{D\dagger} H_1^+ + \rho^{D\dagger} H_2^+)D^R + \bar{D}_L(\kappa^{D\dagger} H_1^0 + \rho^{D\dagger} H_2^0)D^R + \text{h.c.}, \quad (2.30)
\end{aligned}$$

where<sup>2</sup>

$$\kappa^Q \equiv \frac{v_1^* \eta_1^Q + v_2^* \eta_2^Q}{v}, \quad \rho^Q \equiv \frac{-v_2 \eta_1^Q + v_1 \eta_2^Q}{v}. \quad (2.31)$$

Note that  $\rho^Q \rightarrow e^{-i\chi} \rho^Q$  with respect to the rephasing  $H_2 \rightarrow e^{i\chi} H_2$ . Since  $\langle H_1^0 \rangle = v/\sqrt{2}$  and  $\langle H_2^0 \rangle = 0$ , it follows that the  $\kappa^{U,D}$  are proportional to the diagonal quark mass matrices,  $M_U$  and  $M_D$ , whose matrix elements are real and non-negative,

$$M_U = \frac{v\kappa^U}{\sqrt{2}} = \text{diag}(m_u, m_c, m_t), \quad M_D = \frac{v\kappa^D}{\sqrt{2}} = \text{diag}(m_d, m_s, m_b). \quad (2.32)$$

---

<sup>2</sup>As noted in eq. (A.6), the  $\rho^Q$  are U(2)-pseudoinvariant combinations of the Yukawa coupling matrices and the vevs, whereas the  $\kappa^Q$  are U(2)-invariants.

The Yukawa couplings of the Higgs doublets to the leptons can be similarly treated by replacing  $U \rightarrow N$ ,  $D \rightarrow E$ ,  $M_U \rightarrow 0$ ,  $M_D \rightarrow M_E$  and  $K \rightarrow \mathbf{1}$ , where  $N = (\nu_e, \nu_\mu, \nu_\tau)$ ,  $E = (e, \mu, \tau)$  and  $M_E$  is the diagonal charged lepton mass matrix.

Since the Yukawa matrices  $\rho^{U,D,E}$  are independent complex  $3 \times 3$  matrices, it follows that the Yukawa Lagrangian exhibited in eq. (2.30) generically exhibits tree-level Higgs mediated FCNCs. The off-diagonal elements of the  $\rho^{U,D}$  matrices are highly constrained by experimental data to be very small. As first shown by Glashow, Weinberg and Paschos (GWP) [31, 32], it is possible to *naturally* eliminate tree-level Higgs mediated FCNCs if for some choice of basis of the scalar fields, at most one Higgs multiplet is responsible for providing mass for quarks or leptons of a given electric charge. In the 2HDM, the GWP condition can be imposed in four different ways by employing the appropriate  $\mathbb{Z}_2$  discrete symmetry [35, 36, 37, 50, 51]:

1. Type-I Yukawa couplings:  $\eta_1^U = \eta_1^D = \eta_1^L = 0$ ,
2. Type-II Yukawa couplings:  $\eta_1^U = \eta_2^D = \eta_2^L = 0$ .
3. Type-X Yukawa couplings:  $\eta_1^U = \eta_1^D = \eta_2^L = 0$ ,
4. Type-Y Yukawa couplings:  $\eta_1^U = \eta_2^D = \eta_1^L = 0$ .

For example, it follows from eq. (2.31) that in the Type-I 2HDM,

$$\rho^{U,D,L} = \frac{v_1}{v_2^*} \kappa^{U,D,L}, \quad (2.33)$$

and in the Type-II 2HDM,

$$\rho^U = \frac{v_1}{v_2^*} \kappa^U, \quad \rho^{D,L} = -\frac{v_2}{v_1^*} \kappa^{D,L}. \quad (2.34)$$

In light of eq. (2.32), the  $\rho^F$  ( $F = U, D, L$ ) are diagonal matrices in which case the neutral Higgs–fermion Yukawa interactions are flavor-diagonal at tree-level.

If only phenomenological considerations are invoked in choosing the Higgs–fermion Yukawa couplings, then it is possible to consider the more general case of the flavor-aligned 2HDM introduced in Ref. [33]. In this model applied to the Higgs basis, one imposes the following conditions

$$\rho^U = \alpha^U \kappa^U, \quad \rho^D = \alpha^D \kappa^D, \quad \text{and} \quad \rho^L = \alpha^L \kappa^L, \quad (2.35)$$

which generalize the Type-I and II results exhibited in eqs. (2.33) and (2.34). In eq. (2.35), the alignment parameters,  $\alpha^{U,D,L}$ , are arbitrary complex constants.<sup>3</sup> The flavor-alignment condition shown in eq. (2.35) is not imposed by any symmetry, and is strictly unnatural (i.e., it can be achieved only by a fine-tuning of the model parameters). Equivalently, as observed in Ref. [38], the flavor-alignment is preserved under RGE running only in the case of Type I, II, X and Y Yukawa couplings, which correspond to the conditions

---

<sup>3</sup>In practice, if the magnitude of the alignment constants are too large, then some of the Higgs–fermion Yukawa couplings will develop Landau poles below the Planck scale. In our analysis, we will determine the allowed regions of the flavor-aligned 2HDM parameter space where such Landau poles are absent.

$$\alpha^U = \alpha^{D^*} = \alpha^{L^*} \quad (\text{type-I}), \quad (2.36)$$

$$\alpha^U = -\frac{1}{\alpha^D} = -\frac{1}{\alpha^L} \quad (\text{type-II}), \quad (2.37)$$

$$\alpha^U = \alpha^{D^*} = -\frac{1}{\alpha^L} \quad (\text{type-X}), \quad (2.38)$$

$$\alpha^U = -\frac{1}{\alpha^D} = \alpha^{L^*} \quad (\text{type-Y}). \quad (2.39)$$

Nevertheless, one can imagine the possibility of new dynamics above the electroweak scale that could be responsible for an approximately flavor-aligned 2HDM. Thus, in our analysis we shall employ the more general eq. (2.35), which is sufficient for satisfying the phenomenological FCNC constraints.

# Chapter 3

## Renormalization Group Stability and Perturbativity Analysis

In this chapter, we examine the theoretical consistency of *the most general* 2HDM between the electroweak scale and the Planck scale, using the one-loop RGEs of the model to investigate the possible occurrence of Landau poles and instability of the scalar potential. We focus on the decoupling regime of the 2HDM where the 125 GeV Higgs boson is SM-like [41, 52], and assume Yukawa alignment in the flavor sector [33] to avoid Higgs-mediated tree-level FCNCs. Our aim is to exhibit the allowed regions of the 2HDM parameter space that are free from both Landau poles and vacuum instability below the Planck scale. In particular, a 2HDM that satisfies these constraints does not require further BSM physics to

stabilize the theory.

Let us assume that the observed SM-like Higgs boson (with  $m_h \simeq 125$  GeV) is part of a 2HDM in the decoupling limit with a flavor-aligned Yukawa sector, with no other new physics present beyond the 2HDM below the Planck scale.<sup>1</sup> We shall examine whether there are regions of the 2HDM parameter space that yield a consistent model under RG running from the electroweak to the Planck scale. In general, two potential problems can arise in the RG evolution. First, Landau poles could arise from the divergence of the 2HDM quartic scalar couplings and/or Yukawa couplings. Second, the 2HDM scalar potential could become unstable at a higher energy scale. The case of Landau poles is fairly straightforward, although the precise energy scale at which they arise cannot be strictly determined, since it lies outside the perturbative regime of the RGEs. In practice, we shall consider that a Landau pole occurs when the relevant coupling exceeds 100 for some energy scale  $\Lambda \leq M_{PL}$ . Indeed, once such a large coupling is reached, it will very quickly diverge at an energy scale very close to  $\Lambda$ . In our analysis, we employ the one-loop RGEs for the quartic scalar couplings of the 2HDM in the Higgs basis given in Appendix A. These equations are strongly coupled, and thus a divergence in one quartic scalar coupling will cause a divergence in the rest. The leading effects of two-loop running will be assessed at the end of this section.

---

<sup>1</sup>Incorporating light neutrino masses via the seesaw mechanism [53, 54, 55, 56, 57] with the mass scale of the right-handed neutrino sector assumed to be of order a typical grand unified scale has a very minor impact on the considerations in this paper.

In the SM, the requirement that the scalar potential is stable at all energy scales below the scale  $\Lambda$  is easily implemented. It is sufficient to require that the SM quartic scalar coupling is positive, i.e.  $\lambda_{\text{SM}}(\Lambda) > 0$  for  $\Lambda > v$ . Requiring that the 2HDM scalar potential is stable at all energy scales below the scale  $\Lambda$  leads to a more complicated set of conditions. In the 2HDM with an unbroken, or softly broken,  $\mathbb{Z}_2$  discrete symmetry that sets  $\lambda_6 = \lambda_7 = 0$  in eq. (2.1), the stability conditions were first obtained in Ref. [58],

$$\lambda_1 > 0, \tag{3.1}$$

$$\lambda_2 > 0, \tag{3.2}$$

$$\lambda_3 > -\sqrt{\lambda_1 \lambda_2}, \tag{3.3}$$

$$\lambda_3 + \lambda_4 - |\lambda_5| > -\sqrt{\lambda_1 \lambda_2}. \tag{3.4}$$

However, in the case of a completely general scalar potential, the corresponding stability conditions are far more complicated (with no simple analytic form). Ref. [42] provides an algorithm for deriving the stability conditions for a general 2HDM, with no symmetry or CP assumptions imposed on the 2HDM scalar potential. In terms of the Higgs basis parameters, this algorithm is summarized in Appendix 2.2. Except for special cases for the quartic scalar couplings, the corresponding stability conditions must be determined numerically.

We now describe in detail the procedure used in our analysis. We assume that we are in the decoupling regime of the 2HDM, where the mass scale of the heavy

Higgs sector is of  $\mathcal{O}(\Lambda_H)$ . In light of eqs. (2.7), (2.12) and (2.13), we henceforth set  $\Lambda_H^2 \equiv Y_2$ .

1. Start with the SM Higgs potential defined at the scale of the 125 GeV Higgs boson.
2. Use SM RG evolution to run the Higgs-self coupling parameter  $\lambda$  and the fermion mass matrices up to the scale  $\Lambda_H$ .<sup>2</sup>
3. Match the one-doublet Higgs potential with the 2HDM potential by taking  $Z_1 = \lambda(\Lambda_H)$  and  $\kappa^F = \sqrt{2}M_F(\Lambda_H)/v$  (for  $F = U, D$ ). This establishes the low energy boundary conditions. The effects of the lepton masses are negligible and have been ignored.
4. Scan over all other 2HDM quartic scalar coupling parameters  $Z_i$  and Yukawa alignment parameters  $\alpha^F$  ( $F = U, D$ ). The latter fix the values of the  $\rho^F(\Lambda_H)$ .
5. Run the 2HDM RGEs for the  $Z_i$ ,  $\kappa^F$  and  $\rho^F$  up to higher energies  $\Lambda$ . Check for stability of the potential at the scale  $\Lambda$  using the procedure summarized in Section 2.2.

---

<sup>2</sup>Starting the RG evolution at  $m_Z$ , we use a five flavor scheme to run up to  $m_t$  and a six flavor scheme above  $m_t$ . Running quark mass masses at  $m_Z$  and  $m_t$  are obtained from the RunDec Mathematica software package [59], based on quark masses provided in Ref. [29]. For simplicity, the effects of the lepton masses are ignored, as these contribute very little to the running of the  $Z_i$ .

6. Stop the running if a Landau pole is encountered or if the stability conditions cannot be satisfied.

For the scalar sector, we scanned over the parameter space using 100,000 points, with  $|Z_i| \lesssim \mathcal{O}(1)$ , for  $i = 2, \dots, 7$ , to enforce the decoupling limit. These points were also subject to the constraint that they obey the stability conditions presented in Appendix 2.2. Note that when  $|Z_i| \ll 1$  for  $i = 2, \dots, 7$ , we recover the SM Higgs sector. The choice of  $\Lambda_H$  is subject to the condition  $\Lambda_H^2 \gg v^2$ , so that we are safely in the decoupling regime. Moreover, in order for the 2HDM to be distinguishable from the SM Higgs sector,  $\Lambda_H$  should not be significantly larger than  $\mathcal{O}(1 \text{ TeV})$ . We considered two different values,  $\Lambda_H = 500 \text{ GeV}$  and  $1 \text{ TeV}$ , although the allowed parameter regime in which the 2HDM remains consistent up to the Planck scale is not especially sensitive to the precise value of  $\Lambda_H$  in the desired mass range. In the case of  $\Lambda_H = 500 \text{ GeV}$ , it is plausible that the heavy Higgs boson states could be detected in high luminosity LHC running. Indeed, as we shall demonstrate later in this section, differences in the squared-masses of the heavy Higgs states can provide an important consistency check of this framework.

The Yukawa couplings play a fundamental role in this analysis. As discussed in Section 2.3, we have employed the flavor-aligned 2HDM to describe the Yukawa sector, with random complex alignment parameters whose moduli were varied by several orders of magnitude. The evolution of the Yukawa couplings in the flavor-

aligned 2HDM was first performed in Ref. [60]. Notice that the running of the Yukawa couplings can also generate Landau poles. Due to the large size of the top quark mass, at least one of the Yukawa couplings will be of order one at the electroweak scale, so that a Landau pole in the top-quark Yukawa coupling below the Planck scale can be generated by the RG running. The alignment parameters, unique for both the up and down quark sectors, were log random generated in such a way as to prevent such Landau poles in the running of the Yukawa couplings up to Planck scale. In the RG running, the initial value of the top Yukawa coupling was taken to be  $y_t(m_t) = 0.94$ , corresponding to an  $\overline{\text{MS}}$  top quark mass of  $m_t(m_t) = 163.71 \pm 0.9$  GeV [29]. The non-occurrence of Landau poles then leads to the constraints

$$|\alpha^U| \lesssim 0.95 \quad \text{and} \quad |\alpha^D| \lesssim 81.5 \quad (\Lambda_H = 500 \text{ GeV}), \quad (3.5)$$

$$|\alpha^U| \lesssim 0.97 \quad \text{and} \quad |\alpha^D| \lesssim 84 \quad (\Lambda_H = 1 \text{ TeV}), \quad (3.6)$$

as seen in Fig. 3.1<sup>3</sup>. These results are quite consistent with those obtained in Ref. [60].

The effect of the alignment parameters in the one-loop quartic scalar coupling RGEs is to bolster the negative Yukawa terms, thereby further driving the quartic scalar couplings to be negative during RGE evolution. The influence of the Yukawa

---

<sup>3</sup>For  $\Lambda_H = 1$  TeV, the figure corresponding to Fig. 3.1 looks nearly identical, so we do not display it here.

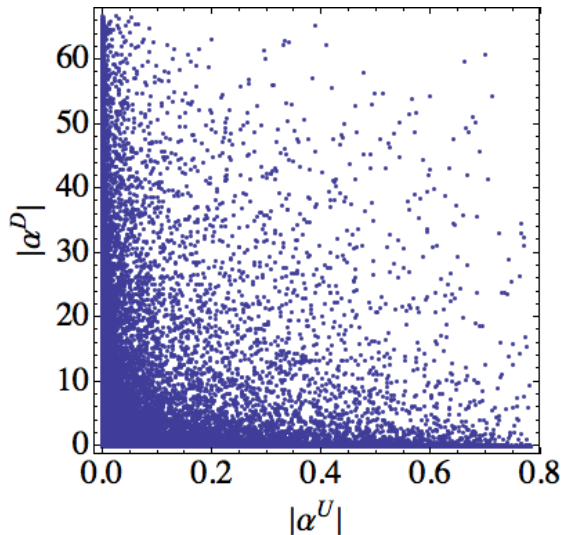


Figure 3.1: Distribution of absolute values of the flavor-alignment parameters, for regions of 2HDM parameter space which remain valid up to the Planck scale, assuming  $\Lambda_H = 500$  GeV.

couplings in the scalar couplings RG evolution is dominated by  $y_t^4$  terms (where  $y_t$  is the top quark Yukawa coupling) in the one-loop  $\beta$ -functions, where they provide a negative contribution. In this manner, the large size of the top quark Yukawa coupling tends to drive  $Z_1$  negative at large energy scales, thus provoking an instability in the potential. This will occur unless the starting point value (at the electroweak scale) of  $Z_1$  is large enough. Since  $Z_1$  is directly related to the lightest CP-even mass in the decoupling regime, requiring the stability of the scalar potential between the electroweak scale and the Planck one therefore yields a lower bound on  $m_h$ . Similarly, if the initial value of  $Z_1$  at the electroweak scale

is too large, then a Landau pole will appear in the running of  $Z_1$  below the Planck scale due to the fact that the leading  $Z_i$  contributions to the  $\beta$ -functions of the quartic scalar couplings are positive, thereby driving the quartic scalar couplings to larger values as the energy scale increases. Preventing the occurrence of Landau poles thus establishes an upper bound on  $Z_1$ , and thus on  $m_h$ .

Within the SM, these demands can only be satisfied up to the Planck scale by a rather narrow window of Higgs boson masses, which excludes the observed value of 125 GeV. As we shall now see, the complexity of the 2HDM scalar potential “opens up” that narrow window to include the known value of the Higgs mass.

## 3.1 Numerical Analysis

### 3.1.1 Results from one-loop RG running

Let us now compare the effect of the one-loop running of the SM scalar coupling, with its effect on the 2HDM quartic scalar couplings. The results of our calculations are shown in Fig. 3.2, which we now analyze in detail. The full 2HDM running begins at  $\Lambda_H = 1$  TeV, where the  $Z_i$  for  $i = 2, \dots, 7$  are chosen.<sup>4</sup> The red points in Fig. 3.2 correspond to choices of parameters  $Z_i$  for which an instability of the potential occurred for a given higher scale  $\Lambda > \Lambda_H$ . The blue points cor-

---

<sup>4</sup>The corresponding plot for  $\Lambda_H = 500$  GeV looks nearly identical, so we do not exhibit it here.

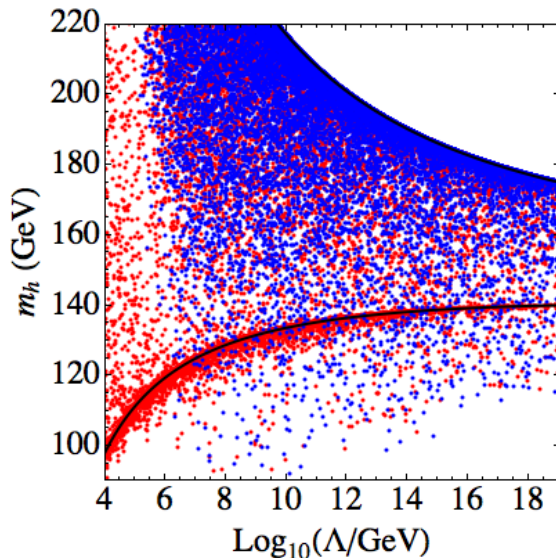


Figure 3.2: RG running of 2HDM quartic scalar couplings, with  $\Lambda_H = 1$  TeV. Red points correspond to parameter choices for which an instability occurs in the scalar potential; blue points indicate the presence of a Landau pole. The upper solid black line indicates the occurrence of a Landau pole in the SM. The lower solid black line indicates the limit for which the SM potential becomes unstable.

respond to parameter choices for which a Landau pole occurred during the RG running at some scale  $\Lambda > \Lambda_H$ . These results are to be compared with the corresponding results of the SM Higgs sector also shown in Fig. 3.2: the upper solid line indicates the maximally allowed value of  $m_h$  to avoid a Landau pole and the lower solid line indicates the minimal value of  $m_h$  needed to avoid a negative SM quartic scalar coupling, at all energy scales below  $\Lambda$ . We recover the well-known one-loop SM result that  $140 \lesssim m_h \lesssim 175$  GeV in order to preserve vacuum sta-

bility and avoid Landau poles in the running of the quartic scalar coupling at all energy scales up to  $M_{\text{PL}}$  [13, 61, 62] .

The distribution of red and blue points in Fig. 3.2 has some interesting features. First, there are no blue points above the SM-Landau pole line. In fact, although the 2HDM scalar potential has several scalar couplings, their contributions to the 2HDM  $\beta$ -functions are mostly positive. As such, when one of these couplings starts to become very large in its RG evolution, the others will not be able to counteract that growth, and a Landau pole is reached. Consequently, the upper limit for the quartic scalar coupling  $Z_1$  that controls the value of  $m_h$  hardly differs from the corresponding SM result. Second, note the appearance of many blue points *below* the SM-instability line. These correspond to Landau poles that occur for relatively low values of  $m_h$ , which is equivalent to low values of  $Z_1$ . However, even though the initial value of  $Z_1$  at  $\Lambda_H$  may be small, the values of other  $Z_i$  can be large, and thus Landau poles in these couplings can be generated, yielding those blue points below the SM instability line.

The most interesting aspect of our results concerns the distribution of the red points, which correspond to the violation of one or more of the 2HDM stability conditions at the energy scale  $\Lambda$ . We see a great “density” of points around the SM-instability line. These points may be interpreted as regions of 2HDM parameter space that constitute small deviations from SM behavior. But the

remarkable difference with the SM result is the appearance of many points *below and to the right* of the SM-instability line. For these points, the instability of the scalar potential occurs at a larger value of  $\Lambda$  for a given value of  $m_h$  as compared to the SM.

Indeed, the full impact of the 2HDM on the RG evolution may be best appreciated by examining the rightmost boundary of Fig. 3.2 corresponding to  $\Lambda = M_{\text{PL}}$ . On this boundary, we find both blue and red points, for a range of Higgs masses from about 118 GeV up to 175 GeV. Thus we see that a range of 2HDM parameters exists for which it is possible to have a SM-like Higgs boson with a mass of 125 GeV, without that mass value implying an instability of the potential (or a Landau pole) between the electroweak and Planck scales.

Let us now analyze more closely the region of parameter space for which the 2HDM is consistent up to the Planck scale. According to Fig. 3.2, only a narrow range of  $m_h$  (which corresponds to a narrow interval of values of  $Z_1$ ) is consistent with a 2HDM with a stable vacuum and no Landau poles from the electroweak to the Planck scale. Since the 2HDM quartic couplings are all coupled together in their RG running, it follows that the allowed ranges for all  $Z_i$ , not only  $Z_1$ , will likewise be quite narrow. This has interesting implications on the scalar mass spectrum. In fact, in light of eq. 2.14, the squared-mass splitting of the two heavy neutral Higgs states depends primarily on  $|Z_5|$ . Likewise, eq. 2.15 shows that the

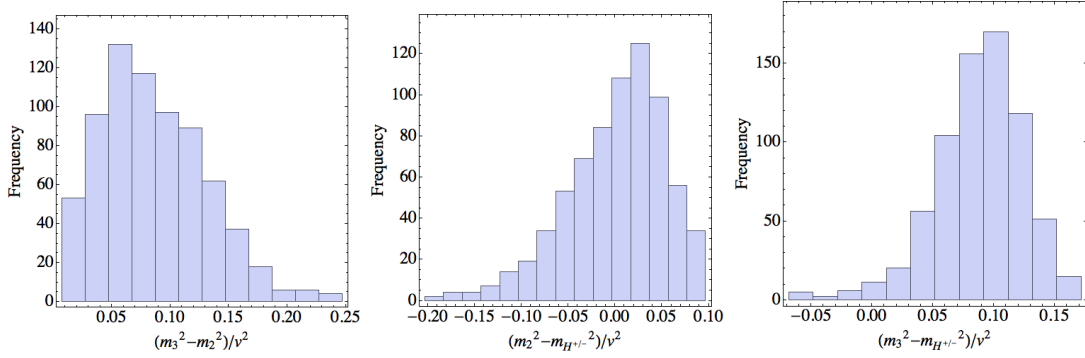


Figure 3.3: Histograms of squared-mass differences of the heavy scalar states for  $\Lambda_H = 500$  GeV. The left panel shows values of squared-mass difference between the two heavier neutral states. The middle and right panels show the values of the squared-mass difference between the lighter and heavier of the two heavy neutral states and the charged Higgs boson, respectively. The histograms correspond to 2HDM parameters for which there are no Landau poles and vacuum stability is satisfied at all energies below the Planck scale.

squared-mass splitting of the heavier neutral Higgs boson and the charged Higgs boson primarily depends on  $Z_4$  and  $|Z_5|$ . Since the possible values of  $Z_4$  and  $|Z_5|$  are restricted to a narrow range of values, it follows that the squared-mass splittings of the heavy Higgs states should also be strongly constrained.

For a 125 GeV SM-like Higgs boson, we have evaluated the squared-mass splittings of the heavier Higgs bosons for 2HDM parameters that are consistent with a stable scalar potential and an absence of Landau poles up to the Planck scale. The histograms shown in Figs. 3.3 and 3.4 exhibit the distribution of

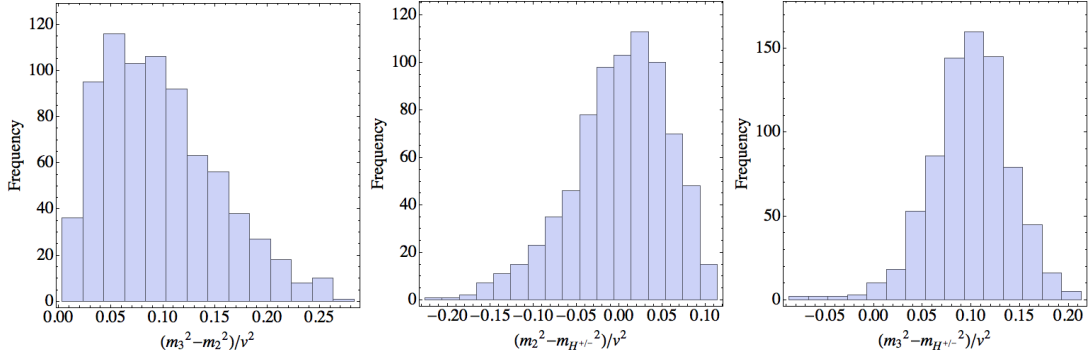


Figure 3.4: Histograms of squared-mass differences of the heavy scalar states for  $\Lambda_H = 1$  TeV. The left panel shows values of squared-mass difference between the two heavier neutral states. The middle and right panels shows the values of the squared-mass difference between the lighter and heavier of the two heavy neutral states and the charged Higgs boson, respectively. The histograms correspond to 2HDM parameters for which there are no Landau poles and vacuum stability is satisfied at all energies below the Planck scale.

squared-mass differences between the two heavy neutral states (these differences are positive by definition) and between the lighter of the two heavy neutral states and the charged Higgs pair, for  $\Lambda_H = 500$  GeV and 1 TeV, respectively. Given the formulae in section 2.1.2, all the heavier scalars have masses of order  $\Lambda_H$  in the decoupling limit. The statistics of these histograms are summarized in Tables 3.1 and 3.2.

If the 2HDM is valid up to the Planck scale, then the mass differences among the heavy Higgs states must be quite small. This presents a challenge for heavy

	min	max	mean	std. dev.
$(m_3^2 - m_2^2)/v^2$	0.01	0.26	0.09	0.05
$(m_2^2 - m_{H^\pm}^2)/v^2$	-0.20	0.11	0	0.05
$(m_3^2 - m_{H^\pm}^2)/v^2$	-0.07	0.19	0.09	0.04

Table 3.1: Squared mass splittings of the heavier Higgs bosons of the 2HDM with  $\Lambda_H = 500$  GeV, for  $124 \lesssim m_h \lesssim 126$  GeV, for points that survive up to the Planck scale, using one-loop calculations.

Higgs searches at future colliders. It may be that such a spectrum could only be reliably determined at a multi-TeV lepton collider. Indeed, if the heavy Higgs spectrum could be determined at some future collider, it would provide a nontrivial check of the present framework in which the 2HDM is valid up to the Planck scale.

The results shown in Table 3.1 are not particularly sensitive to the value of  $\Lambda_H$ . For example, if  $\Lambda_H = 1$  TeV, then the distribution of possible squared-mass differences yields the results shown in Table 3.2. Of course, in this case the corresponding mass differences are even smaller, and the separate discovery of each of these new scalar states at a future collider is even more challenging.

	min	max	mean	std. dev.
$(m_3^2 - m_2^2)/v^2$	0	0.29	0.09	0.05
$(m_2^2 - m_{H^\pm}^2)/v^2$	-0.23	0.12	0	0.06
$(m_3^2 - m_{H^\pm}^2)/v^2$	-0.08	0.19	0.09	0.04

Table 3.2: Squared mass splittings of the heavier Higgs bosons of the 2HDM with  $\Lambda_H = 1$  TeV, for  $124 \lesssim m_h \lesssim 126$  GeV, for points that survive up to the Planck scale, using one-loop calculations.

### 3.1.2 The effects of two-loops RG running

In the SM, the inclusion of the two-loop terms in the RGEs will shift the scalar potential instability boundary to a higher energy scale, which lowers the minimum Higgs boson mass that is consistent with a stable scalar potential all the way up to the Planck scale. In particular, the results in Ref. [2] yield a minimal value of  $m_h \simeq 129$  GeV for vacuum stability. It is further argued that given the currently observed value of 125 GeV for the Higgs boson, the SM vacuum is metastable under the assumption of no new physics beyond the Standard Model below about  $10^{10}$  GeV. This means that the effect of including the two-loop effects in the running lowers the minimal acceptable value of the Higgs mass from  $\sim 140$  GeV to  $\sim 129$  GeV.

We expect that employing the full two-loop RG analysis for the 2HDM would

provide a similar downward shift in the lower bound of Higgs masses that survive up to the Planck scale, as well as increase the fraction of points that survive. In practice, implementing this full two-loop procedure is very delicate and computationally expensive. Instead, we present a procedure to estimate the two-loop RG results. Note that the stability curve for the SM scalar potential at two-loops is both shifted to a higher energy scale, and is less steep as a function of the Higgs mass, relative to the one-loop SM scalar potential stability curve. In essence, going from one-loop to two-loops shifts the stability curve energy scale to a higher scale for a particular Higgs mass. From our one-loop SM calculations and the two-loop SM calculations of Ref. [2], we determine the energy scale shift of the SM scalar potential stability curves due to the inclusion of two-loop RG running. Taking  $\Lambda_H = 1$  TeV, the resulting scale shift function is shown in the left panel of Fig. 3.5, which then yields our “two-loop” result shown in the right panel, which is obtained by applying the scale shift to our one-loop calculation. This shift is applied only to those points in which the scalar potential became unstable, not for points that hit a Landau pole before the Planck scale. The upper bound on the SM Higgs mass due to the absence of Landau poles does not exhibit a similar shift from one-loop to two-loop calculations. As in the case of Fig. 3.2, the case of  $\Lambda_H = 500$  GeV yields nearly identical results.

In our one-loop calculations, only 707 (or 0.707%) of the 100,000 points ana-

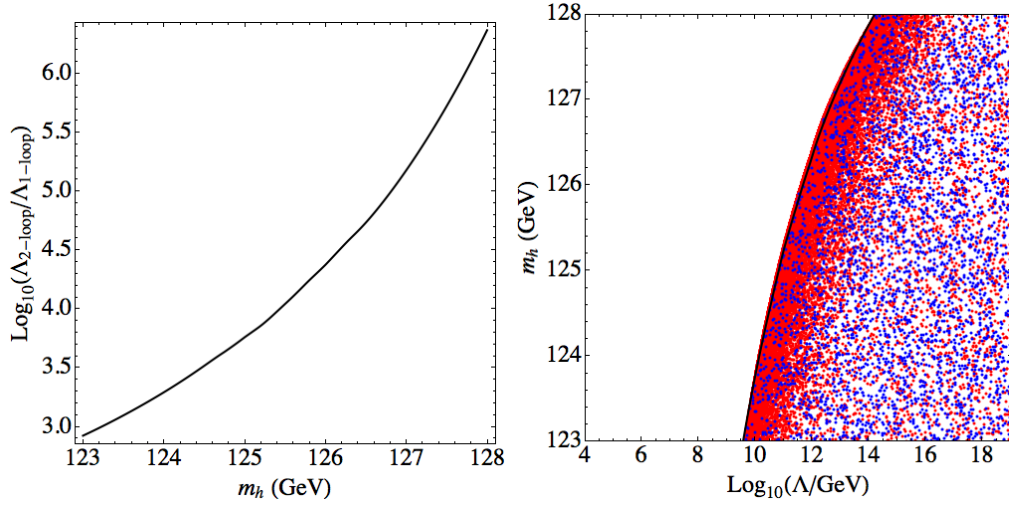


Figure 3.5: Left panel: Scale shift for converting the one-loop scalar potential instability boundary to the two-loop scalar potential instability boundary for a SM-like Higgs boson. Right panel: Higgs boson mass bounds in the flavor-aligned 2HDM, incorporating the scale shift shown in the left panel, assuming that  $\Lambda_H = 1$  TeV. Red points indicate an instability in the running; blue points indicate the presence of a Landau pole.

lyzed survive to the Planck scale in the 123 GeV to 128 GeV region. With the conversion shift and a double check that they satisfy the stability requirement for 2HDM quartic scalar coupling parameters, 1,371 more points reach the Planck scale for a total of 2,078 (or 2.078%) at the Planck scale, an increase of 94% relative to the one-loop results. With an increase in the number of points, the “two-loop” squared mass splittings of the heavier Higgs bosons for points that

	min	max	mean	std. dev.
$(m_3^2 - m_2^2)/v^2$	0	0.31	0.11	0.05
$(m_2^2 - m_{H^\pm}^2)/v^2$	-0.23	0.12	0	0.05
$(m_3^2 - m_{H^\pm}^2)/v^2$	-0.09	0.23	0.11	0.04

Table 3.3: Squared-mass splittings of the heavy Higgs bosons of the 2HDM with  $\Lambda_H = 1$  TeV, for  $m_h \simeq 125$  GeV, for points that survive to the Planck scale, using the two-loop extended procedure.

survive up to the Planck scale are shown in Fig. 3.6 and statistics summarized in Table 3.3. Comparing Tables 3.2 and 3.3, we see that there exists only slight differences in the squared-mass splittings of the heavier Higgs bosons when the approximate two-loop effects are included. Nonetheless, the increase in the number of points for which the model remains consistent all the way up to the Planck scale is according to what one should expect, in light of the observation that the two-loop contributions increase the stability of the SM potential. Thus, this quick estimate suggests that the 2HDM parameter space for which RG running of the quartic scalar couplings up to the Planck scale leaves the potential stable, and for which no Landau poles occur during that running, is larger than the one-loop calculation may lead to believe.

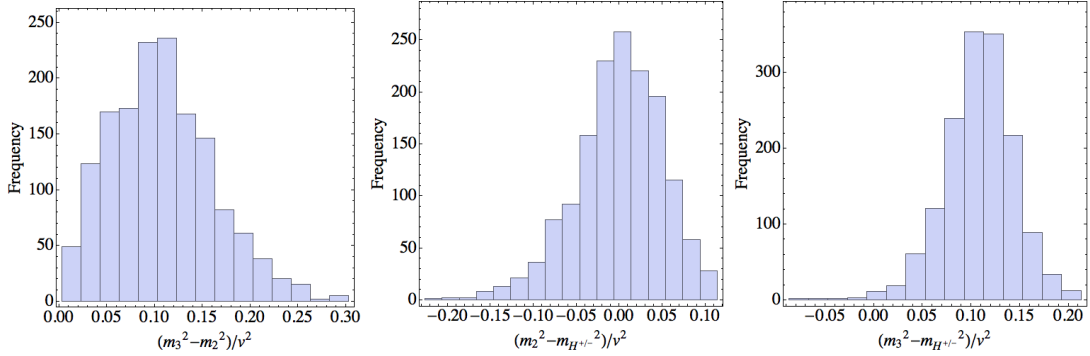


Figure 3.6: Histograms of squared-mass differences of the heavy scalar states for  $\Lambda_H = 1$  TeV, using the two-loop extended procedure. The left panel shows values of squared-mass difference between the two heavier neutral states. The middle and right panels shows the values of the squared-mass difference between the lighter and heavier of the two heavy neutral states and the charged Higgs boson, respectively. The histograms correspond to 2HDM parameters for which there are no Landau poles and vacuum stability is satisfied at all energies below the Planck scale.

# Chapter 4

## Flavor Violation via Planck Scale

### Flavor-Alignment

The most general 2HDM typically exhibits FCNCs which are incompatible with experimental data. To avoid large FCNC requires either an artificial fine-tuning of parameters in the Yukawa sector or the existence of a symmetry that automatically removes FCNC in the tree-level approximation. The flavor-alignment ansatz reviewed in Section 2.3 asserts a proportionality between the two sets of Yukawa matrices making them simultaneously bi-diagonalizable, thereby eliminating FCNCs at tree-level. In addition, the flavor-aligned 2HDM (A2HDM) preserves the relative hierarchy in the quark mass matrices, and provides additional sources of CP-violation in the Yukawa Lagrangian via introduction of three

complex alignment parameters. In special cases, flavor-alignment can be implemented by a symmetry in the low-energy effective theory. Examples of this include the type I, II, X and Y Yukawa sectors of the 2HDM. For these models, flavor-alignment is stable with respect to RG running [38]. However, the generic form of flavor-alignment requires a fine tuning of parameters of the Yukawa sector, and can only be implemented at a particular momentum scale.

In this chapter, we imagine that new physics beyond the SM enforces flavor-alignment near the Planck scale. In this case, we can employ RG running to compute the matrix Yukawa couplings at the electroweak scale. In this set up, deviations from flavor-alignment will emerge at the electroweak flavor scale, creating a source for tree-level FCNCs. This is similar work performed in [63], who use meson mixing and  $B$  decays to constrain the CP-conserving flavor-aligned 2HDM parameter space, via flavor-alignment at the Planck scale. They arrive at their results first analytically in the leading log approximation, and then numerically by evolving the one-loop RGEs down from the Planck scale, but miss a key contribution from off-diagonal sources that are negligible in the leading log approximation, but not in full numerical calculations. Our work includes these contributions in the context of the more general CP-violating A2HDM. We consider experimental constraints on top quark and  $B$  decays, and find that  $B_s \rightarrow \mu^+ \mu^-$  can be used to provide constraints on the A2HDM parameter space.

## 4.1 Planck scale flavor-alignment

To study the maximal amount of FCNCs that can be generated in the A2HDM at the electroweak scale, we establish flavor-alignment at the Planck scale, and run the one-loop RGEs from the Planck scale to the electroweak scale. Thus, we impose the following boundary conditions for the running of the one-loop 2HDM Yukawa RGEs (provided in Appendix A):

$$\kappa^Q(\Lambda_H) = Y^Q(\Lambda_H), \quad (4.1)$$

$$\rho^Q(M_{PL}) = \alpha^Q \kappa^Q(M_{PL}), \quad (4.2)$$

where  $Y^Q$  are the SM Yukawa matrices in the quark-mass eigenstate, and  $\Lambda_H$  is the scale of the heavier doublet, taken in this chapter to be  $\Lambda_H = 400$  GeV, such that we are sufficiently in the decoupling limit. Satisfying these two boundary conditions is not trivial, since they are imposed at opposite ends of the RGE running. For example, to set flavor-alignment at the Planck scale, we must know the values of  $\kappa^Q(M_{PL})$ . This involves running up  $\kappa^Q(\Lambda_H)$  to the Planck scale, but since the one-loop RGEs are strongly coupled to the  $\rho^Q$  matrices, we must supply values for  $\rho^Q(\Lambda_H)$  to begin the running. With no *a priori* knowledge of which values of  $\rho^Q(\Lambda_H)$  lead to flavor-alignment at the Planck scale, we begin by asserting flavor-alignment at  $\Lambda_H$  via a low-scale alignment parameter  $\alpha'^Q$ :

$$\rho^Q(\Lambda_H) = \alpha'^Q \kappa^Q(\Lambda_H). \quad (4.3)$$

In general, this flavor-alignment will be broken during RGE evolution to the Planck scale, and a procedure is needed to reestablish flavor-alignment at the Planck scale. To accomplish this, we decompose  $\rho^Q(M_{PL})$  into portions that are aligned and misaligned with  $\kappa^Q(M_{PL})$ :

$$\rho^Q(M_{PL}) = \alpha^Q \kappa^Q(M_{PL}) + \delta\rho^Q, \quad (4.4)$$

where  $\alpha^Q$  represents the aligned portion (in general, different from  $\alpha'^Q$ ), and  $\delta\rho^Q$  the corresponding degree of misalignment at the Planck scale. To minimize the misaligned portion of  $\rho^Q(M_{PL})$ , we implement the cost function

$$\Delta^Q \equiv \sum_{i,j=1}^3 |\delta\rho_{ij}^Q|^2 = \sum_{i,j=1}^3 |\rho_{ij}^Q(M_{PL}) - \alpha^Q \kappa_{ij}^Q(M_{PL})|^2, \quad (4.5)$$

which once minimized, provides the optimal value of  $\alpha^Q$  for flavor-alignment at the Planck scale:

$$\alpha^Q \equiv \frac{\sum_{i,j=1}^3 \kappa_{ij}^{Q*} \rho_{ij}^Q}{\sum_{i,j=1}^3 \kappa_{ij}^{Q*} \kappa_{ij}^Q}, \quad (4.6)$$

based on the alignment parameters  $\alpha'^Q$  at  $\Lambda_H$ . We subsequently reassert flavor-alignment at the Planck scale using this optimized alignment parameter,

$$\rho^Q(M_{PL}) = \alpha^Q \kappa^Q(M_{PL}), \quad (4.7)$$

and evolve the one-loop RGEs back down to  $\Lambda_H$ . At  $\Lambda_H$ , we use eq. 4.1 to match the boundary conditions for the 2HDM and SM, and then run the SM down (using the one-loop SM RGEs provided in Ref. [64]) to the electroweak scale to check the accuracy of the resulting quark masses. If any of the quark masses differ from their experimental values<sup>1</sup> by more than 3%, we reestablish the correct quark masses at the electroweak scale, run back up to  $\Lambda_H$ , and then rerun this procedure repeatedly until the two boundary conditions are satisfied. The result is flavor-alignment between  $\kappa^Q(M_{PL})$  and  $\rho^Q(M_{PL})$ , and a set of  $\rho^Q$  matrices at the electroweak scale that provide a source of FCNCs.

Note that this work is similar to the analysis done by Ref. [63], in which they implement Planck scale flavor-alignment in a CP-conserving A2HDM, and constrain the A2HDM parameter space using experimental constraints from  $B_s^0 \leftrightarrow \bar{B}_s^0$  mixing and  $B_s \rightarrow \mu^+ \mu^-$ . They perform their analysis first in the leading logarithm approximation, showing that in this limit,  $|\rho_{32}^D|/|\rho_{23}^D| \simeq 0.019$ , thus the dominant contribution to FCNCs in  $B$  mixing and decays is from  $\Delta_{23}^D$ . Next, they perform their full numerical analysis, relying on the observation,  $|\rho_{23}^D| \gg$

---

<sup>1</sup>Starting the RG evolution at  $m_Z$ , we use a five flavor scheme to run up to  $m_t$  and a six flavor scheme above  $m_t$ . Running quark mass masses at  $m_Z$  and  $m_t$  are obtained from the RunDec Mathematica software package [59], based on quark masses provided in Ref. [65]. For simplicity, the effects of the lepton masses are ignored, as these contribute very little to the running of the  $Z_i$ .

$|\rho_{32}^D|$ , independent of scale, obtained from their approximate analytic results, and subsequently place limits on the flavor-alignment parameter space.

Our implementation is more flexible in a number of ways. First, we choose a framework allowing for CP-violation in both the scalar potential in the Yukawa sector, via complex alignment parameters. Second, we observe that in the large alignment parameter limit,  $\rho_{32}^D(\Lambda_H)$  is non-negligible, and in fact we find via our numerical running,  $|\rho_{32}^D(\Lambda_H)| \gg |\rho_{23}^D(\Lambda_H)|$ . This is the result of the off-diagonal elements in  $\beta_{\rho^D}$  being driven by large values of the alignment parameters, making the leading log approximation unreliable. In the large alignment parameter limit, the terms that couple to the CKM matrix dominate the off-diagonal elements of  $\beta_{\rho^D}$ , favoring for example, the growth of  $\rho_{32}^D$  relative to  $\rho_{23}^D$ . In the small parameter limit, however, we indeed recover  $|\rho_{32}^D(\Lambda_H)|/|\rho_{23}^D(\Lambda_H)| \simeq 0.019$ , showing consistency between our calculations.

#### 4.1.1 Leading logarithm approximation

In the small alignment parameter limit, it is possible to obtain approximate analytic solutions to the one-loop  $\beta$ -functions provided for the Yukawa matrices in Appendix A. For  $Y^D$ , the SM down-type Yukawa matrix in the quark mass eigenstate, the off-diagonal terms in the  $\beta$ -function are generated by the term

$$\beta_{Y_{ij}^D} = 16\pi^2 \frac{dY_{ij}^D}{dt}, \quad (4.8)$$

$$= -\frac{3}{2}[K^\dagger Y^U Y^{U\dagger} K Y^D]_{ij}. \quad (4.9)$$

for  $i \neq j$ , where  $K$  is the CKM matrix,  $t = \ln(\mu/m_t)$ , and  $\mu$  is the renormalization energy scale. The off-diagonal elements of  $\beta_{Y_{ij}^D}(m_t)$  are very small, and so to very good approximation, we can approximate  $Y_{ij}^D(\Lambda)$  to leading log order

$$Y_{ij}^D(\Lambda) \approx Y_{ij}^D(m_t) + \frac{\beta_{Y_{ij}^D}(m_t)}{16\pi^2} \log\left(\frac{\Lambda}{m_t}\right). \quad (4.10)$$

Since  $Y_{ij}^D(m_t) = 0$  (for  $i \neq j$ ), eq. 4.10 simplifies to

$$Y_{ij}^D(\Lambda) = \frac{\beta_{Y_{ij}^D}(m_t)}{16\pi^2} \log\left(\frac{\Lambda}{m_t}\right), \quad (4.11)$$

$$= -\frac{1}{16\pi^2} \frac{3}{2}[K^\dagger Y^U(m_t) Y^{U\dagger}(m_t) K Y^D(m_t)]_{ij} \log\left(\frac{\Lambda}{m_t}\right). \quad (4.12)$$

Note that,

$$\frac{|Y^D(m_t)_{32}|}{|Y^D(m_t)_{23}|} = \frac{|[K^\dagger Y^U(m_t) Y^{U\dagger}(m_t) V_{CKM} Y^D(m_t)]_{32}|}{|[K^\dagger Y^U(m_t) Y^{U\dagger}(m_t) K Y^D(m_t)]_{23}|}, \quad (4.13)$$

$$= \frac{|[K^\dagger M_U^2 V_{CKM} M_D]_{32}|}{|[K^\dagger M_U^2 K M_D]_{23}|}, \quad (4.14)$$

$$\simeq 0.019, \quad (4.15)$$

independent of the scale  $\Lambda$ . Furthermore, the boundary condition between  $\kappa^D(\Lambda_H)$  and  $Y^D(\Lambda_H)$  (eq. 4.1) implies that  $|\kappa^D(\Lambda_H)_{32}|/|\kappa^D(\Lambda_H)_{23}| \approx 0.019$ . In the small

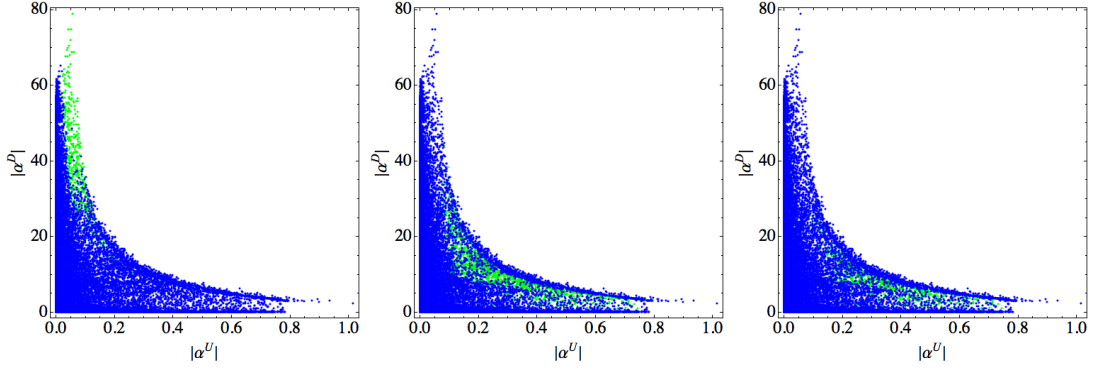


Figure 4.1: Regions of the A2HDM parameter space where  $|\rho_{ij}^U| \gg |\rho_{ji}^U|$  (green points) and  $|\rho_{ij}^U| \ll |\rho_{ji}^U|$  (blue points), for  $i > j$ . The left panel is for  $i, j = 2, 1$ , the middle panel is for  $i, j = 3, 1$ , and the right panel is for  $i, j = 3, 2$ .

alignment parameter limit, this ratio also holds for  $\rho^D(\Lambda_H)$ , and in fact, more generally, one finds

$$\frac{|\rho^Q(\Lambda_H)_{ij}|}{|\rho^Q(\Lambda_H)_{ji}|} \ll 1, \quad (4.16)$$

for  $i > j$ . This is the basis for Ref. [63] ignoring  $\rho_{32}^D$  in lieu of  $\rho_{23}^D$ .

In the large alignment parameter, however, the leading log approximation fails. Indeed, the terms in  $\beta_{\rho^Q}$  that couple to the CKM matrix dominate the RG running, and drive

$$\frac{|\rho^Q(\Lambda_H)_{ij}|}{|\rho^Q(\Lambda_H)_{ji}|} \gg 1, \quad (4.17)$$

for  $i > j$ . Hence,  $\rho_{ij}^Q$  with  $i > j$  cannot be neglected in the large alignment

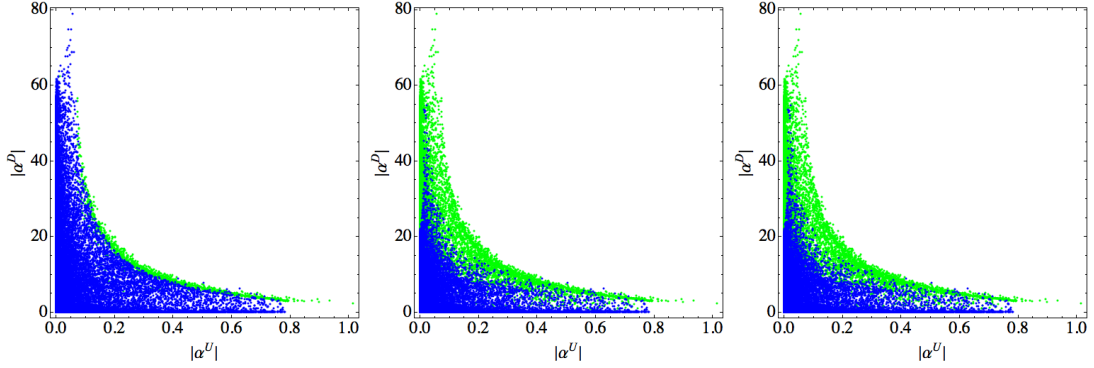


Figure 4.2: Regions of the A2HDM parameter space where  $|\rho_{ij}^D| \gg |\rho_{ji}^D|$  (green points) and  $|\rho_{ij}^D| \ll |\rho_{ji}^D|$  (blue points), for  $i > j$ . The left panel is for  $i, j = 2, 1$ , the middle panel is for  $i, j = 3, 1$ , and the right panel is for  $i, j = 3, 2$ .

parameter limit, particularly in the down sector, as they generate the largest sources of FCNCs during RG running (though the  $\rho_{ji}^Q$  still contribute appreciably), and hence will be the most useful in placing constraints on the A2HDM. Fig. 4.1 show the regions of the A2HDM parameter space where  $|\rho_{ij}^U| \gg |\rho_{ji}^U|$  and  $|\rho_{ij}^U| \ll |\rho_{ji}^U|$ , for  $i > j$ , and Fig. 4.2 shows these limits for  $\rho^D$ .

## 4.2 Experimental Bounds

For our numerical analysis, we use the procedure described in the previous section, taking the A2HDM to be in the decoupling limit such that the lightest Higgs boson resembles that of the SM. The two heavier neutral scalars are denoted by  $H$  and  $A$ , corresponding to the CP-even and CP-odd eigenstates, and are

roughly degenerate in mass  $m_H \approx m_A \approx \Lambda_H$  in the decoupling limit, where  $\Lambda_H$  is subject to the condition  $\Lambda_H^2 \gg v^2$ . The decoupling limit also enforces the condition  $\cos(\beta - \alpha) \approx 0$ , where  $\alpha$  is the CP mixing angle between the two heavy neutral Higgs bosons, and  $\beta$  is given by the ratio of the vevs in a generic basis,  $\tan \beta = v_2/v_1$ . In the calculations that follow, we take  $m_H = m_A = 400$  GeV, and  $(\beta - \alpha) = \pi/2 + 0.1$ , to be consistent with the Higgs data. For  $B_s \rightarrow \mu^+\mu^-$ , we define the coupling  $\rho_{22}^L \equiv 10y_\mu = 10\sqrt{2}m_\mu/v$ .

### 4.2.1 Flavor-changing top decays

We calculate the tree-level branching ratios for  $t \rightarrow qh$ , for  $q = u, c$ , arising from misalignment generated via radiative corrections during RG running, given in Ref. [66]:

$$\begin{aligned} \text{BR}(t \rightarrow uh) &= \frac{1}{2} \cos^2(\beta - \alpha) (|\rho_{13}^U|^2 + |\rho_{31}^U|^2) \\ &\quad \times \frac{2v^2}{m_t^2} \frac{(1 - m_h^2/m_t^2)}{(1 - m_W^2/m_t^2)} \left(1 + \frac{2m_W^2}{m_t^2}\right) \eta_{QCD}, \end{aligned} \quad (4.18)$$

$$\begin{aligned} \text{BR}(t \rightarrow ch) &= \frac{1}{2} \cos^2(\beta - \alpha) (|\rho_{23}^U|^2 + |\rho_{32}^U|^2) \\ &\quad \times \frac{2v^2}{m_t^2} \frac{(1 - m_h^2/m_t^2)}{(1 - m_W^2/m_t^2)} \left(1 + \frac{2m_W^2}{m_t^2}\right) \eta_{QCD}, \end{aligned} \quad (4.19)$$

where  $\eta_{QCD} = 1 + 0.97\alpha_s = 1.10$  is the NLO QCD correction to the branching ratio. These expressions are based on the leading order formulae for both  $t \rightarrow Wb$  and  $t \rightarrow qh$  decay rates, assuming the top quark decay width is dominated by

the SM value of  $\Gamma(t \rightarrow Wb)$ . The results of our calculations for the A2HDM, presented in Fig. 4.3, give  $\text{BR}(t \rightarrow qh) \lesssim 10^{-11}$ , for both  $q = u, c$ . The SM contribution to the branching ratio is of order  $10^{-13} - 10^{-15}$ , as calculated in Refs. [67, 68, 69, 70]. Indirect bounds placed on the branching ratio for  $t \rightarrow ch$  are given in Refs. [71, 72] to be of order  $\sim 10^{-3}$ , whereas Ref. [73] uses LHC results to obtain  $\text{BR}(t \rightarrow ch) < 2.7\%$ . These experimental constraints are many orders of magnitude greater than our calculated branching ratios, and thus we find that these top quark decays cannot provide constraints to the A2HDM parameter space.

Note that the A2HDM alignment parameter space probed in this analysis is constrained to be perturbative, that is, that none of the Yukawa couplings encounter a Landau pole during one-loop RGE running, producing similar bounds to eq. 3.5 for  $\Lambda_H = 400$  GeV. The parameter space of the A2HDM obeying the Landau pole constraints, and having gone through the iterative boundary condition matching procedure described in the previous section, can be seen in either Figs. 4.1 or 4.2. For constraints on the A2HDM parameter space to be placed using  $t \rightarrow qh$  for ( $q = u, c$ ), then this would require the off-diagonal elements  $\rho_{13}^U$  and  $\rho_{23}^U$  (and their respective permutations) to be several orders of magnitude larger than is currently allowed. The size of these terms are bound by Landau poles, and thus the inability to place constraints using these flavor-

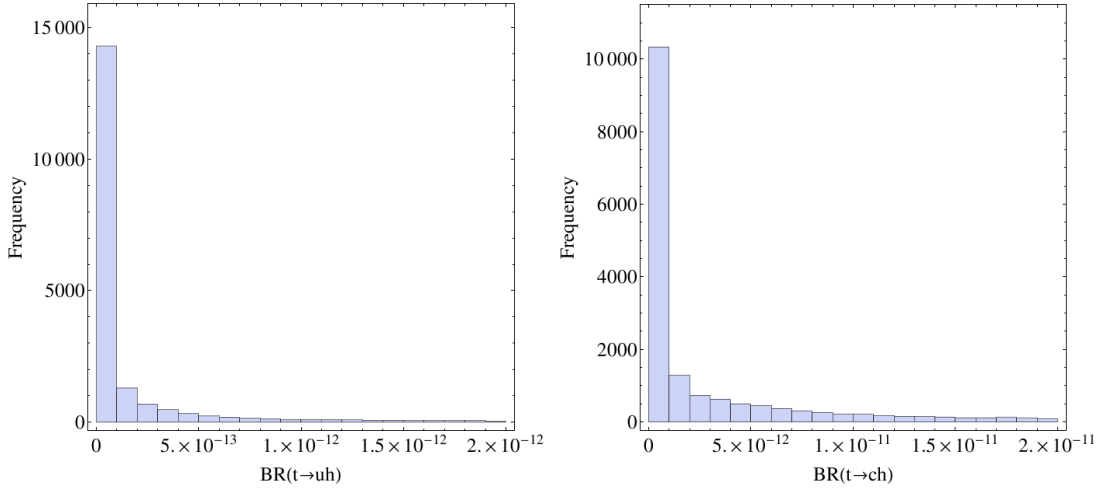


Figure 4.3: Histogram of branching ratios for  $t \rightarrow uh$  and  $t \rightarrow ch$ , in the left and right panels, respectively. Although enhancements with respect to the SM rate are possible, the resulting decay rate is many orders of magnitudes below the current experimental bound of  $\text{BR}(t \rightarrow qh) \lesssim 10^{-3}$ , for both  $q = u, c$ .

changing top decays can be traced back to constraints on the A2HDM parameter space via Landau poles.

### 4.2.2 Leptonic $B$ decays

In the down sector,  $B_s \rightarrow \ell^+ \ell^-$  can be mediated by the neutral Higgs bosons at tree-level in the most general 2HDM, but not at tree-level in the SM. In the A2HDM, misalignment and hence tree-level FCNCs can be generated at the electroweak scale via RG running, if flavor-alignment is imposed at a high energy scale, such as the Planck scale, whereas  $B_s \rightarrow \tau^+ \tau^-$  should be favored since the

coupling depends on the lepton masses. However, these  $\tau$ 's decay to jets and leptons whose invariant mass does not reconstruct the  $\tau$ , and thus cannot be tagged in detectors.  $B_s \rightarrow \mu^+ \mu^-$  is more easily tagged (Ref. [63]). For our calculations, we follow the approach of Ref. [74], who show that in the presence of new physics, we can calculate

$$\frac{\text{BR}(B_s \rightarrow \mu^+ \mu^-)}{\text{BR}(B_s \rightarrow \mu^+ \mu^-)_{SM}} \simeq (|S|^2 + |P|^2) \times \left( 1 + y_s \frac{\text{Re}(P^2) - \text{Re}(S^2)}{|S|^2 + |P|^2} \right) \left( \frac{1}{1 + y_s} \right), \quad (4.20)$$

where  $\text{BR}(B_s \rightarrow \mu^+ \mu^-)_{SM}$  is the SM prediction for the branching ratio extracted from an untagged rate,  $y_s = (8.8 \pm 1.4)\%$  has to be taken into account when comparing experimental and theoretical results, and

$$S \equiv \frac{m_{B_s}}{2m_\mu} \frac{(C_S - C'_S)}{C_{10}^{SM}} \sqrt{1 - \frac{4m_\mu^2}{m_{B_s}^2}}, \quad (4.21)$$

$$P \equiv \frac{m_{B_s}}{2m_\mu} \frac{(C_P - C'_P)}{C_{10}^{SM}} + \frac{(C_{10} - C'_{10})}{C_{10}^{SM}}. \quad (4.22)$$

The  $C_i$  are the Wilson coefficients corresponding to the operators

$$O_S^{(\prime)} = \frac{m_b}{m_{B_s}} (\bar{s} P_{R(L)} b) (\bar{\ell} \ell), \quad (4.23)$$

$$O_P^{(\prime)} = \frac{m_b}{m_{B_s}} (\bar{s} P_{R(L)} b) (\bar{\ell} \gamma^5 \ell), \quad (4.24)$$

$$O_{10}^{(\prime)} = (\bar{s} \gamma_\mu P_{R(L)} b) (\bar{\ell} \gamma^\mu \gamma^5 \ell), \quad (4.25)$$

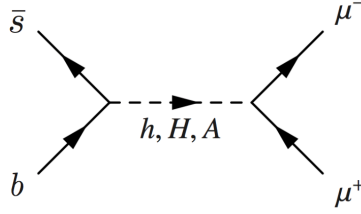


Figure 4.4: Tree level neutral Higgs boson mediated  $B_s \rightarrow \mu^+ \mu^-$  in the 2HDM.

which based on the tree-level diagram given in Fig. 4.4, we calculate for the 2HDM as

$$C_P = \frac{m_{B_s}}{m_b} \rho_{32}^{D*} \rho_{22}^L \frac{1}{m_A^2}, \quad (4.26)$$

$$C'_P = \frac{m_{B_s}}{m_b} \rho_{23}^{D*} \rho_{22}^L \frac{1}{m_A^2}, \quad (4.27)$$

$$C_S = -\frac{m_{B_s}}{m_b} \rho_{32}^{D*} \rho_{22}^L \frac{1}{m_H^2}, \quad (4.28)$$

$$C'_S = \frac{m_{B_s}}{m_b} \rho_{23}^{D*} \rho_{22}^L \frac{1}{m_H^2}, \quad (4.29)$$

The authors of Ref. [74] provide  $\text{BR}(B_s \rightarrow \mu^+ \mu^-)_{SM} = (3.32 \pm 0.17) \times 10^{-9}$ , obtained from recent lattice results presented in Refs. [75, 76, 77]. This in good agreement with  $\text{BR}(B_s \rightarrow \mu^+ \mu^-)_{exp} = (2.4 \pm 0.16) \times 10^{-9}$ , which they obtain using a combination of LHC results provided in Refs. [78, 79, 80].

Fig. 4.5 shows the results of our evaluation of eq. 4.20 as a function of the down-type alignment parameter. The largest deviations of the predicted A2HDM branching ratio from the SM prediction occur in the limit  $|\rho_{32}^D| \gg |\rho_{23}^D|$ , which corresponds to the large alignment parameter limit, as seen in Fig. 4.2. In the

large alignment parameter limit, the terms in  $\beta_{\rho^D}$  that couple to the CKM matrix dominate, and drive the off-diagonal elements of  $\rho^D$  to be very large during RG running, with contributions from  $\rho_{32}^D$  dominating those from  $\rho_{23}^D$ . Since the SM prediction is in good agreement with experimental results, we can place constraints on the A2HDM parameter space, by requiring that  $|\rho_{32}^D| \ll |\rho_{23}^D|$ , so that the branching ratio not differ significantly from that of the SM. This in turn implies that the A2HDM must be in the small alignment parameter limit. Fig. 4.6 shows regions of the A2HDM parameter space that produce a branching ratio of  $B_s \rightarrow \mu^+ \mu^-$  within 10%, 10%-20%, and  $> 20\%$  of the SM calculation, and thus provides upper bounds on the values of the alignment parameters at the Planck scale.

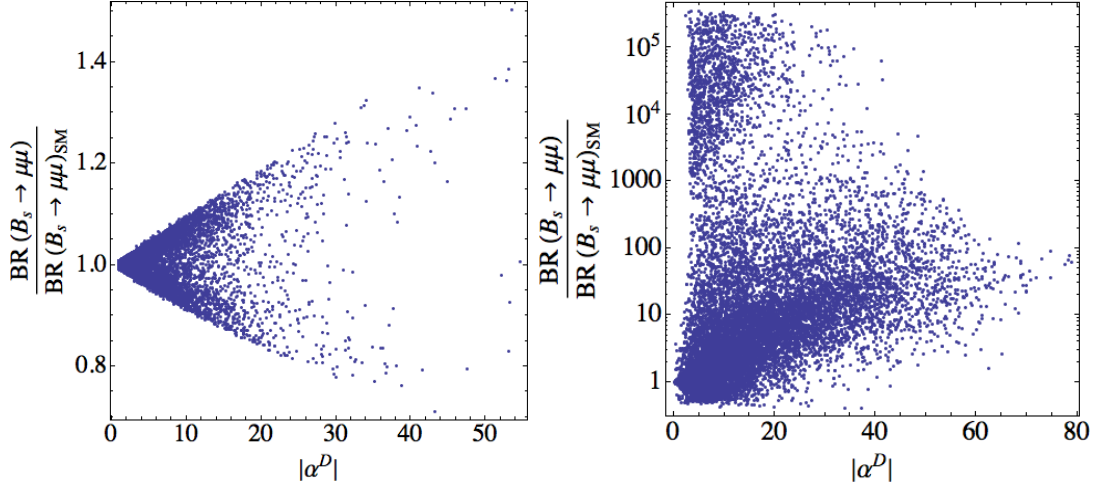


Figure 4.5: A2HDM branching ratio for  $B_s \rightarrow \mu^+ \mu^-$  relative the the SM, as a function of  $|\alpha^D|$ . Left panel: results for  $|\rho_{32}^D| \ll |\rho_{23}^D|$ , corresponding to the small alignment parameter limit. Right panel: results for  $|\rho_{32}^D| \gg |\rho_{23}^D|$ , corresponding to the large alignment parameter limit, implying large branching ratios relative to the SM are generated only when  $|\rho_{32}^D| \gg |\rho_{23}^D|$ .

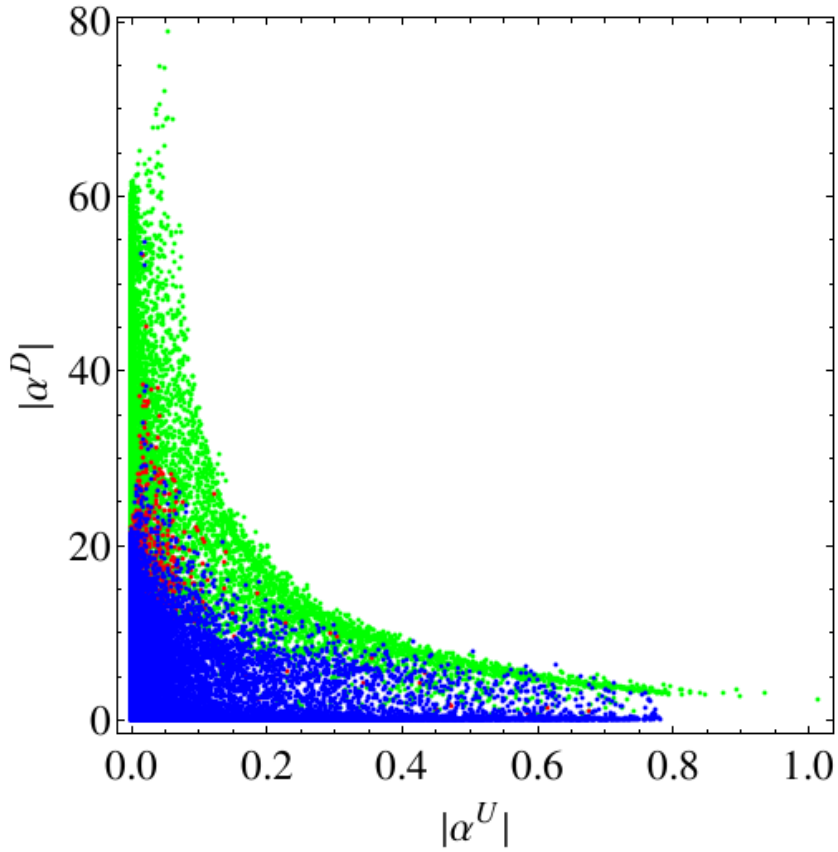


Figure 4.6: Constraints on the A2HDM parameter space from  $B_s \rightarrow \mu^+\mu^-$ . The blue points correspond to regions of parameter space that deviate from  $\text{BR}(B_s \rightarrow \mu^+\mu^-)_{SM}$  by less than 10%. The red points correspond to regions of parameter space that deviate from  $\text{BR}(B_s \rightarrow \mu^+\mu^-)_{SM}$  between 10% - 20%. The green points indicate the region of parameter space that deviate from  $\text{BR}(B_s \rightarrow \mu^+\mu^-)_{SM}$  by more than 20%.

# Chapter 5

## Conclusions

The discovery of a SM-like Higgs boson with a mass  $m_h = 125$  GeV has focused attention on the validity of the Standard Model at higher energies. Putting aside the question of the origin of the electroweak symmetry breaking (e.g., accepting the fine-tuning of parameters inherent in fixing the electroweak scale), one can ask whether the Standard Model is consistent all the way up to the Planck scale. Refined calculations of the radiatively-corrected scalar potential suggest that the Standard Model vacuum is at best metastable (and long-lived), with a deeper vacuum located at field values near  $10^{10}$  GeV, well below the Planck scale.

Adding new degrees of freedom has the potential of ameliorating the problem of an unstable vacuum. In this thesis we considered the two Higgs doublet extension of the Standard Model (2HDM) and examined the range of parameters for which

the 2HDM is stable and perturbative at all energy scales below the Planck scale. Our aim was to make the minimal number of assumptions regarding the structure of the 2HDM required by the experimental data. Since the observed Higgs boson is SM-like (within the accuracy of the limited Higgs data set), we considered the 2HDM with the most general scalar potential in the decoupling regime. The Yukawa sector was treated using the flavor-alignment ansatz, in which the second set of Yukawa matrices is proportional to the SM-like set at the electroweak scale to protect against tree-level Higgs-mediated FCNCs. Although the flavor-alignment condition is not protected by a low-energy symmetry (except in special cases, which lead to 2HDMs of Types I, II, X or Y), it provides a more general framework which at present is consistent with experimental data.

We scanned over the scalar potential parameters and the flavor-alignment parameters to fix the boundary conditions at the scale of the heavy Higgs states. We then employed one-loop RGEs to run the 2HDM parameters up to the Planck scale, and required that no Landau poles are encountered, without generating an instability in the scalar potential. In contrast to the Standard Model, it is possible to have a SM-like Higgs boson with a mass of 125 GeV while maintaining the validity of the 2HDM up to the Planck scale. We also presented a scheme to estimate the effects of the RG-running at two-loops, by applying a scale shift seen in going from the one-loop SM scalar potential stability curve to the two-loop SM

scalar potential stability curve. Such effects *increase* the number of points in the 2HDM parameter scan that survive Landau pole and stability requirements up to the Planck scale.

The larger range of allowed values of  $m_h$  in the 2HDM (as compared with the SM) is a direct consequence of the fact that the 2HDM scalar potential contains more quartic scalar couplings than the SM, which increases the stability of the potential at all scales between the electroweak and the Planck scale. In contrast, we observed that the theoretical upper bound on  $m_h$  in the 2HDM based on the non-existence of Landau poles up to Planck scale hardly differs from the corresponding SM behavior. This can be understood as follows. In the SM, the negative top Yukawa contribution in the quartic scalar coupling  $\beta$ -function drives that coupling to negative values during RG running, unless its starting point is sufficiently large. In the 2HDM, even if the initial values of *some* of the quartic scalar couplings are small, and even though the top quark contributions to the  $\beta$ -functions are still negative, other couplings are allowed to have large values, which (in some cases) counterbalance any putative instabilities arising due to RG running. The 2HDM scalar potential is thus comparatively more stable than that of the SM.

Thus, we have obtained bounds on the square-mass differences of the heavier Higgs bosons in the parameter regime where the 2HDM remains valid up to the

Planck scale. If the 2HDM is realized in nature, this could provide an important check of the consistency of the model.

In addition, we explored the consequences of asserting flavor-alignment at the Planck scale on electroweak flavor observables. In the flavor-aligned 2HDM, all sources of FCNCs are eliminated at tree-level if flavor-alignment is imposed at the electroweak scale. If flavor-alignment is instead imposed at a higher energy scale, such as the Planck scale, perhaps enforced by new physics beyond the SM, then the tree-level flavor-alignment will be broken during one-loop RG running down to the electroweak scale, generating sources of FCNCs. These FCNCs are constrained by experimental bounds on flavor-changing observables, and subsequent bounds can be placed on the flavor-aligned 2HDM parameter space by requiring that the model be consistent with current experimental results.

We required that the alignment parameters at the high scale remain perturbative, that is, they avoid Landau poles during RG running. The effect of this requirement is that it provides an upper bound on the values of the alignment parameters at the Planck scale. This in turn provided an upper bound on the size of FCNCs generated at the electroweak scale. The flavor-changing observables we considered to constrain the flavor-aligned 2HDM parameter space were  $t \rightarrow uh$ ,  $t \rightarrow ch$ , and  $B_s \rightarrow \mu^+\mu^-$ . In the case of the top quark decays, we found that the branching ratios for both of these decay modes is far below that given by current

experimental bounds, and thus were not able to place constraints on the flavor-aligned 2HDM. The inability to place constraints using top decays is related to the requirement that the alignment parameters remain perturbative during RG running.

By considering the leptonic decay  $B_S \rightarrow \mu^+ \mu^-$  corresponding to the flavor transition  $b \rightarrow s$ , we placed constraints on the parameter space of the flavor-aligned 2HDM by requiring that the predicted tree-level branching ratio in the 2HDM not deviate significantly from that of the SM. Our bounds on the flavor-aligned 2HDM parameter space correspond to the small alignment parameter limit, that is, that the alignment parameters be much smaller than the bounds provided by requiring the parameters remain perturbative.

# Appendix A

## One-Loop Renormalization

### Group Equations for 2HDM

The one-loop RGEs for the SM used in this analysis are provided by Ref. [64]. The 2HDM one-loop RGEs in various bases are given in Refs. [38, 42, 81, 82, 83]. The one-loop RGEs found in the literature typically assume a 2HDM scalar potential with a  $\mathbb{Z}_2$  symmetry,  $\Phi_1 \rightarrow \Phi_1$ ,  $\Phi_2 \rightarrow -\Phi_2$ , to avoid FCNCs and/or are explicitly CP-conserving. Here, we present one-loop RGEs for the full 2HDM, using a basis-independent approach and making no CP assumptions.

## A.1 Yukawa Couplings

In a general 2HDM, the Higgs fermion interactions are governed by the following interaction Lagrangian:

$$-\mathcal{L}_Y = \overline{Q}_L^0 \tilde{\Phi}_{\bar{a}} \eta_a^{U,0} U_R^0 + \overline{Q}_L^0 \Phi_a (\eta_{\bar{a}}^{D,0})^\dagger D_R^0 + \overline{E}_L^0 \Phi_a (\eta_{\bar{a}}^{E,0})^\dagger E_R^0 + \text{h.c.}, \quad (\text{A.1})$$

summed over  $a, \bar{a} = 1, 2$ , where  $\Phi_{1,2}$  are the Higgs doublets,  $\tilde{\Phi}_{\bar{a}} \equiv i\sigma_2 \Phi_{\bar{a}}^*$ ,  $Q_L^0$  and  $E_L^0$  are the weak isospin quark and lepton doublets, and  $U_R^0, D_R^0, E_R^0$  are weak isospin quark and lepton singlets. [The right and left-handed fermion fields are defined as usual:  $\psi_{R,L} \equiv P_{R,L}\psi$ , where  $P_{R,L} \equiv \frac{1}{2}(1 \pm \gamma_5)$ .] Here,  $Q_L^0, E_L^0, U_R^0, D_R^0, E_R^0$  denote the interaction basis states, which are vectors in the quark and lepton flavor spaces, and  $\eta_1^{U,0}, \eta_2^{U,0}, \eta_1^{D,0}, \eta_2^{D,0}, \eta_1^{E,0}, \eta_2^{E,0}$  are  $3 \times 3$  matrices in quark and lepton flavor spaces.

The neutral Higgs states acquire vacuum expectation values,

$$\langle \Phi_a^0 \rangle = \frac{v \hat{v}_a}{\sqrt{2}}, \quad (\text{A.2})$$

where  $\hat{v}_a \hat{v}_a^* = 1$  and  $v = 246$  GeV. It is also convenient to define

$$\hat{w}_b \equiv \hat{v}_a^* \epsilon_{ab}, \quad (\text{A.3})$$

where  $\epsilon_{12} = -\epsilon_{21} = 1$  and  $\epsilon_{11} = \epsilon_{22} = 0$ .

It is convenient to define invariant and pseudo-invariant matrix Yukawa couplings [12, 40],

$$\kappa^{F,0} \equiv \hat{v}_a^* \eta_a^{F,0}, \quad \rho^{F,0} \equiv \hat{w}_a^* \eta_a^{F,0}, \quad (\text{A.4})$$

where  $F = U, D$  or  $E$ . Inverting these equations yields

$$\eta_a^{F,0} = \kappa^{F,0} \hat{v}_a + \rho^{F,0} \hat{w}_a. \quad (\text{A.5})$$

Note that under the  $U(2)$  transformation,  $\Phi_a \rightarrow U_{ab} \Phi_b$  [cf. eq. (A.41)],

$$\kappa^{F,0} \text{ is invariant and } \rho^{F,0} \rightarrow (\det U) \rho^{F,0}. \quad (\text{A.6})$$

The Higgs fields in the Higgs basis are defined by [40]

$$H_1 \equiv \hat{v}_a^* \Phi_a, \quad H_2 \equiv \hat{w}_a^* \Phi_a, \quad (\text{A.7})$$

which can be inverted to yield  $\Phi_a = H_1 \hat{v}_a + H_2 \hat{w}_a$ . One can rewrite eq. (A.1) in terms of the Higgs basis fields,

$$\begin{aligned} -\mathcal{L}_Y = & \overline{Q}_L^0 (\tilde{H}_1 \kappa^{U,0} + \tilde{H}_2 \rho^{U,0}) U_R^0 + \overline{Q}_L^0 (H_1 \kappa^{D,0\dagger} + H_1 \rho^{D,0\dagger}) D_R^0 \\ & + \overline{E}_L^0 (H_1 \kappa^{E,0\dagger} + H_1 \rho^{E,0\dagger}) E_R^0 + \text{h.c.}, \end{aligned} \quad (\text{A.8})$$

The next step is to identify the quark and lepton mass-eigenstates. This is accomplished by replacing  $H_1 \rightarrow (0, v/\sqrt{2})$  and performing unitary transformations of the left and right-handed up and down quark multiplets such that the resulting quark and charged lepton mass matrices are diagonal with non-negative entries. In more detail, we define:

$$\begin{aligned} P_L U &= V_L^U P_L U^0, & P_R U &= V_R^U P_R U^0, & P_L D &= V_L^D P_L D^0, & P_R D &= V_R^D P_R D^0, \\ P_L E &= V_L^E P_L E^0, & P_R E &= V_R^E P_R E^0, & P_L N &= V_L^E P_L N^0, \end{aligned} \quad (\text{A.9})$$

and the Cabibbo-Kobayashi-Maskawa (CKM) matrix is defined as  $K \equiv V_L^U V_L^{D\dagger}$ . Note that for the neutrino fields, we are free to choose  $V_L^N = V_L^E$  since neutrinos are exactly massless in this analysis. (Here we are ignoring the right-handed neutrino sector, which gives mass to neutrinos via the seesaw mechanism).

In particular, the unitary matrices  $V_L^F$  and  $V_R^F$  (for  $F = U, D$  and  $E$ ) are chosen such that

$$M_U = \frac{v}{\sqrt{2}} V_L^U \kappa^{U,0} V_R^{U\dagger} = \text{diag}(m_u, m_c, m_t), \quad (\text{A.10})$$

$$M_D = \frac{v}{\sqrt{2}} V_L^D \kappa^{D,0} V_R^{D\dagger} = \text{diag}(m_d, m_s, m_b), \quad (\text{A.11})$$

$$M_E = \frac{v}{\sqrt{2}} V_L^E \kappa^{E,0} V_R^{E\dagger} = \text{diag}(m_e, m_\mu, m_\tau). \quad (\text{A.12})$$

It is convenient to define

$$\kappa^U = V_L^U \kappa^{U,0} V_R^{U\dagger}, \quad \kappa^D = V_R^D \kappa^{D,0} V_L^{D\dagger}, \quad \kappa^E = V_R^D \kappa^{E,0} V_L^{E\dagger}, \quad (\text{A.13})$$

$$\rho^U = V_L^U \rho^{U,0} V_R^{U\dagger}, \quad \rho^D = V_R^D \rho^{D,0} V_L^{D\dagger}, \quad \rho^E = V_R^D \rho^{E,0} V_L^{E\dagger}. \quad (\text{A.14})$$

Eq. (A.6) implies that under the  $U(2)$  transformation,  $\Phi_a \rightarrow U_{a\bar{b}} \Phi_b$ ,

$$\kappa^F \text{ is invariant and } \rho^F \rightarrow (\det U) \rho^F, \quad (\text{A.15})$$

for  $F = U, D$  and  $E$ . Indeed,  $\kappa^F$  is invariant since eqs. (A.10)–(A.12) imply that

$$M_F = \frac{v}{\sqrt{2}} \kappa^F, \quad (\text{A.16})$$

which is a physical observable. The matrices  $\rho^U$ ,  $\rho^D$  and  $\rho^E$  are independent pseudoinvariant complex  $3 \times 3$  matrices. The Higgs-fermion interactions given in

eq. (A.8) can be rewritten in terms of the quark and lepton mass eigenstates,

$$\begin{aligned}
-\mathcal{L}_Y &= \bar{U}_L(\kappa^U H_1^{0\dagger} + \rho^U H_2^{0\dagger})U_R - \bar{D}_L K^\dagger(\kappa^U H_1^- + \rho^U H_2^-)U_R \\
&+ \bar{U}_L K(\kappa^{D\dagger} H_1^+ + \rho^{D\dagger} H_2^+)D_R + \bar{D}_L(\kappa^{D\dagger} H_1^0 + \rho^{D\dagger} H_2^0)D_R \\
&+ \bar{N}_L(\kappa^{E\dagger} H_1^+ + \rho^{E\dagger} H_2^+)E_R + \bar{E}_L(\kappa^{E\dagger} H_1^0 + \rho^{E\dagger} H_2^0)E_R + \text{h.c.} \quad (\text{A.17})
\end{aligned}$$

We now write down the renormalization group equations (RGEs) for the Yukawa matrices  $\eta_a^{U,0}$ ,  $\eta_a^{D,0}$  and  $\eta_a^{E,0}$ . Defining  $\mathcal{D} \equiv 16\pi^2\mu(d/d\mu)$ , the RGEs are given by [38]:

$$\begin{aligned}
\mathcal{D}\eta_a^{U,0} &= -(8g_s^2 + \frac{9}{4}g^2 + \frac{17}{12}g'^2)\eta_a^{U,0} + \left\{ 3\text{Tr}[\eta_a^{U,0}(\eta_b^{U,0})^\dagger + \eta_a^{D,0}(\eta_b^{D,0})^\dagger] \right. \\
&\quad \left. + \text{Tr}[\eta_a^{E,0}(\eta_b^{E,0})^\dagger] \right\} \eta_b^{U,0} - 2(\eta_b^{D,0})^\dagger \eta_a^{D,0} \eta_b^{U,0} + \eta_a^{U,0}(\eta_b^{U,0})^\dagger \eta_b^{U,0} \\
&\quad + \frac{1}{2}(\eta_b^{D,0})^\dagger \eta_b^{D,0} \eta_a^{U,0} + \frac{1}{2}\eta_b^{U,0}(\eta_b^{U,0})^\dagger \eta_a^{U,0}, \quad (\text{A.18})
\end{aligned}$$

$$\begin{aligned}
\mathcal{D}\eta_a^{D,0} &= -(8g_s^2 + \frac{9}{4}g^2 + \frac{5}{12}g'^2)\eta_a^{D,0} + \left\{ 3\text{Tr}[(\eta_b^{D,0})^\dagger \eta_a^{D,0} + (\eta_b^{U,0})^\dagger \eta_a^{U,0}] \right. \\
&\quad \left. + \text{Tr}[(\eta_b^{E,0})^\dagger \eta_a^{E,0}] \right\} \eta_b^{D,0} - 2\eta_b^{D,0} \eta_a^{U,0}(\eta_b^{U,0})^\dagger + \eta_b^{D,0}(\eta_b^{D,0})^\dagger \eta_a^{D,0} \\
&\quad + \frac{1}{2}\eta_a^{D,0} \eta_b^{U,0}(\eta_b^{U,0})^\dagger + \frac{1}{2}\eta_a^{D,0}(\eta_b^{D,0})^\dagger \eta_b^{D,0}, \quad (\text{A.19})
\end{aligned}$$

$$\begin{aligned}
\mathcal{D}\eta_a^{E,0} &= -(\frac{9}{4}g^2 + \frac{15}{4}g'^2)\eta_a^{E,0} + \left\{ 3\text{Tr}[(\eta_b^{D,0})^\dagger \eta_a^{D,0} + (\eta_b^{U,0})^\dagger \eta_a^{U,0}] \right. \\
&\quad \left. + \text{Tr}[(\eta_b^{E,0})^\dagger \eta_a^{E,0}] \right\} \eta_b^{E,0} + \eta_b^{E,0}(\eta_b^{E,0})^\dagger \eta_a^{E,0} \\
&\quad + \frac{1}{2}\eta_a^{E,0}(\eta_b^{E,0})^\dagger \eta_b^{E,0}. \quad (\text{A.20})
\end{aligned}$$

The RGEs above are true for any basis choice. Thus, they must also be true

in the Higgs basis in which  $\hat{v} = (1, 0)$  and  $\hat{w} = (0, 1)$ . In this case, we can simply choose  $\eta_1^{F,0} = \kappa^{F,0}$  and  $\eta_2^{F,0} = \rho^{F,0}$  to obtain the RGEs for the  $\kappa^{F,0}$  and  $\rho^{F,0}$ . Alternatively, we can multiply eqs. (A.19)–(A.20) first by  $\hat{v}_a^*$  and then by  $\hat{w}_a^*$ . Expanding  $\eta_{\hat{a}}^\dagger$ , which appears on the right-hand sides of eqs. (A.19)–(A.20), in terms of  $\kappa^\dagger$  and  $\rho^\dagger$  using eq. (A.5), we again obtain the RGEs for the  $\kappa^{F,0}$  and  $\rho^{F,0}$ . Of course, both methods must yield the same results, since the diagonalization matrices employed in eqs. (A.10)–(A.12) are defined as those that bring the mass matrices to their diagonal form at the electroweak scale. No scale dependence is assumed in the diagonalization matrices, and as such they are not affected by the operators  $\mathcal{D}$ .

$$\begin{aligned}
\mathcal{D}\kappa^{U,0} = & -\left(8g_s^2 + \frac{9}{4}g^2 + \frac{17}{12}g'^2\right)\kappa^{U,0} + \left\{3\text{Tr}[\kappa^{U,0}\kappa^{U,0\dagger} + \kappa^{D,0}\kappa^{D,0\dagger}] \right. \\
& \left. + \text{Tr}[\kappa^{E,0}\kappa^{E,0\dagger}]\right\}\kappa^{U,0} + \left\{3\text{Tr}[\kappa^{U,0}\rho^{U,0\dagger} + \kappa^{D,0}\rho^{D,0\dagger}] \right. \\
& \left. + \text{Tr}[\kappa^{E,0}\rho^{E,0\dagger}]\right\}\rho^{U,0} - 2(\kappa^{D,0\dagger}\kappa^{D,0}\kappa^{U,0} + \rho^{D,0\dagger}\kappa^{D,0}\rho^{U,0}) \\
& + \kappa^{U,0}(\kappa^{U,0\dagger}\kappa^{U,0} + \rho^{U,0\dagger}\rho^{U,0}) + \frac{1}{2}(\kappa^{D,0\dagger}\kappa^{D,0} + \rho^{D,0\dagger}\rho^{D,0})\kappa^{U,0} \\
& + \frac{1}{2}(\kappa^{U,0}\kappa^{U,0\dagger} + \rho^{U,0}\rho^{U,0\dagger})\kappa^{U,0}, \tag{A.21}
\end{aligned}$$

$$\begin{aligned}
\mathcal{D}\rho^{U,0} = & -\left(8g_s^2 + \frac{9}{4}g^2 + \frac{17}{12}g'^2\right)\rho^{U,0} + \left\{3\text{Tr}[\rho^{U,0}\kappa^{U,0\dagger} + \rho^{D,0}\kappa^{D,0\dagger}] \right. \\
& + \text{Tr}[\rho^{E,0}\kappa^{E,0\dagger}] \left. \right\}\kappa^{U,0} + \left\{3\text{Tr}[\rho^{U,0}\rho^{U,0\dagger} + \rho^{D,0}\rho^{D,0\dagger}] \right. \\
& + \text{Tr}[\rho^{E,0}\rho^{E,0\dagger}] \left. \right\}\rho^{U,0} - 2(\kappa^{D,0\dagger}\rho^{D,0}\kappa^{U,0} + \rho^{D,0\dagger}\rho^{D,0}\rho^{U,0}) \\
& + \rho^{U,0}(\kappa^{U,0\dagger}\kappa^{U,0} + \rho^{U,0\dagger}\rho^{U,0}) + \frac{1}{2}(\kappa^{D,0\dagger}\kappa^{D,0} + \rho^{D,0\dagger}\rho^{D,0})\rho^{U,0} \\
& + \frac{1}{2}(\kappa^{U,0}\kappa^{U,0\dagger} + \rho^{U,0}\rho^{U,0\dagger})\rho^{U,0}, \tag{A.22}
\end{aligned}$$

$$\begin{aligned}
\mathcal{D}\kappa^{D,0} = & -\left(8g_s^2 + \frac{9}{4}g^2 + \frac{5}{12}g'^2\right)\kappa^{D,0} + \left\{3\text{Tr}[\kappa^{D,0\dagger}\kappa^{D,0} + \kappa^{U,0\dagger}\kappa^{U,0}] \right. \\
& + \text{Tr}[\kappa^{E,0\dagger}\kappa^{E,0}] \left. \right\}\kappa^{D,0} + \left\{3\text{Tr}[\rho^{D,0\dagger}\kappa^{D,0} + \rho^{U,0\dagger}\kappa^{U,0}] \right. \\
& + \text{Tr}[\rho^{E,0\dagger}\kappa^{E,0}] \left. \right\}\rho^{D,0} - 2(\kappa^{D,0}\kappa^{U,0}\kappa^{U,0\dagger} + \rho^{D,0}\kappa^{U,0}\rho^{U,0\dagger}) \\
& + (\kappa^{D,0}\kappa^{D,0\dagger} + \rho^{D,0}\rho^{D,0\dagger})\kappa^{D,0} + \frac{1}{2}\kappa^{D,0}(\kappa^{U,0}\kappa^{U,0\dagger} + \rho^{U,0}\rho^{U,0\dagger}) \\
& + \frac{1}{2}\kappa^{D,0}(\kappa^{D,0\dagger}\kappa^{D,0} + \rho^{D,0\dagger}\rho^{D,0}), \tag{A.23}
\end{aligned}$$

$$\begin{aligned}
\mathcal{D}\rho^{D,0} = & -\left(8g_s^2 + \frac{9}{4}g^2 + \frac{5}{12}g'^2\right)\rho^{D,0} + \left\{3\text{Tr}[\kappa^{D,0\dagger}\rho^{D,0} + \kappa^{U,0\dagger}\rho^{U,0}] \right. \\
& + \text{Tr}[\kappa^{E,0\dagger}\rho^{E,0}] \left. \right\}\kappa^{D,0} + \left\{3\text{Tr}[\rho^{D,0\dagger}\rho^{D,0} + \rho^{U,0\dagger}\rho^{U,0}] \right. \\
& + \text{Tr}[\rho^{E,0\dagger}\rho^{E,0}] \left. \right\}\rho^{D,0} - 2(\kappa^{D,0}\rho^{U,0}\kappa^{U,0\dagger} + \rho^{D,0}\rho^{U,0}\rho^{U,0\dagger}) \\
& + (\kappa^{D,0}\kappa^{D,0\dagger} + \rho^{D,0}\rho^{D,0\dagger})\rho^{D,0} + \frac{1}{2}\rho^{D,0}(\kappa^{U,0}\kappa^{U,0\dagger} + \rho^{U,0}\rho^{U,0\dagger}) \\
& + \frac{1}{2}\rho^{D,0}(\kappa^{D,0\dagger}\kappa^{D,0} + \rho^{D,0\dagger}\rho^{D,0}), \tag{A.24}
\end{aligned}$$

$$\begin{aligned}
\mathcal{D}\kappa^{E,0} = & -\left(\frac{9}{4}g^2 + \frac{15}{4}g'^2\right)\kappa^{E,0} + \left\{ 3\text{Tr}[\kappa^{D,0\dagger}\kappa^{D,0} + \kappa^{U,0\dagger}\kappa^{U,0}] \right. \\
& + \text{Tr}[\kappa^{E,0\dagger}\kappa^{E,0}] \left. \right\} \kappa^{E,0} + \left\{ 3\text{Tr}[\rho^{D,0\dagger}\rho^{D,0} + \rho^{U,0\dagger}\rho^{U,0}] \right. \\
& + \text{Tr}[\rho^{E,0\dagger}\rho^{E,0}] \left. \right\} \rho^{E,0} + (\kappa^{E,0}\kappa^{E,0\dagger} + \rho^{E,0}\rho^{E,0\dagger})\kappa^{E,0} \\
& + \frac{1}{2}\kappa^{E,0}(\kappa^{E,0\dagger}\kappa^{E,0} + \rho^{E,0\dagger}\rho^{E,0}), \tag{A.25}
\end{aligned}$$

$$\begin{aligned}
\mathcal{D}\rho^{E,0} = & -\left(\frac{9}{4}g^2 + \frac{15}{4}g'^2\right)\rho^{E,0} + \left\{ 3\text{Tr}[\kappa^{D,0\dagger}\rho^{D,0} + \kappa^{U,0\dagger}\rho^{U,0}] \right. \\
& + \text{Tr}[\kappa^{E,0\dagger}\rho^{E,0}] \left. \right\} \kappa^{E,0} + \left\{ 3\text{Tr}[\rho^{D,0\dagger}\rho^{D,0} + \rho^{U,0\dagger}\rho^{U,0}] \right. \\
& + \text{Tr}[\rho^{E,0\dagger}\rho^{E,0}] \left. \right\} \rho^{E,0} + (\kappa^{E,0}\kappa^{E,0\dagger} + \rho^{E,0}\rho^{E,0\dagger})\rho^{E,0} \\
& + \frac{1}{2}\rho^{E,0}(\kappa^{E,0\dagger}\kappa^{E,0} + \rho^{E,0\dagger}\rho^{E,0}). \tag{A.26}
\end{aligned}$$

Using eqs. (A.13) and (A.14), we immediately obtain the RGEs for the  $\kappa^F$  and  $\rho^F$ ,

$$\begin{aligned}
\mathcal{D}\kappa^U = & -(8g_s^2 + \frac{9}{4}g^2 + \frac{17}{12}g'^2)\kappa^U + \left\{ 3\text{Tr}[\kappa^U\kappa^{U\dagger} + \kappa^D\kappa^{D\dagger}] + \text{Tr}[\kappa^E\kappa^{E\dagger}] \right\} \kappa^U \\
& + \left\{ 3\text{Tr}[\kappa^U\rho^{U\dagger} + \kappa^D\rho^{D\dagger}] + \text{Tr}[\kappa^E\rho^{E\dagger}] \right\} \rho^U - 2K(\kappa^{D\dagger}\kappa^D K^\dagger\kappa^U \\
& + \rho^{D\dagger}\kappa^D K^\dagger\rho^U) + \kappa^U(\kappa^{U\dagger}\kappa^U + \rho^{U\dagger}\rho^U) + \frac{1}{2}K(\kappa^{D\dagger}\kappa^D + \rho^{D\dagger}\rho^D)K^\dagger\kappa^U \\
& + \frac{1}{2}(\kappa^U\kappa^{U\dagger} + \rho^U\rho^{U\dagger})\kappa^U, \tag{A.27}
\end{aligned}$$

$$\begin{aligned}
\mathcal{D}\rho^U &= -(8g_s^2 + \frac{9}{4}g^2 + \frac{17}{12}g'^2)\rho^U + \left\{ 3\text{Tr}[\rho^U \kappa^{U\dagger} + \rho^D \kappa^{D\dagger}] + \text{Tr}[\rho^E \kappa^{E\dagger}] \right\} \kappa^U \\
&+ \left\{ 3\text{Tr}[\rho^U \rho^{U\dagger} + \rho^D \rho^{D\dagger}] + \text{Tr}[\rho^E \rho^{E\dagger}] \right\} \rho^U - 2K(\kappa^{D\dagger} \rho^D K^\dagger \kappa^U \\
&+ \rho^{D\dagger} \rho^D K^\dagger \rho^U) + \rho^U(\kappa^{U\dagger} \kappa^U + \rho^{U\dagger} \rho^U) + \frac{1}{2}K(\kappa^{D\dagger} \kappa^D + \rho^{D\dagger} \rho^D)K^\dagger \rho^U \\
&+ \frac{1}{2}(\kappa^U \kappa^{U\dagger} + \rho^U \rho^{U\dagger})\rho^U, \tag{A.28}
\end{aligned}$$

$$\begin{aligned}
\mathcal{D}\kappa^D &= -(8g_s^2 + \frac{9}{4}g^2 + \frac{5}{12}g'^2)\kappa^D + \left\{ 3\text{Tr}[\kappa^{D\dagger} \kappa^D + \kappa^{U\dagger} \kappa^U] + \text{Tr}[\kappa^{E\dagger} \kappa^E] \right\} \kappa^D \\
&+ \left\{ 3\text{Tr}[\rho^{D\dagger} \kappa^D + \rho^{U\dagger} \kappa^U] + \text{Tr}[\rho^{E\dagger} \kappa^E] \right\} \rho^D - 2(\kappa^D K^\dagger \kappa^U \kappa^{U\dagger} \\
&+ \rho^{D\dagger} \rho^D K^\dagger \rho^U)K + (\kappa^D \kappa^{D\dagger} + \rho^D \rho^{D\dagger})\kappa^D + \frac{1}{2}\kappa^D K^\dagger(\kappa^U \kappa^{U\dagger} + \rho^U \rho^{U\dagger})K \\
&+ \frac{1}{2}\kappa^D(\kappa^{D\dagger} \kappa^D + \rho^{D\dagger} \rho^D), \tag{A.29}
\end{aligned}$$

$$\begin{aligned}
\mathcal{D}\rho^D &= -(8g_s^2 + \frac{9}{4}g^2 + \frac{5}{12}g'^2)\rho^D + \left\{ 3\text{Tr}[\kappa^{D\dagger} \rho^D + \kappa^{U\dagger} \rho^U] + \text{Tr}[\kappa^{E\dagger} \rho^E] \right\} \kappa^D \\
&+ \left\{ 3\text{Tr}[\rho^{D\dagger} \rho^D + \rho^{U\dagger} \rho^U] + \text{Tr}[\rho^{E\dagger} \rho^E] \right\} \rho^D - 2(\kappa^D K^\dagger \rho^U \kappa^{U\dagger} \\
&+ \rho^{D\dagger} \rho^D K^\dagger \rho^U)K + (\kappa^D \kappa^{D\dagger} + \rho^D \rho^{D\dagger})\rho^D + \frac{1}{2}\rho^D K^\dagger(\kappa^U \kappa^{U\dagger} + \rho^U \rho^{U\dagger})K \\
&+ \frac{1}{2}\rho^D(\kappa^{D\dagger} \kappa^D + \rho^{D\dagger} \rho^D), \tag{A.30}
\end{aligned}$$

$$\begin{aligned}
\mathcal{D}\kappa^E &= -(\frac{9}{4}g^2 + \frac{15}{4}g'^2)\kappa^E + \left\{ 3\text{Tr}[\kappa^{D\dagger} \kappa^D + \kappa^{U\dagger} \kappa^U] + \text{Tr}[\kappa^{E\dagger} \kappa^E] \right\} \kappa^E \\
&+ \left\{ 3\text{Tr}[\rho^{D\dagger} \kappa^D + \rho^{U\dagger} \kappa^U] + \text{Tr}[\rho^{E\dagger} \kappa^E] \right\} \rho^E + (\kappa^E \kappa^{E\dagger} + \rho^E \rho^{E\dagger})\kappa^E \\
&+ \frac{1}{2}\kappa^E(\kappa^{E\dagger} \kappa^E + \rho^{E\dagger} \rho^E), \tag{A.31}
\end{aligned}$$

$$\begin{aligned}
\mathcal{D}\rho^E &= -\left(\frac{9}{4}g^2 + \frac{15}{4}g'^2\right)\rho^E + \left\{3\text{Tr}[\kappa^{D\dagger}\rho^D + \kappa^{U\dagger}\rho^U] + \text{Tr}[\kappa^{E\dagger}\rho^E]\right\}\kappa^E \\
&+ \left\{3\text{Tr}[\rho^{D\dagger}\rho^D + \rho^{U\dagger}\rho^U] + \text{Tr}[\rho^{E\dagger}\rho^E]\right\}\rho^E + (\kappa^E\kappa^{E\dagger} + \rho^E\rho^{E\dagger})\rho^E \\
&+ \frac{1}{2}\rho^E(\kappa^{E\dagger}\kappa^E + \rho^{E\dagger}\rho^E). \tag{A.32}
\end{aligned}$$

## A.2 Scalar Parameters

The 2HDM scalar potential in a generic basis shown in eq. (2.1) can be written in a more compact form,

$$\mathcal{V} = Y_{ab}(\Phi_a^\dagger\Phi_b) + \frac{1}{2}Z_{ab\bar{c}\bar{d}}(\Phi_a^\dagger\Phi_b)(\Phi_{\bar{c}}^\dagger\Phi_{\bar{d}}). \tag{A.33}$$

Hermiticity requires that  $Y_{ab} = Y_{ba}^*$  and  $Z_{ab\bar{c}\bar{d}} = Z_{\bar{d}\bar{c}ba}^*$ . In addition, the form of the scalar potential given in eq. (A.33) implies that  $Z_{ab\bar{c}\bar{d}} = Z_{\bar{c}\bar{d}ab}$ . The full one-loop beta-function for  $Z_{ab\bar{c}\bar{d}}$  is given by,

$$\begin{aligned}
\mathcal{D}Z_{ab\bar{c}\bar{d}} &= 4Z_{abe\bar{f}}Z_{cd\bar{f}\bar{e}} + 2Z_{af\bar{e}\bar{d}}Z_{cd\bar{f}\bar{e}} + 2Z_{af\bar{c}\bar{e}}Z_{f\bar{b}e\bar{d}} + 2Z_{abe\bar{f}}Z_{c\bar{e}f\bar{d}} + 2Z_{a\bar{e}f\bar{b}}Z_{c\bar{d}e\bar{f}} \\
&- (3g'^2 + 9g^2)Z_{ab\bar{c}\bar{d}} + \frac{3}{4}(3g^4 - 2g'^2g^2 + g'^4)\delta_{ab}\delta_{\bar{c}\bar{d}} + (3g'^2g^2)\delta_{a\bar{d}}\delta_{\bar{c}b} \\
&- 4N_c\text{Tr}[\eta_a^Q\eta_b^{Q\dagger}\eta_c^Q\eta_d^{Q\dagger}] + 4(\text{Tr}[\eta_{\bar{e}}^{Q\dagger}\eta_a^Q]Z_{e\bar{b}c\bar{d}} + \text{Tr}[\eta_b^{Q\dagger}\eta_e^Q]Z_{a\bar{e}c\bar{d}} \\
&+ \text{Tr}[\eta_{\bar{e}}^{Q\dagger}\eta_c^Q]Z_{a\bar{b}e\bar{d}} + \text{Tr}[\eta_d^{Q\dagger}\eta_e^Q]Z_{a\bar{b}c\bar{e}}). \tag{A.34}
\end{aligned}$$

The squared-mass and coupling coefficients of the 2HDM scalar potential in

the Higgs basis [cf. eq. (2.3)] can be written in the form of invariants or pseudoinvariants with respect to the U(2) transformations,  $\Phi_a \rightarrow U_{ab}\Phi_b$ , as shown in Ref. [12]. The three squared-mass parameters are given by

$$Y_1 \equiv Y_{a\bar{b}} \widehat{v}_a^* \widehat{v}_b, \quad Y_2 \equiv Y_{a\bar{b}} \widehat{w}_a^* \widehat{w}_b, \quad Y_3 \equiv Y_{a\bar{b}} \widehat{v}_a^* \widehat{w}_b, \quad (\text{A.35})$$

and seven coupling parameters are given by

$$Z_1 \equiv Z_{a\bar{b}c\bar{d}} \widehat{v}_a^* \widehat{v}_b \widehat{v}_c^* \widehat{v}_d, \quad Z_2 \equiv Z_{a\bar{b}c\bar{d}} \widehat{w}_a^* \widehat{w}_b \widehat{w}_c^* \widehat{w}_d, \quad (\text{A.36})$$

$$Z_3 \equiv Z_{a\bar{b}c\bar{d}} \widehat{v}_a^* \widehat{v}_b \widehat{w}_c^* \widehat{w}_d, \quad Z_4 \equiv Z_{a\bar{b}c\bar{d}} \widehat{w}_a^* \widehat{v}_b \widehat{v}_c^* \widehat{w}_d, \quad (\text{A.37})$$

$$Z_5 \equiv Z_{a\bar{b}c\bar{d}} \widehat{v}_a^* \widehat{w}_b \widehat{v}_c^* \widehat{w}_d, \quad (\text{A.38})$$

$$Z_6 \equiv Z_{a\bar{b}c\bar{d}} \widehat{v}_a^* \widehat{v}_b \widehat{v}_c^* \widehat{w}_d, \quad (\text{A.39})$$

$$Z_7 \equiv Z_{a\bar{b}c\bar{d}} \widehat{v}_a^* \widehat{w}_b \widehat{w}_c^* \widehat{w}_d. \quad (\text{A.40})$$

Note that under a U(2) transformation,  $\widehat{v}_a \rightarrow U_{a\bar{b}}\widehat{v}_b$ , whereas

$$\widehat{w}_a \rightarrow (\det U)^{-1} U_{a\bar{b}}\widehat{w}_b. \quad (\text{A.41})$$

Consequently,  $Y_1, Y_2, Z_{1,2,3,4}$  are real U(2)-invariants, whereas  $Y_3, Z_{5,6,7}$  are potentially complex U(2)-pseudoinvariants, which are rephased under a U(2) transformation,

$$[Y_3, Z_6, Z_7] \rightarrow (\det U)^{-1} [Y_3, Z_6, Z_7] \quad \text{and} \quad Z_5 \rightarrow (\det U)^{-2} Z_5. \quad (\text{A.42})$$

Using the above results in eq. (A.34), the one-loop RGEs for the quartic cou-

plings in the Higgs basis are:

$$\begin{aligned}
\mathcal{D}Z_1 &= 12Z_1^2 + 4Z_3^2 + 4Z_3Z_4 + 2Z_4^2 + 2|Z_5|^2 + 24|Z_6|^2 - (3g'^2 + 9g^2)Z_1 \\
&\quad + \frac{3}{4}(g'^4 + 2g'^2g^2 + 3g^4) - 4N_c \text{Tr}[\kappa^{Q\dagger}\kappa^Q\kappa^{Q\dagger}\kappa^Q] + 16(2\text{Tr}[\kappa^{Q\dagger}\kappa^Q]Z_1 \\
&\quad + \text{Tr}[\kappa^{Q\dagger}\rho^Q]Z_6 + \text{Tr}[\rho^{Q\dagger}\kappa^Q]Z_6^*), \tag{A.43}
\end{aligned}$$

$$\begin{aligned}
\mathcal{D}Z_2 &= 12Z_2^2 + 4Z_3^2 + 4Z_3Z_4 + 2Z_4^2 + 2|Z_5|^2 + 24|Z_7|^2 - (3g'^2 + 9g^2)Z_2 \\
&\quad + \frac{3}{4}(g'^4 + 2g'^2g^2 + 3g^4) - 4N_c \text{Tr}[\rho^{Q\dagger}\rho^Q\rho^{Q\dagger}\rho^Q] \\
&\quad + 8(2\text{Tr}[\rho^{Q\dagger}\rho^Q]Z_2 + \text{Tr}[\kappa^{Q\dagger}\rho^Q]Z_7 + \text{Tr}[\rho^{Q\dagger}\kappa^Q]Z_7^*), \tag{A.44}
\end{aligned}$$

$$\begin{aligned}
\mathcal{D}Z_3 &= 2(Z_1 + Z_2)(3Z_3 + Z_4) + 4Z_3^2 + 2Z_4^2 + 2|Z_5|^2 + 4|Z_6|^2 + 4|Z_7|^2 + 8Z_6Z_7^* \\
&\quad + 8Z_6^*Z_7 - (3g'^2 + 9g^2)Z_3 + \frac{3}{4}(g'^4 - 2g'^2g^2 + 3g^4) - 4N_c \text{Tr}[\kappa^{Q\dagger}\kappa^Q\rho^{Q\dagger}\rho^Q] \\
&\quad + 4(2\text{Tr}[\kappa^{Q\dagger}\kappa^Q]Z_3 + 2\text{Tr}[\rho^{Q\dagger}\rho^Q]Z_3 + \text{Tr}[\kappa^{Q\dagger}\rho^Q]Z_6 + \text{Tr}[\rho^{Q\dagger}\kappa^Q]Z_6^* \\
&\quad + \text{Tr}[\kappa^{Q\dagger}\rho^Q]Z_7 + \text{Tr}[\rho^{Q\dagger}\kappa^Q]Z_7^*), \tag{A.45}
\end{aligned}$$

$$\begin{aligned}
\mathcal{D}Z_4 &= 2(Z_1 + Z_2)Z_4 + 8Z_3Z_4 + 4Z_4^2 + 8|Z_5|^2 + 10|Z_6|^2 + 10|Z_7|^2 + 2Z_6Z_7^* \\
&\quad + 2Z_6^*Z_7 - (3g'^2 + 9g^2)Z_4 + \frac{3}{2}g'^2g^2 - 4N_c \text{Tr}[\kappa^{Q\dagger}\rho^Q\rho^{Q\dagger}\kappa^Q] \\
&\quad + 4(2\text{Tr}[\kappa^{Q\dagger}\kappa^Q]Z_4 + 2\text{Tr}[\rho^{Q\dagger}\rho^Q]Z_4 + \text{Tr}[\kappa^{Q\dagger}\rho^Q]Z_6 + \text{Tr}[\rho^{Q\dagger}\kappa^Q]Z_6^* \\
&\quad + \text{Tr}[\kappa^{Q\dagger}\rho^Q]Z_7 + \text{Tr}[\rho^{Q\dagger}\kappa^Q]Z_7^*), \tag{A.46}
\end{aligned}$$

$$\begin{aligned}
\mathcal{D}Z_5 &= 2Z_5(Z_1 + Z_2 + 4Z_3 + 6Z_4) + 10Z_6^2 + 10Z_7^2 + 4Z_6Z_7 - (3g'^2 + 9g^2)Z_5 \\
&\quad - 4N_c \text{Tr}[\kappa^{Q\dagger} \rho^Q \kappa^{Q\dagger} \rho^Q] + 8(\text{Tr}[\kappa^{Q\dagger} \kappa^Q] Z_5 + \text{Tr}[\rho^{Q\dagger} \rho^Q] Z_5 + \text{Tr}[\rho^{Q\dagger} \kappa^Q] Z_6 \\
&\quad + \text{Tr}[\rho^{Q\dagger} \kappa^Q] Z_7), \tag{A.47}
\end{aligned}$$

$$\begin{aligned}
\mathcal{D}Z_6 &= 12Z_1Z_6 + 6Z_3(Z_6 + Z_7) + 4Z_4(2Z_6 + Z_7) + 2Z_5(5Z_6^* + Z_7^*) \\
&\quad - (3g'^2 + 9g^2)Z_6 - 4N_c \text{Tr}[\kappa^{Q\dagger} \kappa^Q \kappa^{Q\dagger} \rho^Q] + 4(3\text{Tr}[\kappa^{Q\dagger} \kappa^Q] Z_6 \\
&\quad + \text{Tr}[\rho^{Q\dagger} \rho^Q] Z_6 + \text{Tr}[\rho^{Q\dagger} \kappa^Q] Z_1 + \text{Tr}[\rho^{Q\dagger} \kappa^Q] Z_3 + \text{Tr}[\rho^{Q\dagger} \kappa^Q] Z_4 \\
&\quad + \text{Tr}[\kappa^{Q\dagger} \rho^Q] Z_5), \tag{A.48}
\end{aligned}$$

$$\begin{aligned}
\mathcal{D}Z_7 &= 12Z_2Z_7 + 6Z_3(Z_6 + Z_7) + 4Z_4(Z_6 + 2Z_7) + 2Z_5(Z_6^* + 5Z_7^*) \\
&\quad - (3g'^2 + 9g^2)Z_7 - 4N_c \text{Tr}[\kappa^{Q\dagger} \rho^Q \rho^{Q\dagger} \rho^Q] + 4(3\text{Tr}[\rho^{Q\dagger} \rho^Q] Z_7 \\
&\quad + \text{Tr}[\kappa^{Q\dagger} \kappa^Q] Z_7 + \text{Tr}[\rho^{Q\dagger} \kappa^Q] Z_2 + \text{Tr}[\rho^{Q\dagger} \kappa^Q] Z_3 + \text{Tr}[\rho^{Q\dagger} \kappa^Q] Z_4 \\
&\quad + \text{Tr}[\kappa^{Q\dagger} \rho^Q] Z_5). \tag{A.49}
\end{aligned}$$

Finally, we note that the anomalous dimensions, which contribute to the quartic coupling beta-functions, are given by

$$\gamma_{a\bar{b}} = -\frac{1}{32\pi^2}(3g'^2 + 9g^2)\delta_{a\bar{b}} + \frac{1}{4\pi^2}\text{Tr}[\eta_a^Q \eta_{\bar{b}}^{Q\dagger}]. \tag{A.50}$$

# Bibliography

- [1] Dario Buttazzo, Giuseppe Degrassi, Pier Paolo Giardino, Gian F. Giudice, Filippo Sala, et al. Investigating the near-criticality of the Higgs boson. *JHEP*, 1312:089, 2013.
- [2] Giuseppe Degrassi, Stefano Di Vita, Joan Elias-Miro, Jose R. Espinosa, Gian F. Giudice, et al. Higgs mass and vacuum stability in the Standard Model at NNLO. *JHEP*, 1208:098, 2012.
- [3] Pedro Ferreira, Howard E. Haber, and Edward Santos. Preserving the validity of the Two-Higgs Doublet Model up to the Planck scale. 2015.
- [4] Stefania Gori, Howard Haber, and Edward Santos. In preparation.
- [5] Georges Aad et al. Observation of a new particle in the search for the Standard Model Higgs boson with the ATLAS detector at the LHC. *Phys.Lett.*, B716:1–29, 2012.

- [6] Serguei Chatrchyan et al. Observation of a new boson at a mass of 125 GeV with the CMS experiment at the LHC. *Phys.Lett.*, B716:30–61, 2012.
- [7] Fedor Bezrukov, Mikhail Yu. Kalmykov, Bernd A. Kniehl, and Mikhail Shaposhnikov. Higgs Boson Mass and New Physics. *JHEP*, 1210:140, 2012.
- [8] Gian Francesco Giudice. Naturally Speaking: The Naturalness Criterion and Physics at the LHC. 2008.
- [9] James D. Wells. The Utility of Naturalness, and how its Application to Quantum Electrodynamics envisages the Standard Model and Higgs Boson. *Stud.Hist.Philos.Mod.Phys.*, 49:102–108, 2015.
- [10] T.D. Lee. A Theory of Spontaneous T Violation. *Phys.Rev.*, D8:1226–1239, 1973.
- [11] G.C. Branco, P.M. Ferreira, L. Lavoura, M.N. Rebelo, Marc Sher, et al. Theory and phenomenology of two-Higgs-doublet models. *Phys.Rept.*, 516:1–102, 2012.
- [12] Sacha Davidson and Howard E. Haber. Basis-independent methods for the two-Higgs-doublet model. *Phys.Rev.*, D72:035004, 2005.
- [13] Guido Altarelli and G. Isidori. Lower limit on the Higgs mass in the standard model: An Update. *Phys.Lett.*, B337:141–144, 1994.

- [14] J.R. Espinosa and M. Quiros. Improved metastability bounds on the standard model Higgs mass. *Phys.Lett.*, B353:257–266, 1995.
- [15] Matthew Gonderinger, Yingchuan Li, Hiren Patel, and Michael J. Ramsey-Musolf. Vacuum Stability, Perturbativity, and Scalar Singlet Dark Matter. *JHEP*, 1001:053, 2010.
- [16] Joan Elias-Miro, Jose R. Espinosa, Gian F. Giudice, Hyun Min Lee, and Alessandro Strumia. Stabilization of the Electroweak Vacuum by a Scalar Threshold Effect. *JHEP*, 1206:031, 2012.
- [17] Oleg Lebedev. On Stability of the Electroweak Vacuum and the Higgs Portal. *Eur.Phys.J.*, C72:2058, 2012.
- [18] Giovanni Marco Pruna and Tania Robens. Higgs singlet extension parameter space in the light of the LHC discovery. *Phys.Rev.*, D88(11):115012, 2013.
- [19] Raul Costa, Antnio P. Morais, Marco O. P. Sampaio, and Rui Santos. Two-loop stability of a complex singlet extended Standard Model. 2014.
- [20] Georg Kreyerhoff and R. Rodenberg. Renormalization Group Analysis of Coleman-Weinberg Symmetry Breaking in Two Higgs Models. *Phys.Lett.*, B226:323, 1989.

- [21] Jan Freund, Georg Kreyerhoff, and Rudolf Rodenberg. Vacuum stability in a two Higgs model. *Phys.Lett.*, B280:267–270, 1992.
- [22] Boris M. Kastening. Bounds from stability and symmetry breaking on parameters in the two Higgs doublet potential. 1992.
- [23] Shuquan Nie and Marc Sher. Vacuum stability bounds in the two Higgs doublet model. *Phys.Lett.*, B449:89–92, 1999.
- [24] Shinya Kanemura, Takashi Kasai, and Yasuhiro Okada. Mass bounds of the lightest CP even Higgs boson in the two Higgs doublet model. *Phys.Lett.*, B471:182–190, 1999.
- [25] P.M. Ferreira and D.R.T. Jones. Bounds on scalar masses in two Higgs doublet models. *JHEP*, 0908:069, 2009.
- [26] John F. Gunion, Howard E. Haber, Gordon L. Kane, and Sally Dawson. The Higgs Hunter’s Guide. *Front.Phys.*, 80:1–448, 2000.
- [27] Michael E. Peskin and Tatsu Takeuchi. A New constraint on a strongly interacting Higgs sector. *Phys.Rev.Lett.*, 65:964–967, 1990.
- [28] Michael E. Peskin and Tatsu Takeuchi. Estimation of oblique electroweak corrections. *Phys.Rev.*, D46:381–409, 1992.
- [29] K.A. Olive et al. Review of Particle Physics. *Chin.Phys.*, C38:090001, 2014.

- [30] S.L. Glashow, J. Iliopoulos, and L. Maiani. Weak Interactions with Lepton-Hadron Symmetry. *Phys.Rev.*, D2:1285–1292, 1970.
- [31] Sheldon L. Glashow and Steven Weinberg. Natural Conservation Laws for Neutral Currents. *Phys.Rev.*, D15:1958, 1977.
- [32] E.A. Paschos. Diagonal Neutral Currents. *Phys.Rev.*, D15:1966, 1977.
- [33] Antonio Pich and Paula Tuzon. Yukawa Alignment in the Two-Higgs-Doublet Model. *Phys.Rev.*, D80:091702, 2009.
- [34] G. D’Ambrosio, G.F. Giudice, G. Isidori, and A. Strumia. Minimal flavor violation: An Effective field theory approach. *Nucl.Phys.*, B645:155–187, 2002.
- [35] Lawrence J. Hall and Mark B. Wise. Flavor Changing Higgs - Boson Couplings. *Nucl.Phys.*, B187:397, 1981.
- [36] Vernon D. Barger, J.L. Hewett, and R.J.N. Phillips. New Constraints on the Charged Higgs Sector in Two Higgs Doublet Models. *Phys.Rev.*, D41:3421–3441, 1990.
- [37] Mayumi Aoki, Shinya Kanemura, Koji Tsumura, and Kei Yagyu. Models of Yukawa interaction in the two Higgs doublet model, and their collider phenomenology. *Phys.Rev.*, D80:015017, 2009.

- [38] P.M. Ferreira, L. Lavoura, and Joao P. Silva. Renormalization-group constraints on Yukawa alignment in multi-Higgs-doublet models. *Phys.Lett.*, B688:341–344, 2010.
- [39] Gustavo C. Branco, Luis Lavoura, and Joao P. Silva. CP Violation. *Int.Ser.Monogr.Phys.*, 103:1–536, 1999.
- [40] Howard E. Haber and Deva O’Neil. Basis-independent methods for the two-Higgs-doublet model. II. The Significance of tan beta. *Phys.Rev.*, D74:015018, 2006.
- [41] Howard E. Haber. The Higgs data and the Decoupling Limit. 2013.
- [42] I.P. Ivanov. Minkowski space structure of the Higgs potential in 2HDM. *Phys.Rev.*, D75:035001, 2007.
- [43] Igor P. Ivanov. Minkowski space structure of the Higgs potential in 2HDM. II. Minima, symmetries, and topology. *Phys.Rev.*, D77:015017, 2008.
- [44] Felix Nagel. *New Aspects of Gauge-Boson Couplings and the Higgs Sector*. PhD thesis, Ruperto-Carola University of Heidelberg, Germany, 2004.
- [45] M. Maniatis, A. von Manteuffel, O. Nachtmann, and F. Nagel. Stability and symmetry breaking in the general two-Higgs-doublet model. *Eur.Phys.J.*, C48:805–823, 2006.

- [46] C.C. Nishi. CP violation conditions in N-Higgs-doublet potentials. *Phys.Rev.*, D74:036003, 2006.
- [47] Celso C. Nishi. The Structure of potentials with N Higgs doublets. *Phys.Rev.*, D76:055013, 2007.
- [48] C.C. Nishi. Physical parameters and basis transformations in the Two-Higgs-Doublet model. *Phys.Rev.*, D77:055009, 2008.
- [49] Howard E. Haber and Deva O’Neil. Basis-independent methods for the two-Higgs-doublet model III: The CP-conserving limit, custodial symmetry, and the oblique parameters S, T, U. *Phys.Rev.*, D83:055017, 2011.
- [50] H.E. Haber, Gordon L. Kane, and T. Sterling. The Fermion Mass Scale and Possible Effects of Higgs Bosons on Experimental Observables. *Nucl.Phys.*, B161:493, 1979.
- [51] John F. Donoghue and Ling Fong Li. Properties of Charged Higgs Bosons. *Phys.Rev.*, D19:945, 1979.
- [52] John F. Gunion and Howard E. Haber. The CP conserving two Higgs doublet model: The Approach to the decoupling limit. *Phys.Rev.*, D67:075019, 2003.
- [53] Peter Minkowski.  $\mu \rightarrow e\gamma$  at a Rate of One Out of  $10^9$  Muon Decays? *Phys.Lett.*, B67:421–428, 1977.

- [54] P. Van Nieuwenhuizen and D.Z. Freedman. SUPERGRAVITY. PROCEEDINGS, WORKSHOP AT STONY BROOK, 27-29 SEPTEMBER 1979. 1979.
- [55] Tsutomu Yanagida. Horizontal Symmetry and Masses of Neutrinos. *Prog.Theor.Phys.*, 64:1103, 1980.
- [56] Rabindra N. Mohapatra and Goran Senjanovic. Neutrino Mass and Spontaneous Parity Violation. *Phys.Rev.Lett.*, 44:912, 1980.
- [57] Rabindra N. Mohapatra and Goran Senjanovic. Neutrino Masses and Mixings in Gauge Models with Spontaneous Parity Violation. *Phys.Rev.*, D23:165, 1981.
- [58] Nilendra G. Deshpande and Ernest Ma. Pattern of Symmetry Breaking with Two Higgs Doublets. *Phys.Rev.*, D18:2574, 1978.
- [59] K.G. Chetyrkin, Johann H. Kuhn, and M. Steinhauser. RunDec: A Mathematica package for running and decoupling of the strong coupling and quark masses. *Comput.Phys.Commun.*, 133:43–65, 2000.
- [60] Johan Bijnens, Jie Lu, and Johan Rathsman. Constraining General Two Higgs Doublet Models by the Evolution of Yukawa Couplings. *JHEP*, 1205:118, 2012.

- [61] C. Ford, D.R.T. Jones, P.W. Stephenson, and M.B. Einhorn. The Effective potential and the renormalization group. *Nucl.Phys.*, B395:17–34, 1993.
- [62] Thomas Hambye and Kurt Riesselmann. Matching conditions and Higgs mass upper bounds revisited. *Phys.Rev.*, D55:7255–7262, 1997.
- [63] Carolin B. Braeuninger, Alejandro Ibarra, and Cristoforo Simonetto. Radiatively induced flavour violation in the general two-Higgs doublet model with Yukawa alignment. *Phys.Lett.*, B692:189–195, 2010.
- [64] H. Arason, D.J. Castano, B. Keszthelyi, S. Mikaelian, E.J. Piard, et al. Renormalization group study of the standard model and its extensions. 1. The Standard model. *Phys.Rev.*, D46:3945–3965, 1992.
- [65] J. Behringer et al. Review of particle physics\*. *Phys. Rev. D*, 86:010001, Jul 2012.
- [66] Admir Greljo, Jernej F. Kamenik, and Joachim Kopp. Disentangling Flavor Violation in the Top-Higgs Sector at the LHC. *JHEP*, 1407:046, 2014.
- [67] G. Eilam, J.L. Hewett, and A. Soni. Rare decays of the top quark in the standard and two Higgs doublet models. *Phys.Rev.*, D44:1473–1484, 1991.
- [68] B. Mele, S. Petrarca, and A. Soddu. A New evaluation of the  $t \rightarrow cH$  decay width in the standard model. *Phys.Lett.*, B435:401–406, 1998.

- [69] J.A. Aguilar-Saavedra. Top flavor-changing neutral interactions: Theoretical expectations and experimental detection. *Acta Phys.Polon.*, B35:2695–2710, 2004.
- [70] Cen Zhang and Fabio Maltoni. Top-quark decay into Higgs boson and a light quark at next-to-leading order in QCD. *Phys.Rev.*, D88:054005, 2013.
- [71] F. Larios, R. Martinez, and M.A. Perez. Constraints on top quark FCNC from electroweak precision measurements. *Phys.Rev.*, D72:057504, 2005.
- [72] J.I. Aranda, A. Cordero-Cid, F. Ramirez-Zavaleta, J.J. Toscano, and E.S. Tututi. Higgs mediated flavor violating top quark decays  $t \rightarrow u_i H$ ,  $u_i \gamma$ ,  $u_i \gamma \gamma$ , and the process  $\gamma \gamma \rightarrow tc$  in effective theories. *Phys.Rev.*, D81:077701, 2010.
- [73] Nathaniel Craig, Jared A. Evans, Richard Gray, Michael Park, Sunil Somalwar, et al. Searching for  $t \rightarrow ch$  with Multi-Leptons. *Phys.Rev.*, D86:075002, 2012.
- [74] Wolfgang Altmannshofer and David M. Straub. Cornering New Physics in  $b \rightarrow s$  Transitions. *JHEP*, 1208:121, 2012.
- [75] C. McNeile, C.T.H. Davies, E. Follana, K. Hornbostel, and G.P. Lepage. High-Precision  $f_{B_s}$  and HQET from Relativistic Lattice QCD. *Phys.Rev.*, D85:031503, 2012.

- [76] A. Bazavov et al. B- and D-meson decay constants from three-flavor lattice QCD. *Phys.Rev.*, D85:114506, 2012.
- [77] Heechang Na, Chris J. Monahan, Christine T.H. Davies, Ron Horgan, G. Peter Lepage, et al. The  $B$  and  $B_s$  Meson Decay Constants from Lattice QCD. *Phys.Rev.*, D86:034506, 2012.
- [78] R. Aaij et al. Strong constraints on the rare decays  $B_s \rightarrow \mu^+\mu^-$  and  $B^0 \rightarrow \mu^+\mu^-$ . *Phys.Rev.Lett.*, 108:231801, 2012.
- [79] Serguei Chatrchyan et al. Search for  $B_s^0 \rightarrow \mu^+\mu^-$  and  $B^0 \rightarrow \mu^+\mu^-$  decays. *JHEP*, 1204:033, 2012.
- [80] Georges Aad et al. Search for the decay  $B_s^0 \rightarrow \mu^+\mu^-$  with the ATLAS detector. *Phys.Lett.*, B713:387–407, 2012.
- [81] M.K. Parida and B. Purkayastha. New formulas and predictions for running masses at higher scales in MSSM. *Eur.Phys.J.*, C14:159–164, 2000.
- [82] C.R. Das and M.K. Parida. New formulas and predictions for running fermion masses at higher scales in SM, 2 HDM, and MSSM. *Eur.Phys.J.*, C20:121–137, 2001.
- [83] Howard E. Haber and Ralf Hempfling. The Renormalization group improved

Higgs sector of the minimal supersymmetric model. *Phys.Rev.*, D48:4280–4309, 1993.